

Spring 2022

# Female Reproductive Toxicity of Harmful Algal Blooms-Produced Toxin Microcystin

Yingzheng Wang

Follow this and additional works at: <https://scholarcommons.sc.edu/etd>



Part of the [Environmental Health Commons](#)

---

## Recommended Citation

Wang, Y.(2022). *Female Reproductive Toxicity of Harmful Algal Blooms-Produced Toxin Microcystin*. (Doctoral dissertation). Retrieved from <https://scholarcommons.sc.edu/etd/6555>

This Open Access Dissertation is brought to you by Scholar Commons. It has been accepted for inclusion in Theses and Dissertations by an authorized administrator of Scholar Commons. For more information, please contact [digres@mailbox.sc.edu](mailto:digres@mailbox.sc.edu).

FEMALE REPRODUCTIVE TOXICITY OF HARMFUL ALGAL BLOOMS-PRODUCED  
TOXIN MICROCYSTIN

by

Yingzheng Wang

Bachelor of Science  
Shandong Agricultural University, 2013

Master of Science  
China Agricultural University, 2016

---

Submitted in Partial Fulfillment of the Requirements

For the Degree of Doctor of Philosophy in

Environmental Health Sciences

The Norman J. Arnold School of Public Health

University of South Carolina

2022

Accepted by:

Geoffrey I. Scott, Major Professor

Shuo Xiao, Committee Member

Saurabh Chatterjee, Committee Member

Holly LaVoie, Committee Member

Tracey L. Weldon, Interim Vice Provost and Dean of the Graduate School

© Copyright by Yingzheng Wang, 2022  
All Rights Reserved.

## DEDICATION

This thesis is dedicated to my beloved parents, sister, girlfriend, and the people who have supported me throughout my education. Their love and endless support helped me be the person I am today.

## ACKNOWLEDGEMENTS

I would like to extend my sincere thanks to my supervisor Dr. Shuo Xiao for his invaluable supervision, advice, and support during my PhD study. I would also like to thank Dr. Geoffrey I. Scott for being my co-advisor to support me to continue my dissertation project after Dr. Xiao moved to Rutgers University. I would like to thank my other PhD committee members Dr. Saurabh Chatterjee and Dr. Holly LaVoie for their valuable insights and support on my study.

In addition, I also appreciate all the support and help from my lab colleagues Dr. Pawat Pattarawat, Dr. Jiyang Zhang, and Mr. Eunchong Kim. I would also like to thank Peihong Zhou, Rita Hahn, and Wen Xia for their treasured help when I worked at Rutgers. It is their kind help and support that have made my study.

Last but not the least, I would like to express my gratitude to my parents, sister, and girlfriend for their encouragement and support in the past few years. Without their tremendous understanding and support, it would be impossible for me to complete this journey.

## ABSTRACT

Harmful algal blooms (HABs) have become a global emerging environmental concern; however, its impact on women's reproductive health is poorly understood. Microcystin-LR (MC-LR) is the most common and hazardous type of HAB toxin. Using both a chronic oral exposure mouse model and an acute exposure mouse model, I found that human-relevant exposure to MC-LR could compromise follicle ovulation via affecting follicle maturation. Both *in vivo* mouse exposure model and encapsulated *in vitro* follicle growth (eIVFG) model revealed that exposure to MC-LR did not affect follicle development, but significantly reduced the expression of some follicle maturation-related genes, such as *Lhcgr* and *Pappa*. Mechanistic studies demonstrated that MC-LR could inhibit the protein phosphatase 1 (PP1) and further block the activation of PI3K/AKT/FOXO1 signaling pathway. In addition, OATP inhibitor Ritonavir could inhibit the accumulation of MC-LR in the follicles and rescue the MC-LR-disrupted follicle ovulation. Taken together, these results demonstrate that human-relevant exposure to MC-LR compromises ovulation via disrupting follicle maturation by inhibiting PP1/PI3K/AKT/FOXO1 signaling pathway in the granulosa cells. More than 279 MC congeners have been identified and a broad spectrum of environmental chemicals and pharmaceutical compounds cause female ovarian toxicity (ovotoxicity). The eIVFG is a robust *in vitro* model for ovotoxicity testing. However, the follicle preparation process is complex and highly dependent on technical skills. Here, I aimed to use vitrification method

to cryopreserve murine immature follicles for a high-content eIVFG, chemical exposure, and ovotoxicity screening. Results indicated that a closed vitrification system combined with optimized vitrification protocols preserved mouse follicle viability and functionality and vitrified follicles exhibited comparable follicle and oocyte reproductive outcomes to freshly harvested follicles during eIVFG, including follicle survival and development, ovarian steroidogenesis, and oocyte maturation and ovulation. Moreover, vitrified follicles consistently responded to ovotoxic chemical, doxorubicin (DOX). I further used vitrified follicles to test the ovotoxicity of 4 MC congeners, including MC-LA, LF, LR, and LY, and found that different congeners of MCs exhibited differential ovotoxicities. In summary, my research study demonstrates a novel toxic mechanism of HAB toxin MC-LR in compromising follicle ovulation and introduces a follicle vitrification strategy to build a long-term-storage and ready-to-use ovarian follicle bank for high-throughput ovotoxicity screening, which identifies endocrine disrupting effects of MCs.

## TABLE OF CONTENTS

Dedication .....	iii
Acknowledgements .....	iv
Abstract .....	v
List of Tables .....	viii
List of Figures .....	ix
Chapter 1 Introduction .....	1
Chapter 2 Literature review .....	6
Chapter 3 Human-relevant exposure to harmful algal bloom toxin microcystin-LR disrupts the PP1-mediated PI3K/AKT/FOXO1 signaling in follicular granulosa cells to compromise female ovarian follicle maturation and ovulation .....	33
Chapter 4 A closed vitrification system enables a murine ovarian follicle bank for high-throughput ovotoxicity screening, which discovers the endocrine disrupting effect of microcystins .....	78
Chapter 5 Conclusion.....	121
References.....	123
Appendix A Copyright permission for chapter.....	138

## LIST OF TABLES

Table 3.1 Established follicle maturation genes and their identified functions in follicle maturation .....	65
Table 3.2 Established ovulatory genes and their identified functions in ovulation.....	66
Table 4.1 Recipes of vitrification and warming solutions .....	103
Table 4.2 A summary of previous studies that vitrified ovarian tissues or individual follicles .....	104

## LIST OF FIGURES

Figure 2.1 The general cyclic structure of microcystins .....	32
Figure 3.1 Chronic exposure of MC-LR using oral gavage on reproductive parameters..	67
Figure 3.2 MC-LR compromises follicle ovulation after short-term exposure during both follicle maturation and ovulation windows .....	68
Figure 3.3 MC-LR compromises mouse follicle ovulation after short-term exposure during follicle maturation window but not the ovulation window .....	69
Figure 3.4 MC-LR accumulates in the ovary and affects the follicle maturation.....	70
Figure 3.5 Effect of MC-LR on follicle survival, follicle development, hormone secretion, and follicle ovulation during encapsulated <i>in vitro</i> follicle growth (eIVFG) .....	71
Figure 3.6 MC-LR treatment affects the follicle maturation and ovulation during eIVFG .....	72
Figure 3.7 Single-follicle RNA-sequencing identifies that PI3K/AKT/FOXO1 signaling pathway is involved in the MC-LR-disrupted follicle maturation.....	73
Figure 3.8 MC-LR inhibits the PP1/PI3K/AKT/FOXO1 signaling pathway .....	74
Figure 3.9 OATP inhibitor Ritonavir blocks the accumulation of MC-LR in follicles and rescues the MC-LR-disrupted follicle ovulation .....	75
Figure 3.10 A proposed model for MC-LR-affected follicle maturation and ovulation ...	76
Figure 3.11 mRNA expression levels of follicle maturation -related genes in the granulosa cells of control and MC-LR treatment follicles on day 6 of eIVFG .....	77
Figure 3.12 Quality control analysis of single-follicle RNA sequencing for the control and MC-LR treatment follicles .....	77

Figure 4.1 Procedures of ovarian follicle vitrification and warming. Freshly harvested follicles were sequentially equilibrated in EG+ PXZ and EDS vitrification solutions containing increasing concentrations of CPAs .....	110
Figure 4.2 Follicle morphology after vitrification and warming .....	111
Figure 4.3 Effect of vitrification on follicle growth and survival during encapsulated <i>in vitro</i> follicle growth (eIVFG).....	112
Figure 4.4 Effect of vitrification on the mRNA expression of ovarian steroidogenesis related genes and 17 $\beta$ -estradiol (E2) secretion .....	113
Figure 4.5 Effect of vitrification on oocyte meiotic maturation after <i>in vitro</i> maturation .....	114
Figure 4.6 Ovotoxicity testing of doxorubicin (DOX) using vitrified and warmed follicles, with representative TUNEL images of follicles treated with DOX at 100 nM for 0, 6, and 12 hours.....	115
Figure 4.7 Effect of different congeners of microcystins (MCs) on follicle growth, survival, and oocyte maturation during encapsulated <i>in vitro</i> follicle growth (eIVFG) using vitrified and warmed follicles .....	116
Figure 4.8 Effect of different congeners and concentrations of microcystins (MCs) on 17 $\beta$ -estradiol (E2) secretion of <i>in vitro</i> cultured vitrified and warmed follicles on day 8 of eIVFG .....	117
Figure 4.9 Representative images of follicles treated with different concentrations of microcystin-LA (MC-LA) on days 0, 2, 4, 6, and 8 during eIVFG.....	118
Figure 4.10 Representative images of follicles treated with different concentrations of microcystin-LR (MC-LR) on days 0, 2, 4, 6, and 8 during eIVFG.....	129
Figure 4.11 Representative images of follicles treated with different concentrations of microcystin-LY (MC-LY) on days 0, 2, 4, 6, and 8 during eIVFG.....	120
Figure 4.12 Effect of different congeners of microcystins (MCs) on follicle growth during encapsulated <i>in vitro</i> follicle growth (eIVFG) using freshly harvested follicles .....	120

# CHAPTER 1

## INTRODUCTION

Harmful algal blooms (HABs) are the overgrowth and accumulation of various microscopic algae and cyanobacteria in marine, brackish, or freshwater ecosystems [1]. Due to the climate change-associated temperature rise and anthropogenic eutrophication, HABs have become an emerging global environmental concern [2]. Planktonic cyanobacteria-related cyanobacterial HABs (CyanoHABs) have received increasing attention due to their prevalence and potential health threats to both humans and animals [3]. CyanoHABs not only worsen water quality, but also produce HAB toxins or cyanotoxins [4]. Among the identified amount of cyanotoxins, microcystins (MCs) are the most widespread cyanotoxins in surface and drinking waters [5].

MCs are non-ribosomally synthesized via an MC synthetase gene cluster in a variety of planktonic and benthic cyanobacteria genera, such as *Microcystis*, *Dolichospermum*, *Planktothrix*, *Nostoc*, etc [6, 7]. The abundance and congener composition of MCs in CyanoHABs are determined by multiple environmental conditions, such as water temperature, pH, photosynthetically active radiation, and nutrient supply, etc [8]. Thus far, at least 279 MC congeners have been identified and MC-LR is the most common and well-characterized MC congener [5, 9].

Humans can be exposed to MC-LR through multiple routes, including ingestion of drinking water or contaminated food, recreational activities, and hemodialysis [10-13]. The World Health Organization (WHO) sets a provisional guideline for MC-LR in lifetime drinking-water at 1 µg/L and the recommended recreational value for MCs released by U.S. Environmental Protection Agency (EPA) is 8 µg/L [14, 15]. However, the concentrations of MC-LR in many water bodies range from 0.06 to 2,100 µg/L which are much higher than the WHO and EPA guidelines [16]. As a hydrophilic and relatively large molecule (molecular mass: approx. 1kDa), MC-LR cannot cross cell membranes via passive diffusion. Organic anion transporting polypeptides (OATPs) have been shown to uptake MC-LR using *in vitro* expression model and gene knockout mouse model [17, 18]. The multidrug resistance-associated protein 2 (MRP2) is largely responsible for the cellular efflux of MC-LR [19]. OATPs are expressed in almost all tissues in animal and human bodies. Distinct tissues express differential OATP isoforms [20, 21]. Thus, the distinct tissue expression patterns of OATPs may impact the distribution of MC-LR as well as its associated toxic effects.

Increasing evidence shows that MC-LR is a toxin targeting multiple organ systems, including liver, kidney, heart, gastrointestinal (GI) tract, lung, skin, brain, immune system, and reproductive system [22-24]. Using both *in vitro* and *in vivo* models, a number of studies have shown that exposure to MC-LR can interfere with male reproduction by inducing testicular damage and sex hormone disorders [25-29]. However, the female reproductive toxicity of MC-LR has not been comprehensively investigated, particularly in mammals. In my second chapter, I comprehensively reviewed the published studies about the toxic effects and mechanisms of MC-LR on the female reproduction. According

to the limited published data, MC-LR is an emerging reproductive environmental toxin which can disrupt female reproduction at different levels in the hypothalamic-pituitary-gonadal (HPG) axis.

The ovary is the primary female reproductive organ and contains of various developmental stages of follicles as the basic functional units. Each follicle contains a central germ cell oocyte surrounded by somatic cells and functions to produce steroid and peptide hormones (steroidogenesis) and to mature an oocyte for ovulation (gametogenesis). The ovarian follicle pool is established during fetal or neonatal life in all mammals and it is non-renewable [30]. Thus, environmental contaminants (e.g., EDCs) or other factors that compromise the quality and quantity of follicles will result in ovarian toxicity (ovotoxicity) and increase women's risks of premature ovarian failure (POF), hormonal imbalance, and infertility [31-33].

Conventional ovarian cell-based assays lack the complexity, functions, and morphology of follicles and do not consider the interactions between oocyte and somatic cells. Our established encapsulated *in vitro* follicle growth (eIVFG) system maintains the 3D architecture of follicles and support follicle development for steroidogenesis, maturation, and ovulation, as well as the acquisition of both oocyte meiotic and developmental competence [34-36]. We further demonstrated that eIVFG is a robust *in vitro* model to perform ovotoxicity testing for environmental contaminants and xenobiotic exposures and drug screening for development of nonhormonal contraceptive [36-40]. Therefore, eIVFG enables us to investigate the direct effects of environmental toxicants and clinical drugs on follicle development, maturation, ovulation, and luteinization at the individual follicle level.

To further investigate the potential toxic effects of MC-LR on the female reproduction, I took advantage of both an *in vivo* mouse exposure model and an *in vitro* 3D follicle culture model to determine the impacts of human-relevant MC-LR exposure on the follicle maturation and ovulation. The third chapter of this thesis demonstrates that exposure to human-relevant MC-LR does not affect follicle survival and growth, but impacts the follicle maturation via programming the gene expression in the granulosa cells and in turn disrupts the following ovulation. In-depth mechanistic studies suggest that MC-LR can block the activation of the PI3K/AKT/FOXO1 signaling pathway via the inhibition of protein phosphatase 1 (PP1) in the granulosa cells. Additionally, OATP inhibitor Ritonavir can inhibit the accumulation of MC-LR in the follicles and rescue the MC-LR-disrupted follicle ovulation.

In addition to MC-LR, the ovarian toxicity of other MC congeners is still largely unknown. Furthermore, over 84,000 chemicals are registered and used daily in consumer products, and about 2,000 new chemicals are being introduced each year, indicating that there is an urgent and unmet need to develop an efficient and reliable ovotoxicity screening platform [41]. Our established eIVFG is a robust *in vitro* model to screen for the ovotoxicity of xenobiotic exposures, however, the follicle preparation procedure for eIVFG is a complex process and requires multiple rounds of follicle isolation and culture. These shortfalls make the eIVFG not optimal for a high-throughput ovotoxicity screening, particularly when a rapid screening is desired in the face of unpredictable and emerging environmental threats such as the Deepwater Horizon oil spill in Gulf of Mexico.

Previous studies have used vitrification methods to cryopreserve preantral follicles from various species as an additional option of female fertility preservation [42-48].

However, the recovered follicles have not undergone a systemic evaluation of folliculogenesis and oogenesis or the follicle and/or oocyte quality are compromised. Additionally, it is also largely unknown whether these vitrified follicles will consistently respond to ovotoxic chemicals compared to freshly harvested follicles.

In the fourth chapter of this thesis, I used a closed vitrification system combined with optimized vitrification protocols to cryopreserve individual murine preantral follicles and demonstrated that vitrification preserved follicle viability and functionality, and vitrified follicles exhibited comparable follicle/oocyte reproductive outcomes to freshly harvested follicles. Moreover, I used doxorubicin (DOX), a commonly used chemotherapeutic chemical that exhibits ovotoxicity [37, 49-51], as the positive control to demonstrate that vitrified and fresh follicles have a comparable response to DOX during eIVFG. Further, I used vitrified follicles and eIVFG to screen for the ovotoxicity of 4 common MCs, including MC-LA, LF, LR, and LY. Results indicate that different MC congeners have differential ovotoxic effects on ovarian follicles, and MC-LF may exhibit endocrine disrupting effects on the ovary.

Overall, the entire research primarily focuses on the ovarian toxicity induced by MC-LR and developing a long-term-storage and ready-to-use ovarian follicle bank for high-throughput ovotoxicity screening of MCs and other environmental contaminants.

CHAPTER 2  
LITERATURE REVIEW

---

Yingzheng Wang and Shuo Xiao. Impacts of harmful algal blooms-produced microcystins on female reproduction. (In preparation)

## 2.1 INTRODUCTION

Harmful algal blooms (HABs) are the overgrowth and accumulation of various microscopic algae and cyanobacteria in marine, brackish, or freshwater ecosystems [1]. Primarily caused by the climate change-associated temperature rise and anthropogenic eutrophication [2], planktonic cyanobacteria and associated cyanobacterial HABs (CyanoHABs) have become an emerging global environmental concern and received an increasing attention due to their prevalence and potential health threats to both wildlife animals and humans [3, 52]. CyanoHABs not only worsen water quality by changing the odor, color, and flavor, but also produce toxic substances that are termed cyanotoxins or HAB toxins [4]. According to the chemical structures, cyanotoxins can be classified into three categories, including cyclic peptides (e.g., microcystin and nodularin), alkaloids (e.g., anatoxin-a, saxitoxin, cylindrospermopsin, aplysiatoxins, lyngbyatoxin-a), and lipopolysaccharides [53]. Among various types of cyanotoxins, microcystins (MCs) are the most widespread cyanotoxins in surface and drinking waters [54].

MCs are frequently produced by a variety of planktonic and benthic cyanobacteria genera, such as *Microcystis*, *Dolichospermum*, *Planktothrix*, *Nostoc*, etc [6]. MCs are non-ribosomally synthesized via an MC synthetase gene (*mcy*) cluster that consists of peptide synthetases (*mcyABC*), polyketide synthases (*mcyD*), and additional modifying enzymes [7, 55]. Thus far, at least 279 MC congeners have been identified [56]. The abundance and congener composition of MCs are determined by multiple environmental conditions, including water temperature, pH, photosynthetically active radiation, and nutrient supply, etc [8, 57, 58]. The general structure of MCs is cyclo-(D-Ala<sup>1</sup>-X<sup>2</sup>-D-MeAsp<sup>3</sup>-Z<sup>4</sup>-Adda<sup>5</sup>-D-Glu<sup>6</sup>-Mdha<sup>7</sup>) with the variable L-amino acids X and Z in positions 2 and 4 (Fig. 2.1). The

different combination of the variable L-amino acids X and Z and modifications of the other amino acids generate a large structural diversity of MCs. While the structural variation has been identified in all seven amino acids of MCs, the X and Z are the most common substitution sites [56]. For example, the substitution of X and Z with leucine (L) and arginine (R), respectively, generates MC-LR which is the most common and well-defined MC congener [54]. In this review, I primarily focused on the impacts of MC-LR on female reproduction and also introduced other MC congeners.

The World Health Organization (WHO) sets a provisional guideline for MC-LR in drinking-water at 1 µg/L, and the recommended value for total MCs in recreational water is 8 µg/L from the U.S. Environmental Protection Agency (EPA) [14, 15]. The concentrations of MC-LR in many water bodies, however, range from 0.06 to 2,100 µg/L, which are much higher than the WHO and EPA standards [16]. Humans can be exposed to MC-LR in a chronic manner via daily drinking water. Because MC-LR can accumulate in various aquatic organisms such as fish and oyster, humans are also exposed to high levels of MC-LR through the consumption of aquatic foods [10, 59]. Eating crop foods and vegetables irrigated with MCs-contaminated water is another critical exposure route in humans [11, 60]. Recreational exposure to MC-LR mainly involves accidentally oral consumption, dermal contact, and inhalation of aerosolized MC-LR [12]. In addition, patients have the potential to be exposed to MC-LR via medical solutions contaminated with MC-LR and other MCs. For instance, contaminated dialysis fluid caused the death of 60 patients who underwent dialysis at a Caruaru hemodialysis unit in Brazil in 1996, which has been related to the acute neurotoxicity and subacute hepatotoxicity upon high levels of MCs exposure [13].

The toxicokinetics of MC-LR have been studied in different species, including rainbow trout [61], rodents [62-65], and pigs [66]. Upon oral ingestion, MC-LR is primarily absorbed through the small intestine of the gastrointestinal (GI) tract to enter the systemic circulation in rainbow trout, mice, and pigs [61, 62, 66]. So far, there are no studies investigating the absorption of MC-LR through the routes of inhalation and dermal exposure. After absorption, MC-LR can distribute to multiple organs via the circulatory system. While liver is the primary distribution site, MC-LR can also reach to other organ systems, such as kidney, brain, heart, muscle, and gonads, but the distribution patterns of MC-LR can be distinctive depending on the species and exposure route [23, 66]. In wild freshwater fishes collected during the CyanoHAB season in the Lake Chaohu in China, intestines and blood had the highest abundance of MC-LR, followed by liver, bile, kidney, and muscle [67]. In ICR female mice that were intraperitoneally administered with the radioactive [<sup>3</sup>H]DihydroMC-LR, however, the highest levels of MC-LR was detected in the liver (72% of administered total radioactivity), followed by the small intestine, large intestine, kidney and gall bladder, lung, and stomach [64]. In rats that were intravenously injected with MCs, including MC-LR, the highest concentration of MCs was found in the kidney, followed by the lung, stomach, liver, small intestine, gonad, spleen, muscle, heart, and brain [65]. The plasma protein composition and albumin binding affinity also impact the distribution of MC-LR [68]. For example, the serum albumin has the highest binding affinity to MC-LR in human compared to five other species, including pig, cattle, silver carp, bighead carp, and crucian carp [68]. These results indicate that although the underlying mechanism remains poorly understood, the distribution of MC-LR depends on the species, exposure routes, as well as the circulating binding proteins.

Glutathione (GSH) conjugation has been shown to be the primary detoxication mechanism of MC-LR in both *in vitro* and *in vivo* models [69-72]. The GSH-conjugated MC-LR is further metabolized to cysteine (Cys)-conjugated MC-LR which can be quickly excreted via urine and feces [73, 74]. Interestingly, both GSH- and Cys- conjugated MC-LR can also be deconjugated to cause the release of free MC-LR based on the results in an *in vitro* deconjugation reactions [75]. The GSH and Cys conjugates of another MC congener, MC-RR, are also able to be reversed to free MC-RR in the bighead carp, indicating that the conjugation of MCs is a reversible process [76]. Although there is limited evidence in mammalian species, the environmental and toxic outcomes of this reversible reaction can be a concern. After metabolism, MC-LR are primarily excreted through urine and feces with the forms of free MC-LR, GSH-MC-LR or Cys-MC-LR [23, 73]. So far, there are limited data regarding the absorption, distribution, metabolism, and excretion of MC-LR in humans. The serum concentrations of MC-LR range from 0.000 to 1.221 ng/mL (with the average at 0.175 ng/mL) in Chinese fishermen who are chronically exposed to MC-LR via daily oral ingestion and dermal exposure [77]. In dialysis patients who have been exposed to a mixture of MCs from contaminated dialysis fluid during a 1996 outbreak in Brazil, the serum concentration of MC-LR equivalents (including MC-LR, MC-YR, and desmethyl MC-LY) reached 7.6 – 31.4 ng/ml (with the average at 20 ng/mL) [78].

As a hydrophilic and relatively large molecule (molecular mass: approx. 1 kDa), MC-LR cannot cross cell membrane via passive diffusion. Organic anion transporting polypeptides (OATPs) have been shown to regulate the cellular uptake of MC-LR based on the results in an *in vitro* expression model and a gene knockout mouse model [17, 18].

The multidrug resistance-associated protein 2 (MRP2) is largely responsible for the cellular efflux of MC-LR [19]. There are more than 300 OATP family members including 11 human transporters [79]. OATPs are expressed in almost all tissues in animals and human bodies. Distinct tissues express differential OATP isoforms [20, 21]. Thus, the distinct tissue expression of OATPs may impact the distribution and accumulation of MC-LR as well as its associated toxic effects. OATP1A2, OATP2A1, OATP3A1, and OATP4A1 have been found to ubiquitously express in a broad range of organs, including brain, kidney, liver, intestine, spleen, lung, testis, and placenta [80, 81]. OATP1B1 is the most abundant OATP isoform in the liver, followed by OATP1B3 and OATP2B1 [82]. OATP2B1 has been detected in the human intestine and regulates the uptake of endogenous compounds and drugs [83]. Although we recognize that the OATP proteins play important roles in the uptake and accumulation of MC-LR, the expression pattern and mechanistic regulation of OATPs, particularly in the GI tract, skin, and nasal systems, remains poorly understood. In addition, previous studies primarily focused on one exposure route, but humans are exposed to MC-LR via different routes. Thus, an experimental model with the mixture of various exposure routes should be considered in future studies. As multispecific transporters, OATPs mediate the cellular uptake of a variety of substrates, including bile acids, steroid conjugates, and numerous xenobiotics [20]. Therefore, whether the exposure to MC-LR alters the transport of other endogenous substrates requires further investigations.

Liver has been identified as the primary target organ of MC-LR. Both epidemiological and bench research demonstrate the association of MC-LR with liver damage and hepatocellular carcinoma [77, 84-86]. Thus, MC-LR is classified as a potential

human carcinogen (Group 2B) by the International Agency for Research on Cancer (IARC). Increasing evidence also reveals that MC-LR is a toxin targeting multiple organ systems, including liver, kidney, heart, GI, lung, skin, brain, immune system, and reproductive system [22-24]. With respect to the reproductive system, a number of studies have shown that exposure to MC-LR can interfere with male reproduction by inducing testicular damage and sex hormone disorders [25-29]. However, the female reproductive toxicity of MC-LR has not been comprehensively investigated, particularly in mammals. Herein, I reviewed previous studies regarding the toxic effects and possible mechanisms of microcystins on female function and also indicated the knowledge gaps; in addition to MC-LR, the most common and well-defined MC congener, I also described the potential reproductive toxicity of other MC congeners.

## 2.2 TOXIC MECHANISMS OF MC-LR

Understanding the molecular initiating event (MIE) of MC-LR is critical for developing protective and/or preventative methods. In this section, I briefly summarized the toxic mechanisms of MC-LR, including the inhibition of protein phosphatases, oxidative stress, and cytoskeleton disruption, *etc*, and more detailed information can be found in previous reviews [23, 87-89].

### 2.2.1 PROTEIN PHOSPHATASE INHIBITION

Protein phosphorylation is a common post-translational modification to regulate numerous cellular processes, such as cell growth, differentiation, apoptosis, and other physiological and pathophysiological changes. As a reversible biological process, protein

phosphorylation is regulated by kinases and phosphatases. Protein phosphatases 1 and 2A (PP1 and PP2A) are the two most abundant serine/threonine phosphatases, and they catalyze the majority of protein dephosphorylation in eukaryotes [90]. MC-LR has been defined as a potent inhibitor of PP1 and PP2A, which has been proposed as a major mode of action (MOA) of MC-LR-induced toxicity [91].

MC-LR binds to the catalytic subunit of PP1 via three distinct surface regions, including the metal-binding site, the hydrophobic groove, and the edge of C-terminal groove [92]. With respect to PP2A, MC-LR binds to the surface pocket of the catalytic subunit of PP2A through the interactions between hydrophobic the Adda side chain of MC-LR and the hydrophobic cage in PP2A [93]. The interaction between MC-LR and PP1/2A is strengthened by the covalent linkage between the terminal carbon atom of the Mdha side chain of MC-LR and the S $\gamma$  atom of Cys273 in PP1 and the S $\gamma$  atom of Cys269 in PP2A, leading to an irreversible inhibition of PP1/2A [92, 93]. The inhibition of PP1/2A by MC-LR disrupts the phosphorylation homeostasis, resulting in the dysregulation of multiple molecules and numerous signaling, such as the mitogen-activated protein kinase (MAPK) and nuclear factor kappa B (NF- $\kappa$ B) signaling pathways [94-96].

Both PP1 and PP2A play essential roles in mitosis and cellular DNA damage response (DDR). The mitotic cycle is governed by the dynamic changes of protein phosphorylation with a peak of protein phosphorylation when a cell undergoes mitosis [90]. The inhibition of specific protein phosphatase activity is essential for a cell to initiate mitosis. For instance, the activated cyclin-dependent kinase 1(CDK1), a master regulator of mitosis, directly inhibits the catalytic activity of PP1 [97, 98], or activates Gwl kinase to further inhibit the PP2A-B55 during mitosis [99, 100]. On the other hand, cells are

constantly exposed to endogenous or exogenous DNA-damaging stresses that pose threats to the integrity of genome. In order to safeguard the genomic stability and integrity, cells develop the DNA-damage response (DDR) mechanisms to recognize the damaged DNA and repair it. When DNA repair is failed or insufficient, the accumulated genetic alterations cause apoptosis or initiate a malignant transformation. Protein phosphatases, including PP1/2A, critically regulate the activation of DDR upon DNA damage and also the inactivation of DDR after the reparation of DNA damage [101]. It has been found that PP1 dephosphorylates p53 at the Ser15 and Ser37 for inactivation to inhibit the DNA damage-dependent activation of p53 signaling pathway [102]. Similar to PP1, PP2A also dephosphorylates p53 at Ser37 to regulate its transcriptional activity [102]. Besides, PP1 also dephosphorylates BRCA1, another essential DNA repair regulator, to control the BRCA1-dependent DNA repair [103]. PP2A is also involved in DDR through regulating the activities of various DDR-related kinases, such as ATM, ATR, DNA-PK, CHK1, and CHK2 [104]. Therefore, according to the ubiquitous expression and essential functions of PP1 and PP2A in the cells, the MC-LR-induced inhibition of PP1/2A may produce multiple effects on different cells and organs.

### 2.2.2 OXIDATIVE STRESS

MC-LR has been found to cause oxidative stress, the imbalance between the production of reactive oxygen species (ROS) and the ability of detoxifying these products in cells. ROS are primarily produced by mitochondria and cells have an antioxidant defensive system to protect themselves from ROS-induced cellular damage. Glutathione (GSH) is an essential low molecular weight antioxidant and contributes to the removal of

ROS. For example, GSH can remove H<sub>2</sub>O<sub>2</sub> by a reduction reaction which is catalyzed by the glutathione peroxidase [105]. It has been established that GSH plays an important role in the detoxification of MC-LR by forming the MC-LR-GSH conjugates [72, 106]. The depletion of GSH by treating the SD rats with a specific GSH synthesis inhibitor-buthionine-(S,R)-sulfoximine (BSO), did not only diminish the detoxification of MC-LR but also remarkably exacerbated MC-LR-induced liver damage [107]. Another follow-up study from the same group reported that the hepatic content of GSH was decreased within 2 hours post-MC-LR exposure [108]. Therefore, exposure to MC-LR may induce oxidative stress by depleting GSH. Mitochondria plays a pivotal role in the ROS production and apoptosis [109, 110]. Meanwhile, the ROS-induced oxidative stress can damage the mitochondrial respiratory chain, alter membrane permeability, and disrupt mitochondrial defense system [111]. MC-LR-induced ROS production could decrease the mitochondrial membrane potential (MMP) and lead to apoptosis in primary rat hepatocyte cells; the pretreatment of antioxidant deferoxamine (DFO) significantly inhibited the ROS production and further blocked the loss of MMP [112]. In agreement with this, ROS generation induced by MC-LR contributed to the hepatocyte apoptosis and liver damage *in vivo* [113, 114]. So far, the detailed mechanism of MC-LR induced-ROS production is elusive. More studies are required to define the origin of ROS after MC-LR exposure, such as the depletion of GSH and mitochondria damage.

### 2.2.3 OTHER TOXIC MECHANISMS OF MC-LR

In addition to the inhibition of PP1/2A and the induction of oxidative stress, several other toxic mechanisms of MC-LR have also been reported, such as the cytoskeletal

disruption, apoptosis, autophagy, and necrosis, *etc* [23, 24]. Cytoskeleton is a well-organized network of intracellular filaments which integrates the activity of a multitude of cytoplasmic proteins and organelles. Both *in vitro* and *in vivo* studies have shown that exposure to MC-LR disrupted cytoskeleton by altering the organization of microfilaments, microtubules, and intermediate filaments in various types of cells, including hepatocytes [115, 116], kidney cells [117], neuroendocrine PC12 cells [94], human umbilical vein endothelial cells [118], testis cells [119], and oocytes [120]. Extensive studies have been performed to decipher the mechanisms of MC-LR-induced cytoskeletal disruption. The altered expression and hyperphosphorylation of cytoskeleton and associated proteins have been identified in different types of cells treated with MC-LR [89]. For example, MC-LR can affect the neuronal cytoskeletal architecture remodeling by enhancing the phosphorylation of tau, a neural microtubule associated protein which is essential for the assembly and stability of microtubules; and this MC-LR-induced cytoskeletal disruption is regulated in a p38 MAPK signaling dependent manner [94]. In human umbilical vein endothelial cells, exposure to MC-LR disrupts cytoskeleton by down-regulating the integrin-mediated FAK/ROCK signaling pathway [118]. Another study demonstrates that ROS production is involved in MC-LR induced cytoskeleton disruption [121]. However, the underlying mechanism of MC-LR-altered the activation of signaling pathways and cytoskeletal disruption requires more investigations; meanwhile, whether the inhibition of PP1/PP2A induced by MC-LR involved in the cytoskeletal disruption is still poorly understood.

Based on the morphological, biochemical, and functional perspectives, cell death can be characterized as multiple types, such as apoptosis, autophagy-dependent cell death,

necrosis, *etc* [122]. The mechanisms of MC-LR-induced cytotoxicity vary according to different cell types and exposure doses. For instance, 10 µg/mL MC-LR reduced the cell viability by about 40% in human colon adenocarcinoma CaCo-2 cells, but did not affect the survival of human astrocytoma IPDDC-A2 and B-lymphoblastoid NCNC cells at the same exposure concentration [123]. MC-LR at nanomolar concentrations stimulated cell proliferation by activating the ERK1/2 signaling pathway in the kidney-derived Vero-E6 cell line; differently, MC-LR at micromolar concentrations induced autophagy, apoptosis and necrosis in a dose and time-dependent manner [124-126], suggesting the non-monotonic effects of MC-LR on cell survival. MC-LR has been reported to induce apoptosis in various types of cells, which is characterized by cytoplasmic shrinkage, cell membrane blebbing, and chromatin condensation [29, 121, 127-129]. By analyzing both transcriptomic and proteomic data, Chen *et al.* reported that 50 µg/kg MC-LR induced apoptosis primarily through the BID-BAX-BCL2 pathway in mouse liver; however, exposure to high dose of MC-LR at 70 µg/kg resulted in apoptosis via the ROS-dependent pathway [130]. These results indicate that different exposure doses can mediate different molecular changes resulting in differential cytotoxicities. In addition, multiple apoptotic pathways are identified using different models, such as mitochondria-mediated apoptosis in human bronchial epithelial cells and rat Sertoli cells [29, 127], NF-κB/iNOS pathway in rat insulinoma (INS-1) cells [131], *etc*.

Autophagy is an intracellular degradation system and functions to deliver cytoplasmic components to the lysosome for degradation/recycling essential cellular components, so it is identified as a cell survival mechanism. Autophagy also plays highly context-specific roles in mediating cell death which is termed autophagy-dependent cell

death [132]. So far, exposure to MC-LR has been found to induce autophagy in different cells accompanied with apoptosis [133-135]. The co-treatment of an autophagy inhibitor 3-methyladenine (3-MA) could inhibit MC-LR-induced autophagy and apoptosis in cultured Sertoli cells, indicating that autophagy contributed to the MC-LR induced cell apoptosis [135]. Inconsistently, the co-treatment of 3-MA and MC-LR increased apoptosis in Chinese hamster ovary (CHO) cells, suggesting that autophagy plays a protective role in MC-LR-induced apoptosis [136]. These inconsistent results may be caused by the use of different cell lines and/or exposure concentrations and times. More studies are required to decipher the role of autophagy in the MC-LR-induced cytotoxicity. Besides the above widely studied cell death routes, necrosis is also found to be related to MC-LR-induced liver injury [137].

Overall, it seems that many different genes, proteins, and organelles are involved in the cellular responses to MC-LR exposure. In future studies, we should take advantage of Multi-Omic strategies and focus on investigating the relationship of identified different mechanisms and their specific roles in the MC-LR-induced toxicity. These proposed mechanisms will shed light on the investigation of female reproductive toxicity of MC-LR.

### 2.3 OVARIAN TOXIC EFFECTS OF MC-LR AND POSSIBLE MECHANISMS INVOLVED

As the female gonad, the ovary contains various stages of follicles as its functional unit. Each follicle consists of a central oocyte, the female germ cell, and surrounding somatic follicular cell layers. Primordial follicles are at the earliest stage and remain dormant from months to decades to establish the ovarian reserve which determines a woman's reproductive life span and menopausal transition. Primordial follicles,

particularly after puberty onset, are activated in a wave of cohorts to become primary follicles which further grow to the secondary, antral, and preovulatory staged follicles to reach maturation. The early phase of follicle activation and development (from the primordial to the secondary stage) is gonadotropin independent; in contrast, the late phase of follicle maturation (from the early antral to the preovulatory stage) is primarily driven by follicle-stimulating hormone (FSH) from the anterior pituitary. At the midpoint of each menstrual cycle, in response to a surge of luteinizing hormone (LH) from the anterior pituitary, a fully grown preovulatory follicle ruptures and ovulates a fertilizable egg at the metaphase II of meiosis. The remaining somatic follicular cells collapse and form a corpus luteum (CL) that can synthesize and secrete progesterone to support the uterine endometrium to become receptive for embryo implantation.

MC-LR has been shown to accumulate in the ovary, including granulosa cells, in mice that received intraperitoneal injection of MC-LR [134, 138]. Using *in vitro* mouse primary granulosa cell culture and immortalized murine granulosa cell (KK-1) models, western blotting and immunofluorescence results suggest that MC-LR can transport into granulosa cells which may be regulated by OATPs [134, 138, 139]. However, due to the positive expression of multiple Oatp genes, such as *Oatp1a4*, *Oatp1a5*, *Oatp2a1*, *Oatp2b1*, *Oatp3a1*, and *Oatp5a1* [138], it is challenging to conclude which specific Oatp isoform(s) regulate the uptake of MC-LR in ovarian cells. Previous studies have shown the adverse effects of MC-LR on follicle development. In an *in vivo* mouse model with 5-week-old BALB/c female mice intraperitoneally injected with 20  $\mu\text{g}/\text{kg}$  MC-LR daily for 28 days, there were significantly fewer primordial follicles than the control group; however, MC-LR did not alter the number of growing follicles, suggesting that exposure to MC-LR might

affect primordial follicles only [140]. However, another study found that when 5-week-old female BALB/c mice were treated with MC-LR at 40 µg/L via drinking water for 6 months, the numbers of both primordial and growing follicles were significantly reduced [139]. The inconsistent results from these two studies indicate that the effects of MC-LR on various stages of follicles may depend on the exposure route, dose, and/or treatment time. Using an *in vitro* 3D follicle culture model, our group treated immature mouse secondary follicles with MC-LR at 0, 0.1, 1, and 10 µM for 8 days and examined the effects of MC-LR on follicle survival, follicle growth, and secretion of estradiol [36]. Results revealed that MC-LR did not affect the follicle survival and estradiol secretion. Moreover, follicles treated with vehicle or MC-LR at 0, 0.1 had comparable size and were able to develop from the secondary to the antral stage. However, 10 µM MC-LR significantly inhibited the follicle development on day 8, indicating that MC-LR might directly affect follicle growth.

The ovarian impacts of MC-LR have also been evaluated using other animal models such as zebrafish and porcine. Unlike mammalian follicles, all staged follicles in zebrafish contain an oocyte surrounded by a single layer of granulosa cells and an outer layer of theca cells [141]. The developmental stages of zebrafish follicles are usually characterized based on the cellular structure of oocytes [141]. Thus, the ovarian toxic effects of MC-LR in zebrafish are investigated by examining the development of different stages of oocytes. In zebrafish treated with MC-LR at 1, 5, and 20 µg/L, there were significantly more pre-vitellogenic oocytes and fewer post-vitellogenic oocytes, indicating that MC-LR may affect oogenesis by inhibiting the growth and maturation of pre-vitellogenic oocytes in zebrafish [142]. MC-LR has also been shown to affect the quality of oocytes by inducing the oocyte vacuolation and nuclear pyknosis as well by disrupting the connection between

and oocyte and the outer layered granulosa and theca cells in zebrafish [143]. The disrupted connection of follicular oocyte and somatic cell layers has also been observed in medaka fish treated with 5 µg/L MC-LR, which might be caused by the loss of contact between the microvillousities of oocyte membranes and follicular cell layer [144]. Exposure to MC-LR has also been shown to affect zebrafish oocyte meiosis *in vivo* and *in vitro*. When zebrafish were exposed to 20 µg/L MC-LR, the GVBD rate of oocytes was significantly increased accompanied by the activation of ERK signaling pathway [143]. Consistently, MC-LR also induced a significant increase of GVBD rate in zebrafish oocytes exposed to 100 µg/L MC-LR *in vitro*, which can be mitigated by the co-treatment of ERK inhibitor U0126 or p38 inhibitor SB203580, suggesting the critical role of MAPK signaling in this process [145]. In another *in vitro* porcine COCs culture model, the cumulus oocyte complexes (COCs) expansion was inhibited and the rate of first polar body extrusion was decreased in a concentration-dependent manner after porcine COCs were cultured with MC-LR at 20, 40, 80, and 120 µM for 44 hours; in addition, exposure to MC-LR also disrupted the spindle morphology and actin distribution in porcine oocytes and the levels of acetylation of  $\alpha$ -tubulin and histone methylation were significantly decreased in MC-LR-treated oocytes. These results indicate that MC-LR-induced oocyte maturation failure might result from the impairment of epigenetic modifications [120].

The ovarian toxic effects of MC-LR have been related to multiple mechanisms, including oxidative stress, ER stress, and autophagy. The malondialdehyde (MDA) contents and the enzymatic activities of antioxidants enzymes such as catalase (CAT), superoxide dismutase (SOD), and glutathione peroxidase (GPx) were significantly increased in the ovary of female zebrafish intraperitoneally injected with MC-LR at 200

$\mu\text{g}/\text{kg}$ , indicating that MC-LR can induce oxidative stress in the ovary [146]. It seems that the ovary can rapidly respond to the oxidative stress through various antioxidant enzymes. In addition, the GSH content was remarkably reduced in the MC-LR-treated ovaries [146]. However, whether the reduction of GSH contributes to the occurrence of oxidative stress in the ovary is still not clear. In an *in vivo* mouse model, exposure to 25 or 40  $\mu\text{g}/\text{kg}$  MC-LR via daily intraperitoneal injection for 14 days induced the production of oxidative products (ROS and MDA) and reduced the activities of antioxidant enzymes (SOD and GSH) in the mouse ovary, suggesting that the roles of oxidative stress in MC-LR induced ovarian toxicities [134]. Oxidative stress has also been observed in cultured immortalized murine ovarian granulosa cells (KK-1 cells), evidenced by the increased production of ROS, decreased antioxidant capacity (SOD and GSH) after the administration of MC-LR at 8.5, 17, or 34  $\mu\text{g}/\text{mL}$  for 24 h [134]. In addition, when primary mouse granulosa cells were exposed to 5 or 20  $\mu\text{M}$  MC-LR for 48 h, the lipid peroxidation was significantly increased and the activity of CAT and SOD was significantly reduced [139]. Using the KK-1 cells, the MC-LR-induced oxidative stress has also been found to dose-dependently promote the expression of apoptotic signal-regulated kinase 1 (ASK1) at both transcriptional and translational levels; the increased ASK1 further activated p38/JNK signaling pathways to induce the alteration of mitochondrial membrane potential and apoptosis [138]. The critical role of ASK1 can be demonstrated by the results that the co-treatment of ASK1 inhibitor NQDI-1 significantly ameliorated MC-LR induced granulosa cell apoptosis *in vivo* [138]. In addition to granulosa cells, exposure to MC-LR also promoted the ROS production in porcine oocytes, which consequently resulted in mitochondrial dysfunction and disrupted oocyte maturation [120, 147].

Recent studies also suggest that exposure to MC-LR can induce ER stress in ovarian granulosa cells. For example, exposure to MC-LR increased the expression of ER stress-related proteins (CHOP, GRP78, P-EIF2 $\alpha$ , and P-PERK) in both *in vitro* cultured immortalized murine granulosa cells and *in vivo* mouse ovaries [134]. Following studies showed that the MC-LR induced ER stress increased the expression of DNA damage inducible transcript 3 (Ddit3) which further promoted the activation of caspase-3 through regulating the expression of Bcl-2 and Dr5 in the KK-1 cells [148]. Similarly, the expression of ER stress related proteins (GRP78, ATF-6, PERK, IRE1, and CHOP) was enhanced in the MC-LR-treated Chinese hamster ovary (CHO) cells in a concentration-dependent manner, and ER stress inhibitor-4-PBA pretreatment could inhibit the MC-LR induce apoptosis and autophagy [136].

Autophagy is another possible mechanism contributing to MC-LR-induced ovarian toxicity. In both *in vitro* and *in vivo* models, exposure to MC-LR has been found to significantly increase the expression of autophagy marker proteins (BECN1, ATG5, ATG12, and LC3-II/LC3-I) in murine granulosa cells, indicating that MC-LR induces autophagy in granulosa cells [134]. MC-LR also induced autophagy in CHO cells, and autophagy inhibitor 3-MA promoted MC-LR-induced apoptosis [136]. Mechanistically, the MC-LR induced autophagy in KK-1 cells depends on the IRE1 and CaMKK $\beta$  signaling pathways, because the knockdown of IRE1 and CaMKK $\beta$  prevented MC-LR-induced ovarian cell autophagy and necrosis of granulosa cells and oocytes [149].

Cytoskeleton destruction is another possible cytotoxic mechanism induced by MC-LR. Exposure to MC-LR has been found to induce the degradation of microfilament mesh, disappearance of stress fibers, and alteration of microtubular structure in the epithelial-like

CHO cells [150]. MC-LR also affected the meiotic maturation of porcine oocytes by disrupting the cytoskeleton dynamics, spindle assembly and homologous chromosome segregation [120, 147]. Collectively, these results suggest that multiple mechanisms are involved in MC-LR-induced ovarian toxicity, but the interactions between these discovered mechanisms remains unknown; moreover, the activation of distinct response pathways may also be controlled by different exposure doses or time.

Our unpublished results have demonstrated that exposure to environmentally-relevant MC-LR compromised follicle ovulation by disrupting the maturation of growing follicles. Overall, previously published results suggest that MC-LR may have adversely effects on ovarian reserve, follicle development, and oocyte maturation. However, further investigations are required to determine the effects of MC-LR on different ovarian activities, such as primordial follicle formation, follicle activation, follicle development, ovulation, and corpus luteum (CL) formation. Additionally, more in-depth mechanistic studies should be performed to elaborate the toxic mechanisms of MC-LR on the ovary.

## 2.4 EFFECTS OF MC-LR ON FERTILIZATION, EMBRYO DEVELOPMENT, AND IMPLANTATION

A successful pregnancy requires a complex process with multiple stages, including fertilization, embryo development, and implantation. After ovulation, the released egg can be fertilized by a sperm in the fallopian tube. The fertilized egg or zygote begins to move toward the uterus while developing to the blastocyst stage. Next, the blastocyst implants into the endometrium of uterus and the subsequently formed placenta that support the development of embryo and fetus. MC-LR has been reported to pose a threat to fertilization

and the health of embryo and placenta. In female zebrafish exposed to 50 µg/L MC-LR for 21 days, the rates of fertilization and hatching were significantly reduced [151]. After female medaka fish were fed with 3.93 µg MC-LR/g dry diet, the survival rate of embryos was significantly decreased [152]. Moreover, to investigate the direct effect of MC-LR on embryo, MC-LR was directly introduced into medaka fish embryos using a microinjection method; MC-LR treatment caused a lower survival rate and a higher earlier hatching rate [153]. When zebrafish embryos were exposed to MC-LR at 5 or 50 µg/L from blastula stage to the end of embryonic development, the larval survival rate was significantly decreased and larval growth was retarded [154]. These results indicate that exposure to MC-LR can disrupt fertilization success and also affect embryo development. However, whether the same effects exist in mammals, including humans, is still largely unknown. The placenta, which connects the maternal and fetal blood, is instrumental for fetal development. When pregnant mice were intraperitoneally injected with MC-LR at 5 or 20 µg/kg from gestational day 13 to day 17, the growth of the fetus and placenta were compromised which was primarily caused by the apoptosis in the placental labyrinthine region induced by the MC-LR-mediated oxidative stress and ER stress [155]. Another study showed that paternal exposure to MC-LR impaired placental angiogenesis and induced fetal growth restriction in mice [156]. Taken together, these results suggest potential impacts of MC-LR on the development of embryo and placenta. The mechanism by which MC-LR damages the development of the embryo and placenta should be further investigated, and the potential risk for human pregnancy should be considered in the future.

## 2.5 THE OVERALL EFFECTS OF MC-LR ON FEMALE REPRODUCTION

Female reproduction is coordinately regulated by the interactions among steroid hormones along the hypothalamic-pituitary-gonadal (HPG) axis. The HPG axis functions to coordinate reproductive events in relation to body condition and environment. Normal ovarian steroidogenesis is not only essential for the maintenance of the reproductive cycle and fertility, but also links to the health of the cardiovascular, brain, and skeletal systems [157-159]. Exposure to MC-LR can affect female reproduction by disrupting the balance of sex hormones and altering the expression of steroidogenesis genes in the HPG axis. Upon the chronic exposure of MC-LR at 5 µg/L to for 30 days, female medaka fish had fewer numbers of spawned eggs [144]. Similar outcomes have also been observed in zebrafish [151, 160, 161]. To investigate the mechanisms of MC-LR-induced defective female reproduction, hormone secretion and the expression of steroidogenesis-related genes have been examined in zebrafish. After adult female zebrafish were exposed to 1, 5, and 20 µg/L MC-LR for 30 days, the serum concentrations of 17β-estradiol (E2), testosterone (T), and follicle-stimulating hormone (FSH) were significantly increased in all MC-LR treatment groups, and the concentrations of luteinizing hormone (LH) were significantly increased in the sera of fish treated with 20 µg/L MC-LR [142]. Furthermore, exposure to MC-LR altered the expression of steroidogenesis-related genes in different organs of the HPG axis, including the hypothalamus (*Gnrh2* and *Gnrh3*), pituitary (*Gnrhr1*, *Gnrhr3*, and *Gnrhr4*), and ovary (*Fshr*, *Lhr*, *Star*, *3β-Hsd*, *17β-Hsd*, and *Cyp19a1*) [142]. Consistently, another research group treated female zebrafish with MC-LR at 0, 1, and 50 µg/L for 21 days, and it was found that MC-LR dramatically increased the concentrations of plasma E2, T, and vitellogenin [151]. Moreover, MC-LR altered the expression of

steroidogenesis-related genes in the brain (*Gnrh2*, *Gnrh3*, *Cyp19b*, and *Erβ*), and ovary (*Fshr*, *Lhr*, *Star*, *Cyp19a*, and *3β-Hsd*) [151]. Interestingly, the toxic effects of MC-LR in adult female zebrafish on abovementioned reproductive parameters, plasma hormone levels, and transcriptional level of HPG axis related genes were reversible by introducing a recovery period with transferring fish to MC-LR-free water for another 21 days [151]. Exposure to different doses of MC-LR may induce differential endocrine disrupting effects. For instance, 10 µg/L MC-LR increased the concentrations of E2 and vitellogenin (VTG); however, 50 µg/L MC-LR decreased the concentrations of E2 and VTG in female zebrafish [161]. In addition, when zebrafish were exposed to MC-LR at 3 and 30 µg/L for a life cycle (90 days), MC-LR did not alter the E2 levels but significantly decreased the T level [162].

In addition to aquatic animals, rodents have also been used to examine the reproductive toxic effects of MC-LR. When 5-week-old BALB/c female mice were intraperitoneally injected with 20 µg/kg MC-LR daily for a consecutive 28 days, estrous cyclicity was disrupted with decreased duration of proestrus and estrus [140]. The dysregulated estrous cyclicity with shortening estrus and prolonged diestrus were also found in mice treated with long-term (3 or 6 months) treatment of 40 µg/L MC-LR via drinking water; moreover, this chronic MC-LR exposure increased the serum concentration of progesterone (P4), but decreased the concentration of E2 [139]. Inconsistently, decreased serum concentrations of P4 were observed in mice treated with 5 and 20 µg/kg MC-LR via intraperitoneal injection for 4 weeks [140]. The inconsistency results may be caused by different exposure routes, doses, and times of exposure. In addition, exposure to MC-LR could promote the secretion of P4 in cultured primary granulosa cells by

upregulating the expression of *Star*, a key gene in regulation of hormone synthesis, via the inhibition of the expression of miR-3473g, suggesting that MC-LR may cause the premature luteinization of granulosa cells [163]. When 10 or 40 µg/L MC-LR-treated female mice were mated to non-treated males, the stillbirth rate was increased and the number of live pups per litter was reduced, indicating that exposure to MC-LR can result in subfertility in mice [139]. The overall toxic effects of MC-LR on female reproduction were also examined using the SD rat model. Female SD rats at 7-8-week old were intraperitoneally injected with 0, 36.5, 54.75, and 73 µg/kg bw MC-LR for 24 hours, and hormone secretion and the expression of genes related to HPG axis were examined [164]. Results demonstrated that exposure to MC-LR significantly decreased the concentration of GnRH, but significantly increased the concentrations of FSH and LH [164]. Moreover, it seems that different doses of MC-LR differentially affect the secretion of T and E2. Specifically, the treatment of MC-LR at 73 µg/kg increased the serum concentration of T; however, MC-LR at 36.5 and 54.75 µg/kg decreased the serum concentration of E2 [164]. Besides, acute exposure to MC-LR also altered the expression of hormone synthesis-associated genes in the hypothalamus (*Kiss1*, *Gpr54*, *Gnrh1*, *Era*, and *Erβ*), pituitary (*Gnrhr*, *Era*, and *Erβ*), and ovary (*Lhr*, *Era*, *Erβ*, *Star*, *Cyp11a1*, *3β-Hsd*, *Cyp17a1*, *17β-Hsd*, and *Cyp19a1*) [164]. These results suggest that MC-LR exerts endocrine-disrupting effects through affecting the HPG axis. Using an *in vitro* luciferase-based reporter gene system in human cell line MELN, it is found that MC-LR may act as an endocrine disruptor at concentrations lower than that in natural environments; moreover, the authors proposed that the MC-LR-induced hyperphosphorylation may mediate its estrogenic effects [165].

In summary, these published data suggest that MC-LR is a potential environmental endocrine-disrupting chemical (EDC). However, there is limited evidence regarding the effects of MC-LR on the HPG axis, hormone secretion, and fertility and inconsistent results exist. To achieve a better understanding of MC-LR action, more investigations should be performed using different models including *in vivo* animal models and *in vitro* cell/organoid culture models. More importantly, human health-based studies are necessary in the future to understand the effects of MC-LR on humans, such as epidemiological studies and *in vitro* human cell/tissue exposure.

## 2.6 TRANSGENERATIONAL EFFECTS OF MC-LR

Oocytes in the growing fetal ovary are vulnerable to prenatal exposures, so the modifications in fetal gonadal development can heighten the risk of transgenerational defects [166]. As MC-LR can accumulate in the ovary, it may transfer the toxicity to the offspring. After adult zebrafish were exposed to MC-LR for 60 days, MC-LR was detected in both F0 gonads and F1 embryos, indicating the direct transport of MC-LR from the F0 to the F1 [167]. After maternal zebrafish were exposed to 5 or 20 µg/L MC-LR for 30 days, the F1 generation were found to hatch prematurely compared to the control group; meanwhile, gestational exposure to MC-LR increased the mortality and deformity rate in the F1 offspring [143]. To further investigate the effect of maternal exposure to MC-LR on the next generation at the molecular level, adult female zebrafish were exposed to 5 or 20 µg/L MC-LR for 30 days and then mated with non-treated male zebrafish in MC-LR-free environment; results showed that MC-LR-exposed zebrafish-generated F1 zebrafish had dramatically elevated ROS levels and altered the transcriptional expression of ER stress

and apoptosis related genes [168]. When pregnant SD rats were exposed to MC-LR at 10 µg/kg BW/day from gestational day 8 to postnatal day 15, neurotoxicity was found in the rat offspring and proteomic analysis revealed that MC-LR remarkably altered the expression of proteins involved in neurodevelopment, oxidative phosphorylation, and metabolism [169]. Collectively, these studies indicate that exposure to MC-LR can result in intergenerational toxicities in F1; however, there are few studies focused on the transgenerational toxicities of MC-LR.

## 2.7 REPRODUCTIVE TOXIC EFFECTS OF ENVIRONMENTAL MIXTURES INCLUDING MC-LR AND OTHER CONTAMINANTS

Human are exposed to chemical mixtures in daily life. Toxicants of co-exposure can interact to induce additive, synergistic, or antagonistic responses. The potential combined toxic effects of MC-LR and other contaminants are big issues. Several studies have investigated the reproductive toxic effects of mixtures of MC-LR and other environmental toxins [170-173]. Nanomaterials have been widely used in our daily life. Nanoparticles, a new category of contaminants of emerging concern (CECs), have a high capability of absorbing environmental toxicants including MCs due to their large specific surface area [174]. It has been found that the co-treatment of nanoparticle TiO<sub>2</sub> (n-TiO<sub>2</sub>) and MC-LR increased the accumulation of MC-LR in the ovaries of zebrafish, which reduced the egg production and E2 secretion in a higher degree compared to MC-LR treatment only [175]. In Chinese hamster ovary (CHO-K1) cells, the co-treatment of MC-LR and 3-chloro-4-dichloromethyl-5-hydroxy-2(5H)-furanone (MX), a common drinking water disinfection byproduct, significantly increased the genotoxicity of MX by inducing

the oxidative stress-related mechanism [176]. Moreover, the mixture of MC-LR and nitrite has also been found to synergistically induce reproductive dysfunctions by interfering with the HPG axis in male zebrafish [177]. While there are limited studies regarding how MC-LR mechanistically interacts with those chemicals, these results suggest that the co-exposure may alter the reproductive toxicities of MC-LR.

## 2.8 CONCLUSIONS AND FUTURE PERSPECTIVES

As we summarized in this review article, MC-LR is an emerging reproductive toxin which can disrupt female reproduction at different levels in the HPG axis. However, there is limited evidence regarding the effects of MC-LR on human reproduction. Thus, epidemiological studies are required to understand the potential reproductive toxic effects of MC-LR exposure in humans. Exposure to HAB toxins, including MC-LR, can be exacerbated by various demographic factors such as geography, race/ethnicity, age, sex, and occupation. Understanding the impacts of these factors on MC-LR exposure is crucial for identifying the racial, ethnic, or underrepresented groups that may be at a higher risk of experiencing the adverse health impacts of MC-LR exposure. Thus far, limited studies of reproductive toxicity of MC-LR have been published by a few groups in the world. So, more investigations of the effects and mechanisms of MC-LR-induced female reproductive toxicity should be performed using different *in vitro* and *in vivo* models. Most importantly, the relationship of different MC-LR-interfered signaling pathways and cellular functions should be clarified. More and more results highlight the inter- or transgenerational effects of MC-LR, so the effects of MC-LR exposure on the next generations are required to be understood. Furthermore, the interaction of the ovary and other organs during MC-LR

exposure is worth to be studied. While MC-LR is considered the most common and toxic MC, the presence of other MCs and cyanotoxins should not be overlooked. The effects of MC-LR and other environmental toxicants mixtures on female reproduction should be considered.

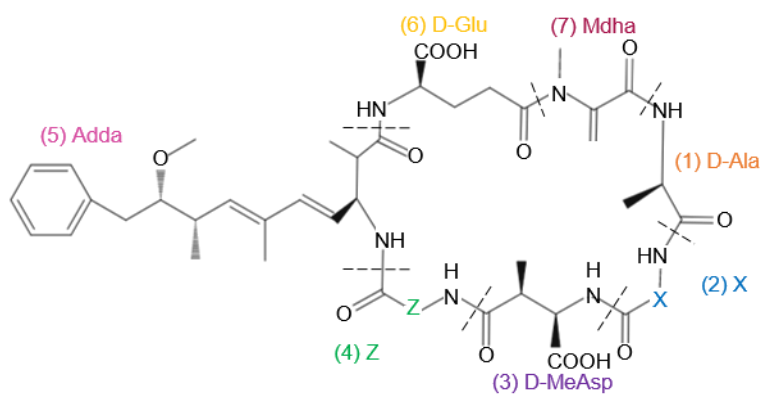


Figure 2.1 The general cyclic structure of microcystins. It contains the following 7 amino acids: (1) D- Alanine (D-Ala); (2) Variable L-amino acid (X); (3) D-erythro- $\beta$ -methyl-aspartic acid (D-MeAsp); (4) Variable L-amino acid (Z); (5) (2S,3S,8S,9S)-3-amino-9-methoxy-2,6,8-trimethyl-10-phenyldeca-4,6-dienoic acid (Adda); (6) D-Glutamic acid (D-Glu); (7) N-methyldehydroalanine (Mdha).

CHAPTER 3

HUMAN-RELEVANT EXPOSURE TO HARMFUL ALGAL BLOOM  
TOXIN MICROCYSTIN-LR DISRUPTS THE PP1-MEDIATED  
PI3K/AKT/FOXO1 SIGNALING IN FOLLICULAR GRANULOSA  
CELLS TO COMPROMISE FEMALE OVARIAN FOLLICLE  
MATURATION AND OVULATION

---

Yingzheng Wang, Pawat Pattarawat, Jiyang Zhang, Lei Liu, Eunchong Kim, Delong Zhang, Ji-Yong Julie Kim, Saurabh Chatterjee, Geoffrey I. Scott, Qiang Zhang, and Shuo Xiao. Human-relevant exposure to harmful algal bloom toxin microcystin-LR disrupts the PP1-mediated PI3K/AKT/FOXO1 signaling in follicular granulosa cells to compromise female ovarian follicle maturation and ovulation. (In preparation)

## Abstract

Harmful algal blooms (HABs) have become a global emerging environmental concern and microcystin-LR (MC-LR) is the most common and hazardous type of HAB toxin; however, its impact on women's reproductive health is poorly understood. Using both a chronic oral exposure mouse model and a short-term superovulation model, we found that human-relevant exposure to MC-LR could compromise follicle ovulation via affecting follicle maturation. Both *in vivo* mouse exposure model and *in vitro* 3D follicle culture model revealed that exposure to MC-LR did not affect follicle development, but significantly reduced the expression of some follicle maturation-related genes, such as *Lhcgr* and *Pappa*. Mechanistic studies demonstrated that MC-LR could inhibit the protein phosphatase 1 (PP1) and further block the activation of PI3K/AKT/FOXO1 signaling pathway. In addition, OATP inhibitor Ritonavir could inhibit the accumulation of MC-LR in the follicles and rescue the MC-LR-disrupted follicle ovulation. Taken together, our results demonstrate that human-relevant exposure to MC-LR compromises ovulation via disrupting follicle maturation by inhibiting PP1/PI3K/AKT/FOXO1 signaling pathway in the granulosa cells.

Keywords: harmful algal bloom, microcystin, protein phosphatase 1, follicle maturation, ovulation

### 3.1 INTRODUCTION

Harmful algal blooms (HABs) are the rapid growth of algae in marine and freshwater ecosystems that produce toxins to cause adverse health effects in humans and wildlife animals [2, 178]. Each decade, HABs increase globally in both severity and frequency, primarily due to the rising water temperatures from climate change and the anthropogenic eutrophication from agricultural runoff and urbanization [179-181]. Produced by cyanobacteria, which are also termed blue-green algae, microcystins (MCs) are the most common and toxic type of HAB toxins [3, 182]. MCs are a family of cyclic heptapeptides with a general structure of cyclo-(D-Ala<sup>1</sup>-X<sup>2</sup>-D-MeAsp<sup>3</sup>-Z<sup>4</sup>-Adda<sup>5</sup>-D-Glu<sup>6</sup>-Mdha<sup>7</sup>), with two variable L-amino acids at positions X<sup>2</sup> and Z<sup>4</sup>, generating nearly 280 different MC congeners [9, 183]. With leucine (L) and arginine (R) occupying the X<sup>2</sup> and Z<sup>4</sup> positions, respectively, MC-LR is the most potent and well-characterized MC congener. MCs persist in the environment due to their high physiochemical stability [184, 185]. Humans are primarily exposed to MCs via drinking water, food, algae dietary supplements and recreational activities in polluted waterbodies (e.g. swimming, fishing) [11, 12, 186]. In addition, humans can be exposed to high levels of MCs through contaminated medical solutions, such as the dialysis fluid during hemodialysis [13, 187].

MC-LR has been shown to be hepatotoxic, neurotoxic, and carcinogenic [89, 188, 189], with the possible toxic mechanisms related to the inhibition of protein phosphatases, induction of oxidative stress, and cytoskeleton disruption [23, 24]. MC-LR selectively inhibits the phosphatase activities of serine/threonine protein phosphatase 1 or 2A (PP1 or PP2A) [93, 190]. By interacting with the catalytic subunits of PP1 or PP2A through irreversible covalent linkage, MC-LR induces a structural rearrangement of these

phosphatases and inactivates their dephosphorylation functions [93]. The inhibition of PP1 and/or PP2A can cause an imbalance in the phosphorylation status of their protein substrates, such as kinases [101], cell cycle regulators [191], and ribonucleoproteins [192], and their disruption can cause oxidative stress, DNA damage, apoptosis, or tumorigenesis, *etc.* [88, 193].

Increasing evidence reveals that MC-LR also exhibits endocrine disrupting effects which may result in endocrine, reproductive, and developmental toxicities [194-198]. With respect to the ovary, the female gonad, MC-LR has been shown to reduce the numbers of primordial or growing follicles in mice, depending on the exposure route, dose, and treatment window [139, 140]. In non-mammalian species, such as zebrafish and medaka fish, exposure to MC-LR disrupts oocyte maturation and meiosis [142, 143, 145], as well as the inter-connections between oocyte and surrounding granulosa cells [143, 144]. While the observed ovarian toxicities of MC-LR have been associated with the induction of oxidative stress [134, 138, 139, 146], endoplasmic reticulum (ER) stress [134, 136, 148], cytoskeleton destruction [120, 147, 150], and autophagy [134, 136, 149], the underlying mechanisms remain poorly understood. So far, there are limited human health-based studies regarding the female reproductive toxic effects of MC-LR. However, as HABs become more prevalent and HAB toxins are not routinely monitored due to the absence of federal/state regulatory standards, there is an urgent need to determine the extent of ovarian toxicities of MCs to females and also the molecular mechanisms involved.

The ovary is a dynamic female reproductive organ housing various stages of follicles as the functional unit. The earliest staged primordial follicles are activated to develop into the primary, secondary, and antral follicles for maturation and ovulation till

menopause. The early phase of follicle development, from the primordial to the secondary stage, is largely gonadotropin-independent [199-202]. In contrast, the progression from the early antral to the antral stage requires follicle-stimulating hormone (FSH) to support follicle maturation [203]. Central to FSH-dependent follicle maturation is the activation of the cAMP/PKA/CREB and IGF/PI3K/AKT/FOXO1 signaling pathways and their cross-talk in the granulosa cells of early antral follicles [204, 205]. FSH activates protein kinase A (PKA) which in turn stimulates PP1; the activated PP1 promotes the dephosphorylation of inhibitory serine residues within insulin receptor substrate 1 (IRS1), permitting the activation of insulin-like growth factor (IGF)-dependent PI3K/AKT/FOXO1 signaling [206, 207]. Together, these two pathways up-regulate a suite of genes critical for estrogen secretion and follicle maturation.

As the selective inhibition of PP1 is one of the molecular initiating events (MIE) of MC-LR [93, 190], and PP1 critically regulates FSH-dependent follicle maturation, we hypothesize that MC-LR may inhibit PP1 in the follicular granulosa cells to disrupt follicle maturation and associated reproductive outcomes. To test this hypothesis, we use an *in vivo* mouse model, and a 3D *in vitro* mouse ovarian follicle culture model to investigate the ovarian toxic effects and mechanisms of MC-LR. Our results demonstrate that MC-LR at human-relevant exposure levels disrupts PP1-mediated activation of PI3K/AKT/FOXO1 signaling in follicular granulosa cells, which compromises FSH-dependent follicle maturation and results in defective ovulation, luteinization, and progesterone secretion. These ovarian disorders in response to MC-LR exposure may heighten a woman's risks of irregular menstrual cycle, anovulation, infertility, and reproductive diseases such as the polycystic ovarian syndrome (PCOS).

## 3.2 MATERIALS AND METHODS

### **Animals**

All animal procedures in this study were performed according to the NIH Guideline for the Care and Use of Laboratory Animals and the approved Institutional Animal Care and Use Committee (IACUC) animal protocol at Rutgers University. The CD-1 mouse breeding colony (Envigo, Indianapolis, IN) was housed in a temperature- and humidity-controlled animal facility at Rutgers with a 12-hour light/dark cycle and provided with food and water *ad libitum*. Female mice were checked daily for the birth of pups to ensure accuracy of the date of birth recorded. Both male and female pups were weaned on postnatal day (PND) 20 and females were housed in groups of 3-5 mice per cage.

### **Chronic low-dose oral exposure to MC-LR *in vivo***

As humans are primarily exposed to HAB toxins, including MC-LR, through oral ingestion of contaminated drinking water, food, algae dietary supplements, or through recreational activities in contaminated marine or lake waters, we chose the oral gavage ingestion method to mimic exposure to MC-LR in humans. The exposure dose of MC-LR was calculated based on a previously published real-world estimated daily intake (EDI) of MC-LR at 25.68 ng/kg/day from drinking water and aquatic foods among residents who lived in the township of Lidu and Yihe in Southwest China; these two townships are located in a joint area of the Yangtze River and the Wu River that provide drinking water and aquatic food resource but had various degrees of HAB contamination [208, 209]. Other indexes used for the exposure dose calculation include the average mouse body weight (BW<sub>m</sub>) at 20 g, the correction factor between mouse and human (K<sub>m</sub>) at 12.3, and the uncertainty factor (UF) of 1000 for the interspecies difference. The ultimate exposure dose

in mice was calculated based on the equation: mouse equivalent dose (MED) = EDI x BW<sub>m</sub> x Km x UF, which generated the exposure dose value of 9.48 µg/kg. Indeed, the World Health Organization (WHO) and US EPA established the Provisional Guideline Value of 1 and 1.6 µg/L of MC-LR in drinking water, respectively, which are equivalent to the Tolerable Daily Intake (TDI) of MC-LR at 100 ng/kg body weight for a young adult woman [210, 211], indicating that the EDI at 25.68 ng/kg we used for calculating the MED is human relevant. Taken together, an oral exposure dose of 10 µg/kg was used in mice to recapitulate the environmentally-relevant exposure level of MC-LR in humans. Specifically, CD-1 female mice at 4-week-old (n = 5 per group) were treated with 1 x phosphate buffered saline (PBS) or MC-LR (Cayman Chemicals, Ann Arbor, MI) at 10 µg/kg body weight via oral gavage daily for six weeks. During vehicle and MC-LR treatment, a daily oral gavage of 100 µL 1xPBS or MC-LR solution was performed by using a straight 20-gauge stainless steel animal feeding needle with a 2-mm ball (Pet Surgical, Sherman Oaks, CA). The mouse body weights were measured and recorded daily before the vehicle or MC-LR administration.

### **Estrous cyclicity examination**

In the last 2-week treatment window, the estrous cycle of vehicle or MC-LR treated mice was determined daily using the method of vaginal smear [212]. The vaginal cells were flushed by introducing 80 µL 1xPBS through multiple pipetting, and the stage of estrous cycle was determined by the microscopic examination of vaginal cell cytology and the proportion of leukocytes, cornified epithelial, and nucleated epithelial cells.

### **Ovarian histology and counting of follicles and corpus luteum (CL)**

The harvested ovaries at the end of 6-week treatment were fixed in Shandon™ Formal-Fixx™ 10% Neutral Buffered Formalin solution (ThermoFisher Scientific, Waltham, MA), embedded in paraffin, and serially sectioned at 5 µm with a RM2165 microtome (Leica Microsystems, Nussloch, Germany). The ovarian histology and counting of follicles and CL were performed as we previously described [51]. Briefly, every 5<sup>th</sup> ovarian section throughout each entire ovary was stained with hematoxylin and eosin (H&E, ThermoFisher Scientific), and the counting of follicles and CL was performed blindly. Primordial follicle was defined as a central oocyte surrounded by single layer of squamous pre-granulosa cells. Primary follicle was characterized as an oocyte surrounded by one layer of cuboidal granulosa cells. Secondary follicle was defined as an oocyte surrounded by two or more layers of cuboidal granulosa cells with no visible antrum. Antral follicle was identified as an oocyte surrounded by five or more layers of granulosa cells with no visible antrum or a clearly defined antral space. Moreover, preovulatory follicles were defined as type 7 and 8 follicles, according to the classification of Pedersen and Peters [213]. Atretic follicles were defined by the appearance of more than 10% of pyknotic granulosa cells surrounding with or without degenerated oocytes. CL was characterized by hypertrophic luteal cells and highly vascularized structure. To avoid repeated counting of CL, when a CL was present for the first time in an ovarian section, it was marked and tracked in the following sections until it disappeared. This procedure was repeated for each CL and the total number of CL in each ovary was recorded.

### **Mouse superovulation, acute MC-LR exposure, and oocyte collection**

An *in vivo* mouse superovulation model was used to investigate the ovarian toxic mechanisms of MC-LR on gonadotropin-dependent follicle maturation and ovulation.

Three MC-LR exposure regimens were performed to distinguish whether MC-LR interferes with FSH-dependent follicle maturation and/or LH-dependent follicle ovulation, including the first exposure regimen covering both windows of follicle maturation and ovulation, the second exposure regimen covering the ovulation window only, and the third exposure regimen covering the FSH-dependent follicle maturation window only. For the first exposure regimen, CD-1 female mice at 21-day-old were treated with vehicle (1xPBS) or 10 µg/kg MC-LR through intraperitoneal (IP) injection daily for 5 days (Fig. 3.2A). The MC-LR treatment through IP injection has been demonstrated to be about 30 -100 times more potent than oral ingestion [85]. Thus, IP injection of 10 µg/kg MC-LR likely recapitulated the scenario of accidental acute high-dose (300-1,000 µg/kg) exposure to MC-LR during HAB seasons in humans. On day 3, mice from vehicle and MC-LR treatment groups were IP injected with 5 IU of pregnant mare serum gonadotropin (PMSG, ProSpec, East Brunswick, NJ) to stimulate early antral follicles to grow to the preovulatory stage to reach maturation [214]. On day 5 (46 hours post-PMSG injection), mice were intraperitoneally injected with 5 IU of human chorionic gonadotropin (hCG, Sigma-Aldrich, St. Louis, MO), an LH analog, to induce ovulation. Mice were sacrificed 16 hours after hCG injection on day 6, and oocytes were harvested from the ampulla region of both sides of the oviducts. The numbers of ovulated oocytes and the percentages of metaphase II (MII) oocytes were examined and recorded. The ovulated ovaries were collected for ovarian histology and counting of un-ovulated late-staged antral follicles. For the second and third MC-LR exposure regimens, the PMSG and hCG treatment methods were the same as the first exposure regimen. However, mice were only treated with 1xPBS or 10 µg/kg MC-LR through IP injection on day 5 (1 hour before hCG injection) for the second

exposure regimen (Fig. 3.3A), and mice were treated with 1xPBS or 10 µg/kg MC-LR daily through IP injection on the first 4 days for the third exposure regimen (Fig. 3.3B).

### **Measurement of antral follicle size and immunohistochemistry**

To examine the effects of MC-LR on follicle growth and maturation *in vivo*, CD-1 female mice at 21-day-old were treated with vehicle/ MC-LR and PMSG as we described in the first MC-LR exposure regimen except that mice were not treated with hCG for ovulation induction and ovaries were collected at the end of day 4 (46 hours post-PMSG injection). Harvested ovaries were processed and ovarian sections were obtained as described above. We first measured the size of late-staged antral follicles to investigate the effects of MC-LR on follicle growth. To ensure the accuracy of measurement, only a preovulatory follicle with clearly visible oocyte nucleus was included. Ninety-one to 95 preovulatory follicles from 6-8 ovaries in the PBS or MC-LR group were assessed using ImageJ software (National Institutes of Health, Bethesda, MD). Briefly, the preovulatory follicle diameter was obtained from two perpendicular measurements from one side to another side of basement membrane per follicle. The first measurement detected the widest diameter of follicle and the second measurement originated at a right angle from the midpoint of the first measurement. Next, the final preovulatory follicle diameter was calculated by averaging these two diameters.

We next examined the ovarian accumulation of MC-LR, and the expression of LH receptor (LHCGR) and PAPPA were determined by immunohistochemistry (IHC). Ovarian sections were deparaffinized in xylene and rehydrated in graded ethanol baths (100%, 95%, 80%, 70%, and 50%). Antigen retrieval was performed by microwaving slides in 0.01 M sodium citrate medium (pH = 6) for 15 minutes (min). Slides were then

incubated in 3% hydrogen peroxide (ThermoFisher Scientific) followed by incubating in the blocking buffer (2% BSA diluted in PBS) for 1 hour at room temperature (RT). Then, slides were incubated in the specific primary antibody diluted in 2% BSA in PBS for 3 hours at 4 °C. Subsequently, slides were rinsed using PBS and incubated with the secondary antibody (1:500, Goat anti-mouse IgG H&L (HRP), ab6789 or Goat anti-rabbit IgG (HRP), ab6271, Abcam, Cambridge, MA) for 1 hour at RT. Protein signals were then detected using DAB substrate kit (Abcam) according to manufacturer's instructions and counterstaining was performed using hematoxylin. Primary antibody against MC-LR (1:200, NBP2-89072) was purchased from Novus Biologicals (Centennial, CO). Primary antibodies against PAPP A (1:200, ab203683) and LHCGR (1:200, ab125214) were purchased from Abcam (Cambridge, MA).

#### **Follicle isolation, encapsulation, eIVFG, and MC-LR exposure**

Ovaries were removed from 16-day-old CD-1 female mice and multilayered secondary follicles were enzymatically isolated using enzymatic solution containing Leibovitz's L-15 medium (Gibco, Grand Island, NY) with Liberase TM (30.8 µg/mL, Roche, Indianapolis, IN) and DNase I (200 µg/mL, Worthington Biochemicals, Freehold, NJ). Morphologically normal follicles with diameters of 130 to 160 µm were selected, encapsulated with alginate hydrogel for eIVFG, and randomly distributed into different experimental groups, as we previously described with minor modifications [35, 36, 38]. Briefly, follicles were individually encapsulated in 0.5% (w/v) alginate hydrogel (Sigma-Aldrich), and alginate beads containing follicles were incubated in the maintenance media containing minimum essential medium (αMEM Glutamax; Gibco) with 1% FBS for 30 min at 37°C in 5% CO<sub>2</sub> incubator. In this study, to recapitulate the dynamic FSH

concentrations during *in vivo* follicle development, two different growth media with different concentrations of were used. Follicles encapsulated within alginate were individually cultured in 96-well plates, with each well containing 100  $\mu$ L growth media for 6 days at 37 °C in a humidified environment of 5% CO<sub>2</sub> in air. The follicle growth media was composed of 50%  $\alpha$ MEM Glutamax and 50% F-12 Glutamax supplemented with 3 mg/mL bovine serum albumin (BSA; Fisher Scientific, Denver, CO), 1 mg/mL bovine fetuin (Sigma-Aldrich), 5  $\mu$ g/mL insulin, 5  $\mu$ g/mL transferrin, and 5 ng/mL selenium (ITS; Sigma-Aldrich) and 5 mIU/mL (day 0-4) or 10 mIU/mL (day 4-6) recombinant follicle-stimulating hormone (rFSH; from A.F. Parlow, National Hormone and Peptide Program, National Institute of Diabetes and Digestive and Kidney Diseases, Bethesda, MD). During eIVFG, follicles were treated with 10  $\mu$ M MC-LR from day 2 to day 6. For the PI3K activator co-treatment experiment, follicles from day 2 of eIVFG were pretreated with PI3K activator 740 Y-P peptide (SelleckChem, Houston, TX) for 1 hour before MC-LR treatment, and follicles were then co-treated with 10  $\mu$ M MC-LR from day 2 to day 6. For each *in vitro* exposure experiment using eIVFG, follicles were imaged at each media change for examining follicle survival and diameter assessment using an Olympus inverted microscope with 10x objective (Olympus Optical Co Ltd, Tokyo, Japan). Follicles were considered dead if they had unhealthy appearing oocytes and/or granulosa cells, or if the integrity of the oocyte and somatic cell interface was visibly compromised. The follicle diameter was calculated by averaging 2 perpendicular measurements from one side to another side of basement membrane per follicle using ImageJ software (National Institutes of Health, Bethesda, MD).

### **Ovulation induction *in vitro***

Grown antral follicles from day 6 of eIVFG were removed from alginate beads by incubating alginate beads in L15 media containing 1% FBS and 10 IU/mL alginate lyase (Sigma-Aldrich) at 37°C for 10 min. Follicles were then treated with  $\alpha$ MEM-based ovulation induction media containing 10% FBS and 1.5 IU/mL hCG (Sigma-Aldrich) at 37°C in 5% CO<sub>2</sub>. At 14 hours post-hCG treatment, follicles were imaged with 10x objective to examine the follicle rupture and resumption of oocyte meiosis. Follicles with broken follicular wall from one side and an expanded cumulus-oocyte complex were defined as “ruptured” follicles; follicles with an intact follicular wall were defined as “unruptured” follicles.

### **Hormone measurement**

To investigate the effects of MC-LR on ovarian steroidogenesis, the concentrations of 17 $\beta$ -estradiol (E2) and testosterone (T) in the conditioned follicle culture media from day 6 of eIVFG was measured using estradiol and testosterone ELISA kits (Cayman Chemical Company, Ann Arbor, MI) according to the manufacturer’s instructions. To evaluate the effects of MC-LR treatment during the follicle maturation window on the subsequent luteinization upon after ovulation induction, after ovulation outcome assessment, hCG-treated follicles were continuously cultured for 48 hours to allow for luteinization and progesterone secretion. The conditioned media was collected to measure the concentration of progesterone (P4) using the progesterone ELISA kit (Cayman Chemical Company) according to the manufacturer’s instructions. The reportable ranges of E2, T, and P4 assay were 0.61-10,000 pg/mL, 3.9-500 pg/mL, 7.8-1,000 pg/mL,

respectively. The inter-assay coefficients of variability and intra-assay coefficients of variability were less than 10% for all assays.

### **Quantitative RT-PCR**

Total RNA of a single follicle from either *in vivo* or *in vitro* exposure experiment was extracted using the Arcturus PicoPure RNA isolation kit (Applied Biosystems, Carlsbad, CA) according to manufacturer's instructions. Total RNA was then reverse transcribed into cDNA using the Superscript III reverse transcriptase with random hexamer primers (Invitrogen, Carlsbad, CA) and stored at -80°C. qPCR was performed in the 384-well plate using Power SYBR Green PCR Master Mix (Applied Biosystems) on ABI ViiA 7 real-time PCR system (Applied Biosystems). qPCR thermocycle was programmed for 10 min at 95 °C, followed by 40 cycles of 15 s at 95 °C and 1 min at 60 °C, and finally a melting stage to determine the specificity of primers. The mRNA expression levels of each gene were normalized by the expression of glyceraldehyde-3-phosphate dehydrogenase (*Gapdh*).

### **Single-follicle RNA sequencing**

To investigate the effects of MC-LR on the whole follicular transcriptome, antral follicles treated vehicle or 10 µM MC-LR were collected from day 6 of eIVFG for single-follicle RNA sequencing (RNA-seq, GEO number:xxxx). Total RNA extraction was performed using the Arcturus PicoPure RNA isolation kit (Applied Biosystems) according to manufacturer's instructions. Next, the library preparation and low-input RNA sequencing were performed on an Illumina NovaSeq PE150 platform by Novogene (Novogene Corporation, Sacramento, CA). High-quality trimmed paired sequencing reads were uploaded into Partek Flow software for data analyses. The potential rDNA and

mtDNA contaminants were filtered using Bowtie 2. Next, the filtered reads were aligned to the whole mouse genome assembly-mm10 using the HISAT 2 aligner. Raw read counts were achieved by quantifying aligned reads to Ensembl Transcripts release 99 using the Partek EM algorithm and then normalized based on the Transcripts Per Million (TPM) method. Differential expression analysis was performed by using the DEseq2(R) and genes with an absolute fold change  $> 1.5$  and a false discovery rate (FDR) adjusted p-value  $< 0.05$  were recognized as differentially expressed genes (DEGs).

### **PP1 and PP2A phosphatase activity measurement**

PP1 and PP2A activity in the MC-LR treated or untreated follicles were measured by using the RediPlate 96 EnzChek Serine/Threonine Phosphatase Assay Kit (ThermoFisher Scientific) according to the manufacturer's protocol. To detect the activity of PP1 and PP2A, cultured multilayered secondary follicles were treated with or without 10  $\mu$ M MC-LR from day 2 to day 6 and then follicles were harvested for PP1 and PP2A activity assay. Firstly, 25-30 follicles in each treatment group were lysed in M-PER Mammalian Protein Extraction Reagent (ThermoFisher). Secondly, the protein concentrations of follicle lysates were determined using the Bradford protein assay kit (Abcam). Next, equal amount of protein in each treatment group was used to determine the activity of PP1 and PP2A. The plate was incubated at room temperature (RT) and then fluorescence was measured at multiple time points on a Spectramax M3 microplate reader (Molecular Devices, Sunnyvale, CA) with excitation and emission wavelengths of 355 and 460 nm, respectively.

## **Western blotting**

Twenty to 25 follicles in each group were lysed in ice-cold Laemmli sample buffer (Bio-Rad, Hercules, CA) containing protease and phosphatase inhibitor cocktail (ThermoFisher Scientific) and separated on 12% acrylamide/bisacrylamide gels. Proteins were transferred to the 0.45 µm nitrocellulose blotting membrane (GE Healthcare Life Science, Pittsburgh, PA). After blocking, membranes were incubated with specific primary antibodies overnight at 4 °C and appropriate horseradish peroxidase-conjugated secondary antibodies at a dilution of 1:2000 for 1 h at RT. The protein was detected using Pierce™ ECL Western Blotting Substrate Kit (ThermoFisher Scientific) according to the manufacturer's instructions. The following antibodies were used: anti-β-actin (1:1000, ab6276, Abcam), anti-PCNA (1:1000, ab2426, Abcam), anti-γ-H2AX (phospho Ser139) (1:1000, ab26350, Abcam), anti-FOXO1A (phospho S253) (1:1000, ab259337), anti-AKT (1:1000, 9272S, Cell Signaling Technology), anti-AKT (phospho T308) (1:1000, ab8933, Abcam), anti-AKT (phospho S473) (1:1000, ab81283, Abcam), anti-MC-LR (1:1000, NBP2-89072, Novus Biologicals).

## **Statistical Analyses**

Student's t-test were used to compare differences between two groups where appropriate. One-way ANOVA followed by a Tukey's multiple comparisons test was performed to analyze the follicle growth, survival, rupture rate, and hormone concentration in comparing multiple groups. A Fisher exact test was performed to analyze the follicle rupture rate for the Ritonavir treatment experiment.  $P < 0.05$  was considered statistically significant.

### 3.3 RESULTS

#### **Chronic oral low dose exposure to MC-LR reduces the number of CL *in vivo***

To investigate the toxic effect of human-relevant MC-LR on female reproduction, CD-1 female mice at 4-week-old were exposed to 1xPBS or 10 µg/kg MC-LR via daily oral gavage for 6 weeks, and the general health of the animals and multiple specific ovarian endpoints were examined through the exposure period (Fig. 3.1A). Exposure to MC-LR did not affect animals' food and water intake (results not shown), and body weight (Fig. 3.1B). The vaginal smear data in the last 2 weeks of MC-LR treatment revealed comparable estrous cyclicity between the control and MC-LR-treated groups (Fig. 3.1C).

At the end of the 6-week exposure, ovaries were collected on diestrus for histological staining and counting of follicles and CL. Ovaries from MC-LR treated mice had comparable numbers of follicles at all stages to the control group (Fig. 3.1D and 3.1E), including primordial follicles ( $687.6 \pm 88.5$  vs.  $667.4 \pm 144.3$ ), primary follicles ( $299.6 \pm 67.4$  vs.  $357.4 \pm 80.1$ ), secondary follicles ( $148.2 \pm 45.0$  vs.  $146.4 \pm 35.3$ ), antral follicles ( $16.0 \pm 4.8$  vs.  $16.4 \pm 4.5$ ), and atretic follicles ( $78.8 \pm 21.0$  vs.  $91.6 \pm 8.0$ ). However, there were nearly 50% fewer CL, a mass of cells that is formed from postovulatory follicular somatic cells, in MC-LR treated ovaries than in the control group ( $6.6 \pm 2.5$  vs.  $11.8 \pm 3.8$ , Fig. 3.1D and 3.1F). These results demonstrate that chronic low-dose oral exposure to MC-LR does not affect the kinetics of folliculogenesis from primordial follicle through antral follicles; however, the significantly reduced numbers of CL in MC-LR treated mice suggest that the processes pertaining to the formation and survival of CL are disrupted by MC-LR. There are several possibilities, involving MC-LR perturbations of preovulatory, ovulatory, or postovulatory events: (1) MC-LR may disrupt the molecular events intrinsic to the

ovulation process per se such that terminally mature follicles fail to rupture and differentiate into CL; (2) Although the antral follicles appear morphologically normal under MC-LR exposure, there could be molecular alterations during follicle maturation that disrupt the readiness of the seemingly mature antral follicles for responding to the ovulatory LH surge; (3) MC-LR may disrupt the luteinization of postovulatory follicular cells to form CL or promote the apoptosis of CL cells. Given the well-characterized inhibitory effect of MC-LR on PP1, a protein phosphatase key to the activation of the IGF/PI3K/AKT/FOXO1 signaling pathway that underpins FSH-dependent follicle maturation and dominance [206, 207], we hypothesize that MC-LR perturbs the maturation of preantral follicles toward the preovulatory stage to block the LH surge-triggered ovulation.

#### **A human-relevant acute exposure to MC-LR disrupts follicle ovulation *in vivo***

To test the hypothesis, we first used an *in vivo* mouse superovulation model to examine the possible adverse effects of MC-LR on two gonadotropin-dependent ovarian events: FSH-dependent follicle maturation and LH-dependent follicle ovulation. As shown in Fig. 3.2A, CD-1 female mice at 21-day-old were treated with 1xPBS or 10 µg/kg MC-LR through daily IP injection for 5 days. As justified in the Materials and Methods, this dosing regimen recapitulated the scenario of acute high-dose exposure to MC-LR in humans during the bloom seasons, such as (1) the HAB outbreak in the Lake Erie in the US in 2014 which was primarily caused by the runoff pollution and (2) the incident of dialysis fluid contamination with microcystins in a Hemodialysis Center in Caruaru, Brazil in 1996 [187, 215]. Mice were then treated with PMSG on day 3 of MC-LR exposure to stimulate follicle maturation followed by the injection of hCG on day 5 to induce ovulation.

The acute *in vivo* exposure experiment showed that at 14 hours post-hCG injection on day 5, there were significantly fewer oocytes harvested from both sides of oviducts in MC-LR treated mice than in the control group ( $25.1 \pm 10.1$  vs.  $38.0 \pm 7.7$ , Fig. 3.2B and 3.2C). For these ovulated oocytes, there were comparable percentages of MII oocytes, with 97.1% and 98.5% of them having the first polar body extrusion in the control and MC-LR groups, respectively (Fig. 3.2D). Histological staining showed that compared to the control group, there were significantly more late-stage antral follicles (class 7-8) that did not ovulate or rupture in the ovaries from MC-LR treated mice ( $15.8 \pm 3.9$  vs.  $9.3 \pm 1.9$ , Fig. 3.2E and 3.2F). Together, these results demonstrate that acute, human-relevant exposure to MC-LR interferes with follicle ovulation *in vivo*, which lead to reduced number of ovulated oocytes and CL as observed in the chronic exposure experiment above. The MC-LR exposure in the current acute experiment is continuous, compassing the day of hCG treatment and ovulation (Fig. 3.2A). Therefore, the failed ovulation under MC-LR exposure might result from either defective follicle maturation or direct impact of MC-LR on the ovulation process per se.

### **MC-LR compromises follicle maturation to disrupt ovulation**

To distinguish whether MC-LR interferes with follicle maturation that causes secondary ovulation defect, or it directly inhibits ovulation per se, we next performed an experiment involving two different MC-LR exposure regimens. Mice in exposure regimen 1 were treated with a single IP injection of 1xPBS or 10  $\mu\text{g}/\text{kg}$  MC-LR during the ovulation window only, *i.e.*, 1 h before hCG injection (Fig. 3.3A). There were comparable numbers of ovulated oocytes ( $41.7 \pm 11.5$  vs.  $39.8 \pm 9.5$ ) and percentages of MII oocytes ( $94.3 \pm 2.9$  vs.  $94.5 \pm 3.3$  %) between vehicle and MC-LR treated mice. In exposure regimen 2, mice

were treated with multiple IP injections of 1xPBS or 10  $\mu\text{g}/\text{kg}$  MC-LR during the follicle maturation window only, with the last injection on day 4 (Fig. 3.3B). There were fewer numbers of ovulated oocytes in the MC-LR treatment group than in the control group ( $23.6 \pm 8.8$  vs.  $36.1 \pm 11.3$ ), but ovulated oocytes had comparable percentages of MII oocytes ( $92.1 \pm 5.5$  vs.  $94.9 \pm 2.6$  %). Taken together, this exposure experiment demonstrated clearly that MC-LR is unlikely to directly block ovulation; rather, the suppressed ovulation is caused by an aberration in the maturation of antral follicles toward the preovulatory stage such that they are less responsive to LH or hCG to ovulate.

### **MC-LR accumulates in the ovary and alters the expression of follicle maturation regulators**

To decipher the underlying mechanism of failed follicle maturation caused by MC-LR, we performed the same exposure experiment as shown in Fig. 3.3B with mice treated with 1xPBS or MC-LR during the follicle maturation window only. Mice were sacrificed on day 5 (46 hours post-PMSG injection) without hCG treatment for ovulation induction. Immunohistochemistry results showed that MC-LR accumulated in the ovarian cells, including stroma cells, theca cells, and granulosa cells in antral follicles (Fig. 3.4A). We also measured the size of late-stage antral follicles (class 7 and 8) and found that ovaries from vehicle and MC-LR treated mice had comparable diameters of large antral follicles, implying that MC-LR does not affect follicle growth (Fig. 3.4B and 3.4C). We further isolated large antral follicles from the ovaries of PBS or MC-LR treated mice and performed single-follicle RT-qPCR to examine the expression of several genes critical for the FSH-induced follicle maturation. The specific genes, their full names, functions in follicle maturation, and references are listed in Table 3.1. Exposure to MC-LR significantly

reduced the expression of several of these genes, including *Inha*, *Comp*, *Lhcgr*, and *Pappa* (Fig. 3.4D). Meanwhile, although no statistically significant, MC-LR also has the tendency to reduce the expression of several other follicle maturation-related genes, including *Inhba*, *Inhbb*, and *Cyp19a1* (Fig. 3.4D). Immunohistochemistry was next performed to examine the protein expression of two essential follicle maturation proteins, LHCGR and PAPPA. Consistent to our qPCR results, the expression of both LHCGR and PAPPA was remarkably reduced in the granulosa cells of antral follicles in MC-LR treated ovaries (Fig. 3.4E and 3.4F). These results demonstrate that MC-LR can accumulate in the ovary and disrupt FSH-dependent follicle maturation without affecting follicle growth, and the reduced expression of follicle maturation-related genes such as *Lhcgr* may contribute to the failed follicle response to LH or hCG for ovulation.

#### **MC-LR disrupts follicle maturation to affect ovulation and luteinization *in vitro***

To further investigate the mechanisms of defective follicle maturation caused by MC-LR and also subsequent reproductive outcomes such as ovulation and luteinization, we used our established 3D *in vitro* follicle culture model, eIVFG, to perform an *in vitro* experiment. We have previously demonstrated that eIVFG faithfully recapitulates the hallmark events of follicle maturation, ovarian steroidogenesis, ovulation, and luteinization [35, 36, 216]. This *in vitro* exposure regimen also enables us to confirm the direct ovarian impact of MC-LR. During eIVFG, immature mouse preantral follicles were treated with various concentrations of MC-LR at 0, 0.1, 1, and 10  $\mu$ M from day 2 to day 6, to recapitulate MC-LR exposure during FSH-dependent follicle maturation. Results showed that follicles from all treatment groups had comparable morphology (Fig. 3.5A) and survival rates (Fig. 3.5B), and follicles from all groups were able to grow from the

secondary stage to the antral stage with comparable follicle size (Fig. 3.5C). The concentrations of estradiol and testosterone in the conditioned media are similar between different groups (Fig. 3.5D and 3.5E). These results are consistent to the observations *in vivo* (Fig. 3.3 and 3.4), demonstrating that exposure to MC-LR during the follicle maturation window does not affect follicle survival, growth, and secretion of estradiol and testosterone.

We next treated grown antral follicles from day 6 of eIVFG with hCG to induce ovulation *in vitro*. Results showed that MC-LR concentration-dependently inhibited follicle ovulation, particularly the rupture of the follicular wall (Fig. 3.5F and 3.5G). In the control and 0.1  $\mu$ M MC-LR treatment groups, nearly 100% follicles ruptured and ovulated MII oocytes in response to hCG stimulation; however, in the 1 and 10  $\mu$ M MC-LR treatment groups, only  $77.5 \pm 7.8\%$  and  $11.9 \pm 3.2\%$  follicles ruptured (Fig. 3.5F and 3.5G). Follicles treated with hCG were next cultured for an additional 48 hours to allow for luteinization and progesterone secretion. ELISA results showed that follicles treated with 10  $\mu$ M MC-LR during the follicle maturation window had significantly lower concentrations of progesterone in the conditioned media, indicating defective luteinization (Fig. 3.5H).

We next used the same exposure regimen with vehicle or 10  $\mu$ M MC-LR during the follicle maturation window to investigate the molecular mechanisms of MC-LR on follicle maturation (Fig. 3.6A). We first collected follicles on day 6 of eIVFG for single-follicle RT-qPCR to examine the expression of follicle maturation-related genes listed in Table 3.1. Results showed that follicles treated with vehicle had a significant increase in mRNA expression from day 0 to day 6 for all examined genes (Fig. 3.6B), confirming that

the eIVFG model preserves the molecular signatures of FSH-dependent follicle maturation. In MC-LR treated follicles, however, the expression levels of all these genes were significantly decreased on day 6 compared to the control group (Fig. 3.6B); particularly for *Pappa* and *Lhcgr*, there were 5.36- and 5.84-fold of reduction on day 6 of eIVFG, respectively. For *Inha* and *Inhbb*, significant reduction was observed starting on day 4 of eIVFG (Fig. 3.6B). To further determine whether the inhibitory effect of MC-LR on these follicle maturation-related genes was specific to granulosa cells, we next isolated mural granulosa cells from cultured follicles on day 6 of eIVFG for qPCR and consistently observed significant reduction of *Comp*, *Inha*, *Lhcgr*, and *Pappa* expression (Fig. 3.11).

We next treated vehicle and MC-LR treated follicles with hCG for ovulation induction. Given that many ovulatory genes were highly induced at 4 hours post-hCG in both *in vivo* and *in vitro* models [217], we collected follicles at 4 hours for qPCR to examine the expression of several known ovulatory genes (Fig. 3.6C). The specific genes, their full names, functions in ovulation are listed in Table 3.2. Results showed that all these ovulatory genes were greatly suppressed in follicles treated with MC-LR during the follicle maturation window only (Fig. 3.6C). Collectively, we demonstrated, using the 3D *in vitro* follicle culture model, that MC-LR disrupts FSH-dependent follicle maturation, which further leads to a secondary disruption on the follicle ovulation, luteinization, and progesterone secretion.

### **Single-follicle RNA-seq analysis reveals MC-LR induces transcriptome-wide changes and alternation of PI3K/AKT/FOXO1 signaling pathway in follicular cells**

To further mechanistically characterize the effects of MC-LR on FSH-dependent follicle maturation in an unbiased manner, we performed the same vehicle and MC-LR

exposure experiment as shown in Fig. 3.6A without hCG treatment and collected follicles on day 6 of eIVFG for single-follicle RNA-seq analysis. High-quality sequencing data were generated from single follicles (Fig. 3.12) and thousands of differentially expressed genes (DEGs) were detected. We first performed principle component analysis (PCA) to determine the global variation in response to MC-LR treatment. The PCA results showed that vehicle and MC-LR treated follicles can be easily separated into two distinct clusters, indicating that MC-LR remarkably altered the follicular transcriptomic profiles (Fig. 3.7A). Differential gene expression analysis further revealed that there were 3,368 DEGs (absolute fold change  $>1.5$  and FDR adjusted p-value  $<0.05$ ) out of a total of 16,563 detected genes between vehicle and MC-LR treated follicles, among which 2,028 were up-regulated and 1,340 were down-regulated in MC-LR-treated follicles, including those established follicle maturation-related genes listed in Table 1 and examined by qPCR (Fig. 3.7B).

DEGs were next used for Gene Ontology (GO) term enrichment and KEGG pathway analyses. Biological process analysis demonstrated that DEGs were primarily enriched in the processes of cell adhesion, angiogenesis, cell migration, inflammatory response, and cell proliferation (Fig. 3.7C). Molecular function analysis showed that DEGs were mainly related to the functions of binding of biomolecules, such as protein, heparin, integrin, calcium ion, extracellular matrix, and fibronectin (Fig. 3.7D). Cellular component analysis revealed that DEGs were closely related to the components of basement membrane, extracellular matrix, and extracellular exosome (Fig. 3.7E). KEGG pathway analysis identified several significantly altered signaling pathways upon MC-LR treatment,

such as pathways related to the ECM-receptor interaction, focal adhesion, and importantly, the PI3K/AKT signaling (Fig. 3.7F).

It is established that the activation of PI3K/AKT/FOXO1 signaling pathway in follicular granulosa cells is essential for the FSH-driven follicle maturation [218]. Based on a previous study that discovered numerous FOXO1 target genes in an *in vitro* granulosa cell culture model, we found that 315 genes were also significantly changed in follicles treated with MC-LR *in vitro*, including 189 and 126 genes that have been shown to be respectively stimulated and suppressed by the FOXO1 (Fig. 3.7G). Among these overlapped genes in the two data sets, many of them critically govern various follicular events during FSH-dependent follicle maturation, such as genes related to the ovarian steroidogenesis (*Cyp17a1*, *Hsd17b1*, and *Cyp19a1*), peptide hormone secretion (*Inha*, *Inhba*, and *Inhbb*), and oocyte meiotic arrest (*Nppc*) (Fig. 3.7H). Moreover, the RNA-seq analysis also identified many new signaling pathways (Fig. 3.7C-3.7F) and genes (Fig. 3.7G and 3.7H), suggesting they may also play important roles in the MC-LR induced defective follicle maturation.

### **MC-LR disrupts PP1-mediated activation of PI3K/AKT/FOXO1 signaling in follicular granulosa cells to compromise the FSH-dependent follicle maturation**

PP1 is an essential molecular component mediating the cross-talk between the FSH-stimulated and IGF-stimulated signal transduction pathways that underpin the FSH-dependent follicle maturation [206, 207]. MC-LR has been shown to selectively and covalently bind to the catalytic subunits of PP1 or PP2A to irreversibly inhibit their phosphatase activities [93, 190], which might be the underlying mechanism of MC-LR induced defective follicle maturation. To test this hypothesis, we first examined the

activities of PP1 and PP2A in follicles treated with vehicle or 10  $\mu$ M MC-LR from day 2-6 of eIVFG. Protein phosphatase assay results showed that the phosphatase activity of PP1 but not PP2A was significantly reduced in MC-LR treated follicles (Fig. 3.8A and 3.8B). Next, follicles with the same vehicle or MC-LR exposure method were collected on day 6 of eIVFG to examine the accumulation of MC-LR, the phosphorylation status of key proteins contributing to activation of PI3K/AKT/FOXO1 signaling pathway, and biomarkers indicated the follicle growth and survival. Western blotting results showed that MC-LR accumulated in cultured follicles (Fig. 3.8C). Exposure to MC-LR significantly increased and decreased the phosphorylation of AKT(Ser473) and AKT(Thr308), respectively (Fig. 3.8C and 3.8D); the phosphorylation modification of these two amino acid residues are indispensable for the full activation of AKT [219]. In addition, western blotting results also revealed that MC-LR did not change the expression of  $\gamma$ H2AX, a DNA damage marker, and PCNA, a cell proliferation marker (Fig. 3.8C and 3.8D).

To further confirm the causal relationship between the disrupted activation of PI3K/AKT/FOXO1 signaling caused by MC-LR and the defective follicle maturation and ovulation, we co-treated follicles with 10  $\mu$ M MC-LR and 25  $\mu$ g/mL 740-YP, a potent PI3K activator. In follicles treated with vehicle or 25  $\mu$ g/mL 740-YP only, there were comparable results regarding the follicle development, survival, expression of follicle maturation-related genes, and ovulation rate, suggesting that the treatment of 740-YP did not affect follicle maturation and ovulation (Fig. 3.8E-3.8H). Notably, compared to the treatment group with MC-LR only, the co-treatment of MC-LR and 740-YP significantly ameliorated the reduced expression of follicle maturation-related genes as well as the follicle ovulation rate (Fig. 3.8G-3.8H). Taken together, these results confirm our

hypothesis that MC-LR does not affect follicle growth and survival but inhibits FSH-dependent follicle maturation by disrupting the PP1-mediated activation of PI3K/AKT/FOXO1 signaling pathway in the follicular granulosa cells.

### **OATPs contribute to the follicular uptake of MC-LR**

The membrane transport proteins, OATPs, have been shown to regulate the uptake of MC-LR in liver cells and HEK293 cells stably expressing OATPs [17, 18]. Both of our *in vivo* and *in vitro* models demonstrated the accumulation of MC-LR in follicular granulosa cells (Fig. 3.4 and 3.8). We next investigated whether OATPs are expressed in the ovary and also their roles in the ovarian accumulation of MC-LR. We first used our single-follicle RNA-seq data to examine the ovarian expression of OATP genes. Among 15 known murine OATP genes, 9 of them were detectable in follicular cells, with *Slco3a1* having the most abundant expression levels, followed by *Slco2b1*, *Slco2a1*, *Slco4a1*, *Slco1c1*, *Slco1a5*, *Slco4c1*, *Slco1a1*, and *Slco5a1* (Fig. 3.9A). RNA-seq data revealed that exposure to MC-LR significantly increased the expression of 4 OATP genes, including *Slco1a1*, *Slco2b1*, *Slco3a1*, and *Slco4a1*, and decreased the expression of *Slco2b1* (Fig. 3.9A). Ritonavir, a FDA-approved antiretroviral protease inhibitor, has been demonstrated to inhibit the OATP-mediated membrane transport of exposed xenobiotics [220, 221]. We co-treated follicles with 10  $\mu$ M MC-LR and Ritonavir at the concentrations of at 0, 0.1, 1, and 10  $\mu$ M from day 2 to day 6 of eIVFG and examined the follicle survival, growth, and ovulation. Results showed that the cotreatment of Ritonavir dose-dependently decreased the follicular accumulation of MC-LR (Fig. 3.9B) and also blocked the MC-LR induced defective follicle ovulation (Fig. 3.9C). Taken together, these results demonstrate that OATPs contribute to the follicular uptake and accumulation of MC-LR.

### 3.3 DISCUSSION

In the present study, we aimed to investigate the effects of harmful algal bloom toxin MC-LR on the female reproduction, which can help us address the knowledge gaps of MC-LR-induced toxicity. Using both *in vivo* mouse exposure model and *in vitro* 3D follicle culture model, we identified an unexpected toxic effect of MC-LR on follicle ovulation. Exposure to human relevant dose of MC-LR could inhibit the activity of PP1 and then disrupt the follicle maturation and following ovulation through blocking the FSH-dependent activation of PI3K/AKT/FOXO1 signaling pathway in the granulosa cells (Fig. 3.10).

The frequency and intensity of HABs in the waterbodies around the world have been increasing in the past few decades [222]. The World Health Organization (WHO) sets a provisional guideline for MC-LR in lifetime drinking-water at 1 µg/L and the recommended recreational value for MCs released by U.S. Environmental Protection Agency (EPA) is 8 µg/L [14, 15]. However, the concentrations of MC-LR in many water bodies range from 0.06 to 2,100 µg/L which are much higher than the WHO and EPA guidelines [16]. In addition, humans can be exposed to MC-LR via multiple exposure routes, including daily drinking water, seafood consumption, crops and vegetables irrigated with MCs-contaminated water, dermal contact, inhalation of aerosolized MC-LR, and hemodialysis [10-13]. The estimated daily intake of MCs from lake water and aquatic products by the fishers in Lake Taihu in China is 4.25-5.95 µg, which is 1.8-2.5 times higher than the WHO tolerable daily intake (TDI, 2.4 µg) for a 60 kg BW adult [223]. In the Chongqing area of the Three Gorges Reservoir Region, the children between 7 and 15

years of age exposed to MCs through drinking water and aquatic food have a total estimated daily MCs intake of 2.03  $\mu\text{g}$ , which is much higher than the WHO TDI (0.4  $\mu\text{g}$ ) for children [84]. Therefore, the ubiquitous exposure of humans to MC-LR highlights the urgent need to understand the toxic effects of MC-LR, including female reproductive toxicity. An important goal of this study is to investigate the toxic effects of environmentally-relevant exposure to MC-LR on female reproduction. Previous studies showed that exposure to MC-LR could affect the estrous cyclicity by decreasing the duration of proestrus and estrus after the 5-week-old BALB/c female mice were intraperitoneally injected with 20  $\mu\text{g}/\text{kg}$  MC-LR daily for 28 days [140]. In addition, the mice had dysregulated estrous cyclicity with shortening estrus and prolonging diestrus after 5-week-old BALB/c mice were administrated with MC-LR at 1, 10, or 40  $\mu\text{g}/\text{L}$  via drinking water for 6 months [139]. However, our results demonstrated that MC-LR-treated mice had normal estrous cyclicity after 4-week-old CD-1 mice orally treated with 10  $\mu\text{g}/\text{kg}$  MC-LR daily for 6 weeks. The inconsistency of the effect of MC-LR on the estrous cyclicity may be caused by different exposure route, time, and age of mice. Exposure to 10  $\mu\text{g}/\text{L}$  MC-LR via drinking water for 6 months did not affect the numbers of primordial follicles and growing follicles in BALB/c mice [139]. Consistently, we found that 10  $\mu\text{g}/\text{kg}$  MC-LR treatment did not affect the follicle development. To our knowledge, we are the first to examine the number of CL in the ovaries post MC-LR exposure. Interestingly, we discovered that MC-LR could remarkably reduce the number of CL, which pointed out that the ovulation might be compromised.

Using a mouse superovulation model and *in vitro* 3D follicle culture model, we confirmed that MC-LR could disrupt follicle ovulation through affecting the follicle

maturation. Both *in vivo* and *in vitro* results showed that MC-LR did not affect the follicle growth, but downregulated the expression of some follicle maturation related genes in the granulosa cells, such as *Lhcgr*, and *Pappa*. Thus, these data indicate that environmentally relevant exposure of MC-LR can program the granulosa cells at the transcriptional levels to interfere the follicle maturation. During follicle development, the acquisition of sufficient numbers of LH receptors in the granulosa cells is the highest priority for follicle maturation which is crucial for the preparation of a LH surge to trigger ovulation [224]. In the granulosa cells, FSH synergizes with insulin-like growth factor-1 (IGF1) to drive the expression of follicle maturation-related genes via PI3K/AKT/FOXO1 signaling pathway [206, 225]. Specifically, FSH can activate protein phosphatase 1 (PP1) via protein kinase A (PKA) to sensitize the insulin receptor substrate 1 (IRS1) which mediates the IGF1-activated PI3K/AKT signaling pathway in granulosa cells [206]. Pregnancy-associated plasma protein-A (PAPPA) is a secreted metalloprotease responsible for cleaving IGF binding protein 4 (IGFBP4) to release bioactive IGF in the ovary [226]. Thus, PAPPA plays a permissive role in the IGF1-activated PI3K/AKT pathway. Herein, we found that MC-LR could significantly reduce the expression of LHCGR and PAPPA at both transcriptional and translational levels in the granulosa cells. Therefore, exposure to MC-LR can compromise the follicle maturation through disrupting the FSH and IGF1 mediated activation of PI3K/AKT/FOXO1 signaling pathway in granulosa cells.

In addition to the function of PP1 in promoting the follicle maturation, PP1 can also participate in the oocyte meiosis resumption during ovulation. Oocytes in follicles are arrested in meiotic prophase stage by cyclic (c)GMP produced in the granulosa cells by natriuretic peptide receptor 2 (NPR2) [227, 228]. Upon the LH surge, the rapid

dephosphorylation of NPR2 mediated by PP1, PP2, and PP6 reduces its activity and decreases the cGMP that causes meiosis to resume in oocytes [229]. Thus, the MC-LR-mediated PP1 inhibition seems to be able to inhibit LH-induced meiosis resumption. However, we did not find that MC-LR affected the MII rate of oocytes upon ovulation both *in vivo* and *in vitro*. Additionally, our RNA-seq data demonstrated that the expression of *Nppc* which encodes C-type natriuretic peptide (CNP, the agonist of NPR2) in mural granulosa cells was significantly decreased in the MC-LR-treated follicles. Interestingly, the downregulated expression of *Nppc* did not induce premature meiotic resumption in the oocytes of preovulatory follicles in both *in vivo* and *in vitro*. One possible reason is that MC-LR-mediated inhibition of PP1 increases the activity of NPR2 which counteracts the effects of decreased NPPC in the granulosa cells. PP2A has also been reported to play roles in follicle development and oocyte meiosis, including downregulating testosterone production in theca cells [230], and regulating oocyte meiotic maturation [231]. However, our phosphatase activity assay revealed that MC-LR could significantly decrease the activity of PP1, but not the activity of PP2A in the follicles. More studies should be performed to understand the underlying mechanism of this specific PP1 inhibition in the follicles. The majority of protein dephosphorylation reactions is catalyzed by PP1 in a highly regulated and selective manner in eukaryotic cells [232]. Thus, it is still required to explore the impacts of MC-LR on the substrates of PP1 and their related functions in the follicle. For instance, AKT has been shown to be a substrate of PP1 and PP1 can dephosphorylate AKT at Ser473 [233]. Consistently, our western blotting results demonstrated that MC-LR treatment significantly increased the expression of pAKT-Ser473, suggesting that AKT was a potential PP1 substrate in follicles. To

comprehensively understand the substrates of PP1 in the follicles will teach us the cellular alteration from MC-LR-mediated PP1 inhibition.

OATPs are ubiquitously expressed in animal and human bodies and distinct tissues express differential OATP isoforms [20]. Thus, the distinct tissue expression patterns of OATPs may impact the distribution of MC-LR as well as its associated toxic effects. Thus far, a number of OATP inhibitors have been identified using in vitro screening model and in silico model [221]. However, whether these OATP inhibitors can be used for preventing the accumulation of MC-LR in the ovary is still unclear. Here, we found that Ritonavir could inhibit the accumulation of MC-LR in the follicles and rescue the MC-LR-damaged follicle ovulation. Our established eIVFG model will allow us to perform a high-throughput screening for the potential OATP inhibitors and the function of specific of OATP should be investigated in future.

In conclusion, our study reveals that human relevant exposure to harmful algal bloom toxin MC-LR can compromise ovulation through affecting follicle maturation via inhibiting the PP1/PI3K/AKT/FOXO1 signaling pathway in the granulosa cells. These results point out that MC-LR is an emerging endocrine-disrupting chemical and pose a threat to human reproductive health and fertility. Meanwhile, the potential impacts of exposure to MC-LR on the fertility in wild and domestic animals should be a big concern.

**Table 3.1:** Established follicle maturation genes and their identified functions in follicle maturation.

<b>Gene symbol</b>	<b>Gene name</b>	<b>Fuctions and references</b>
<i>Inha</i>	Inhibin subunit alpha	Regulation of folliculogenesis and steroidogenesis [234]
<i>Inhba</i>	Inhibin subunit beta A	
<i>Inhbb</i>	Inhibin subunit beta B	
<i>Comp</i>	Cartilage oligomeric matrix protein	A biomarker of follicle maturation [235]
<i>Cyp19a1</i>	Cytochrome P450 family 19 subfamily A member 1	Estrogen synthesis [236]
<i>Fshr</i>	Follicle stimulating hormone receptor	Activation of FSH mediated signaling pathways [237]
<i>Lhcgr</i>	Luteinizing hormone/choriogonadotropin receptor	Activation of LH mediated signaling pathways [225]
<i>Pappa</i>	Pregnancy-associated plasma protein A	IGFBP4 protease; regulation of folliculogenesis and steroidogenesis [226]

**Table 3.2:** Established ovulatory genes and their identified functions in ovulation.

<b>Gene symbol</b>	<b>Gene name</b>	<b>Functions and references</b>
<i>Pgr</i>	Progesterone receptor	Follicle rupture [238]
<i>Runx1</i>	Runt-related transcription factor 1	Progesterone production [239]
<i>Areg</i>	Amphiregulin	Activation of EGF signaling to regulate COC expansion, oocyte maturation, follicle rupture, and luteinization [240]
<i>Ereg</i>	Epiregulin	
<i>Btc</i>	Betacellulin	
<i>Plau</i>	Plasminogen activator, urokinase	ECM remodeling and follicle rupture [241]
<i>Ptgs2</i>	Prostaglandin-endoperoxide synthase 2	Prostaglandin production, COC expansion, and oocyte maturation [242, 243]
<i>Tnfaip6</i>	Tumor necrosis factor-inducible gene 6	COC expansion [244]

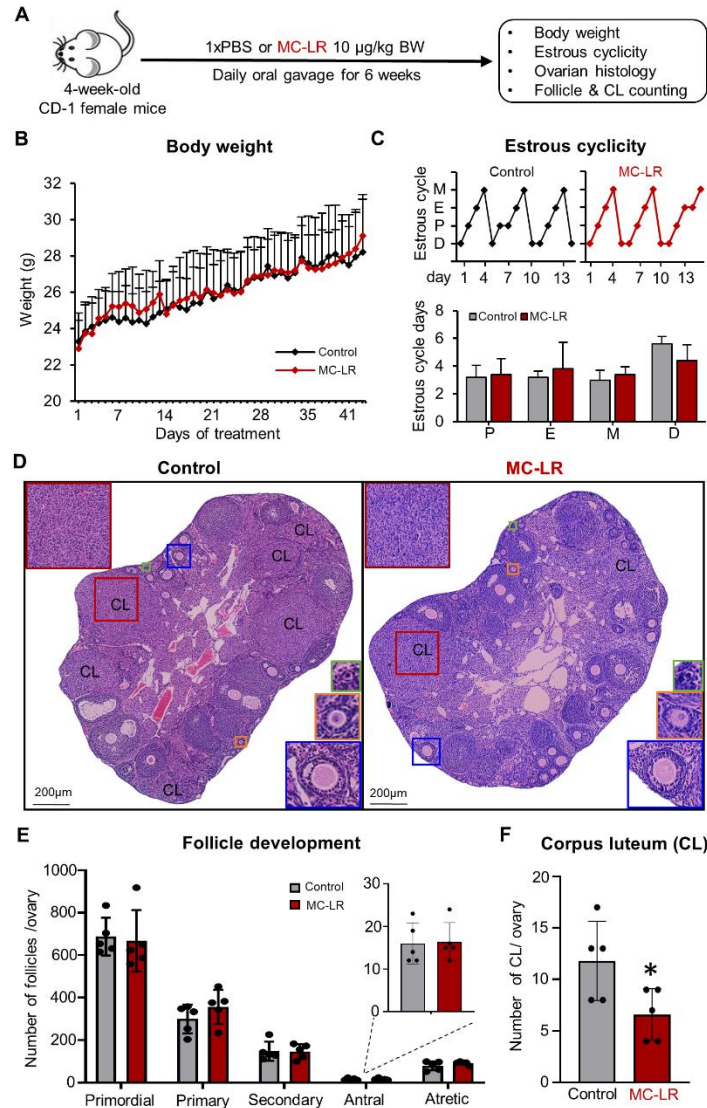


**Figure. 3.1** Chronic exposure of MC-LR using oral gavage on reproductive parameters. (A) A schematic of long-term exposure of MC-LR using oral gavage. Four-week-old CD-1 female mice were daily treated with PBS (n=5) or 10 µg/kg MC-LR (n=5) using oral gavage for 6 weeks and the body weight and estrous cyclicity were examined during treatment. Next, ovaries were harvested for ovarian histology and follicle and corpus luteum (CL) counting. (B) Effect of MC-LR exposure on body weight change. (C) Representative estrous cyclicity in PBS or MC-LR treated mice (top panel). The number of days in each stage of estrous cycle after PBS or MC-LR treatment (bottom panel). Proestrus (P), estrus (E), metestrus (M), and diestrus (D) were determined by vaginal cytology. (D) Representative ovary histological images after PBS or MC-LR treatment. Red squares indicate corpora lutea; Green squares indicate primordial follicles; Orange squares indicate primary follicles; Blue squares indicate secondary follicles. (E) Total number of specific developmental stage of follicles per ovary after PBS or MC-LR treatment. (F) Total number of corpora lutea per ovary in PBS- or MC-LR- treated mice. Error bar: standard deviation; \* $p < 0.05$ .

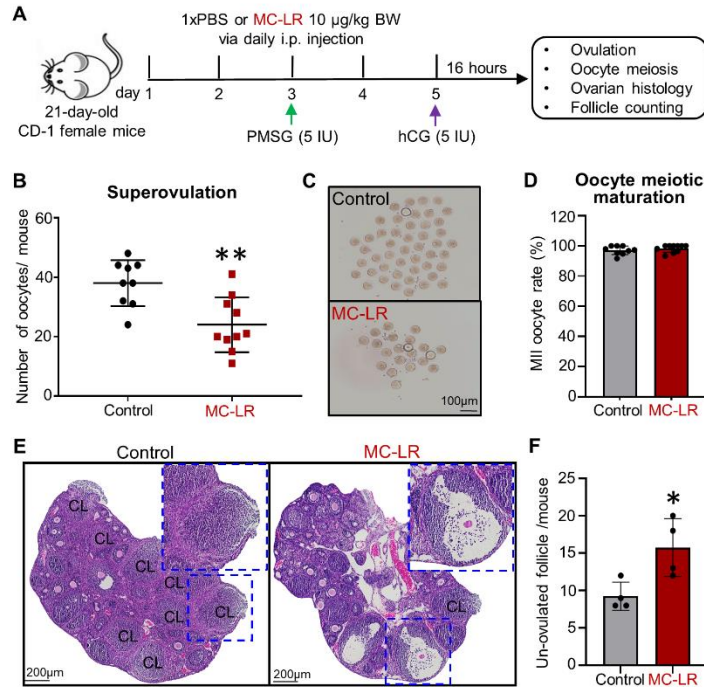


**Figure 3.2** MC-LR compromises mouse follicle ovulation after short-term exposure during both follicle maturation and ovulation windows. (A) A schematic of experimental design of short-term exposure of MC-LR. Twenty-one-day-old CD-1 female mice were daily intraperitoneally (i.p.) injected with PBS or 10 µg/kg MC-LR for 5 days and 5 IU PMSG was injected to stimulate the follicle maturation and 5 IU hCG was injected to induce the ovulation at 46 hours (h) after PMSG treatment. Next, the number of ovulated oocytes and oocyte meiosis were examined. Meanwhile, ovaries were harvested and fixed for histology and un-ovulated follicle counting. (B) Quantification of ovulated oocytes from mice treated with PBS or MC-LR. n = 9-10 female mice in each treatment group. (C) Representative images of harvested oocytes from PBS or MC-LR treated mice. (D) MII oocyte percentage of the ovulated oocytes in the oviduct of mice treated with PBS or MC-LR. (E) Representative histological images of ovaries after the induction of ovulation in the PBS or MC-LR treated mice. Blue dash squares indicate newly-formed corpus luteum or un-ovulated follicle in the PBS or MC-LR treated mouse ovaries, respectively. (F) Total number of un-ovulated follicle per mouse in PBS- or MC-LR- treated mice. n = 4 female mice in each treatment group. Error bar: standard deviation; \*p< 0.05 and \*\*p<0.01.

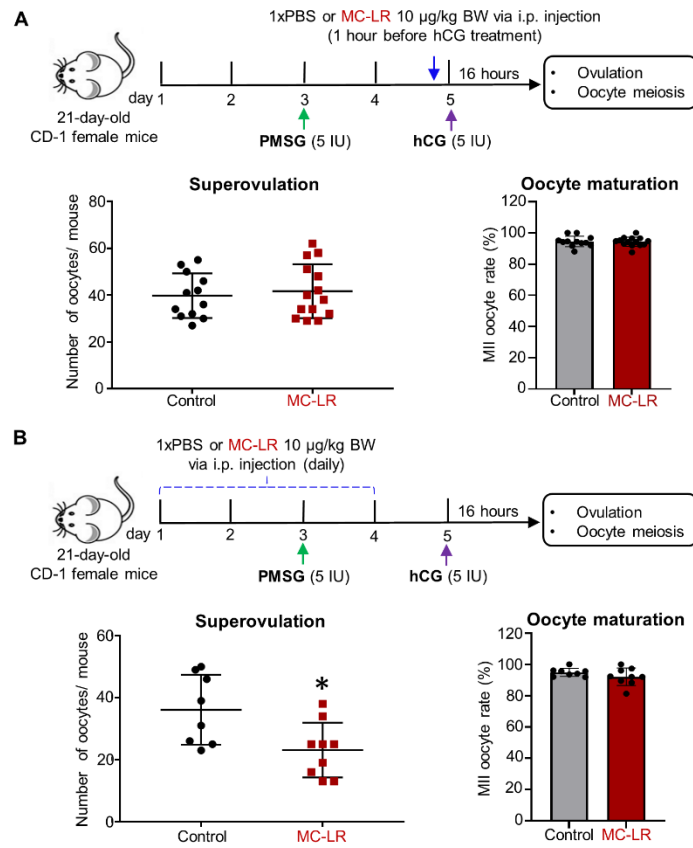


**Figure 3.3** MC-LR compromises mouse follicle ovulation after short-term exposure during follicle maturation window but not the ovulation window. (A) A schematic of experimental design of short-term exposure of MC-LR during ovulation window (top panel). CD-1 female mice were treated with PBS or 10 µg/kg MC-LR at 1 h before hCG treatment and the number of ovulated oocytes and oocyte meiosis were examined at 16 h after hCG treatment. Quantification of ovulated oocytes from mice treated with PBS or MC-LR (bottom left). n = 12-14 female mice in each treatment group. MII oocyte percentage of the ovulated oocytes in the oviduct of mice treated with PBS or MC-LR (bottom right). (B) A schematic of experimental design of short-term exposure of MC-LR during maturation window (top panel). Twenty-one-day-old CD-1 female mice were treated with PBS or 10 µg/kg MC-LR from day 1 to day 4 and the number of ovulated oocytes and oocyte meiosis were examined at 16 h after hCG treatment. Quantification of ovulated oocytes from mice treated with PBS or MC-LR (bottom left). n = 8-9 female mice in each treatment group. MII oocyte percentage of the ovulated oocytes in the oviduct of mice treated with PBS or MC-LR (bottom right). Error bar: standard deviation; \*p < 0.05.

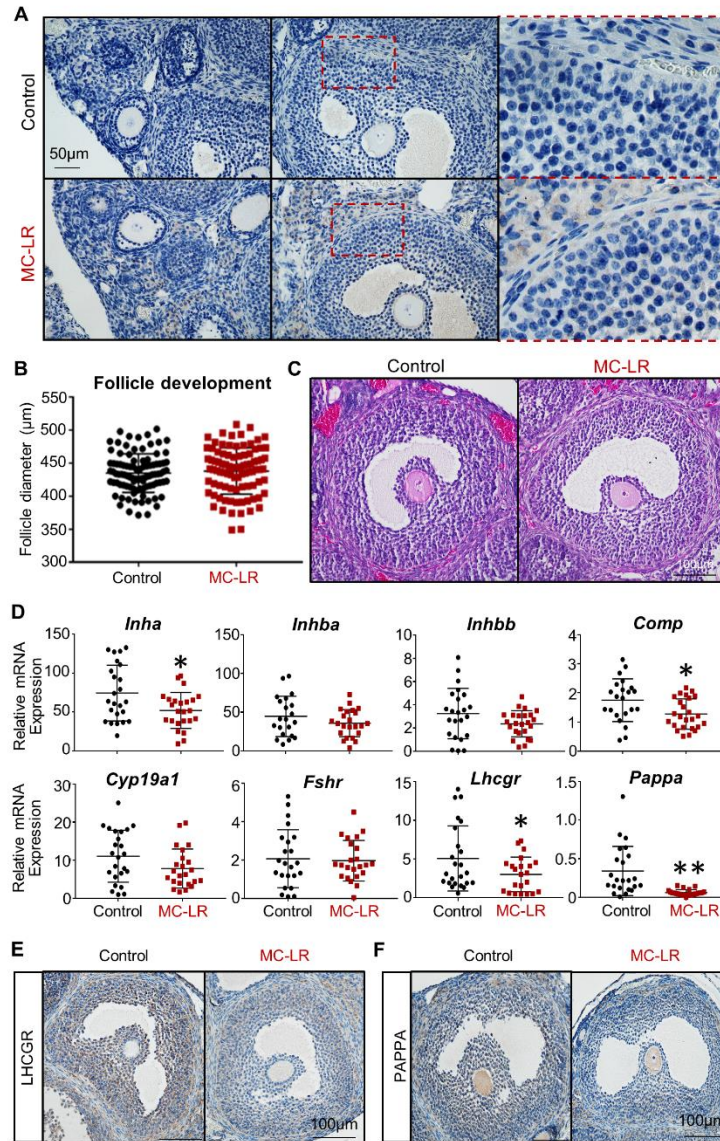


**Figure 3.4** MC-LR accumulates in the ovary and affects the follicle maturation. (A) Accumulation of MC-LR examined by immunohistochemistry (IHC). (B) Preovulatory follicle diameter in PBS or MC-LR treated mouse ovaries.  $n = 91-95$  follicles from 6-8 ovaries in each group. (C) Representative histological images of preovulatory follicles in the PBS or MC-LR treated mice. (D) mRNA expression levels of follicle maturation related genes in isolated preovulatory follicles from PBS or MC-LR treated mice.  $n = 24-25$  follicles from 5 mice in each group. (E and F) Expression of LHCGR (E) and PAPPa (F) proteins in the preovulatory follicles treated with or without MC-LR examined by IHC. Error bar: standard deviation; \* $p < 0.05$  and \*\* $p < 0.01$ .

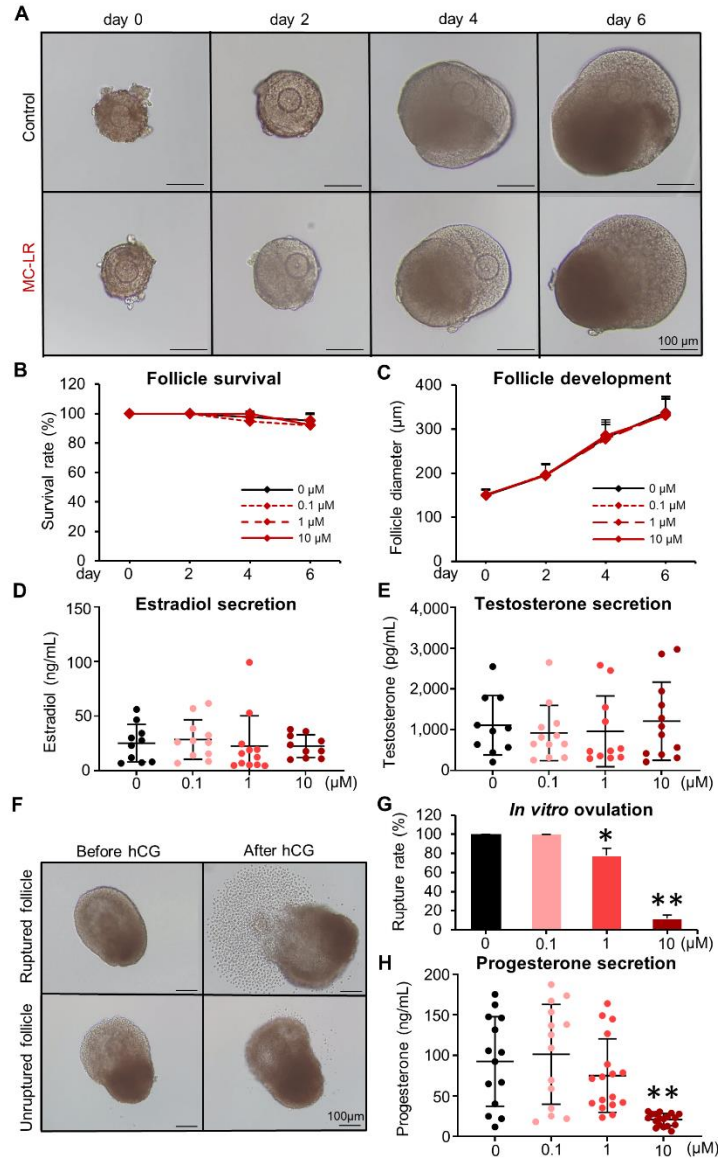


**Figure 3.5** Effect of MC-LR on follicle survival, follicle development, hormone secretion, and follicle ovulation during encapsulated *in vitro* follicle growth (eIVFG). (A) Representative images of follicles treated with or without 10  $\mu\text{M}$  MC-LR on days 0, 2, 4, and 6 of eIVFG. (B) Follicle survival rates and (C) follicle diameters of follicles treated with different concentrations of MC-LR at 0, 0.1, 1, and 10  $\mu\text{M}$  from day 0 to 6 during eIVFG.  $n = 13$ -14 follicles in each experimental group and replicate and 3 replicates were included. (D) 17 $\beta$ -estradiol (E2) and (E) testosterone (T) secretion of different concentrations of MC-LR treated follicles on day 6 of eIVFG.  $n = 10$ -12 follicles in each experimental group. (F) Representative images of ruptured and unruptured follicles before and after hCG treatment. (G) Percentage of ruptured follicles exposed to different concentrations of MC-LR during eIVFG. (H) Progesterone (P4) secretion of different concentrations of MC-LR treated follicles at 48 h after *in vitro* ovulation.  $n = 14$ -17 follicles in each experimental group. Error bar: standard deviation; \* $p < 0.05$  and \*\* $p < 0.01$ .

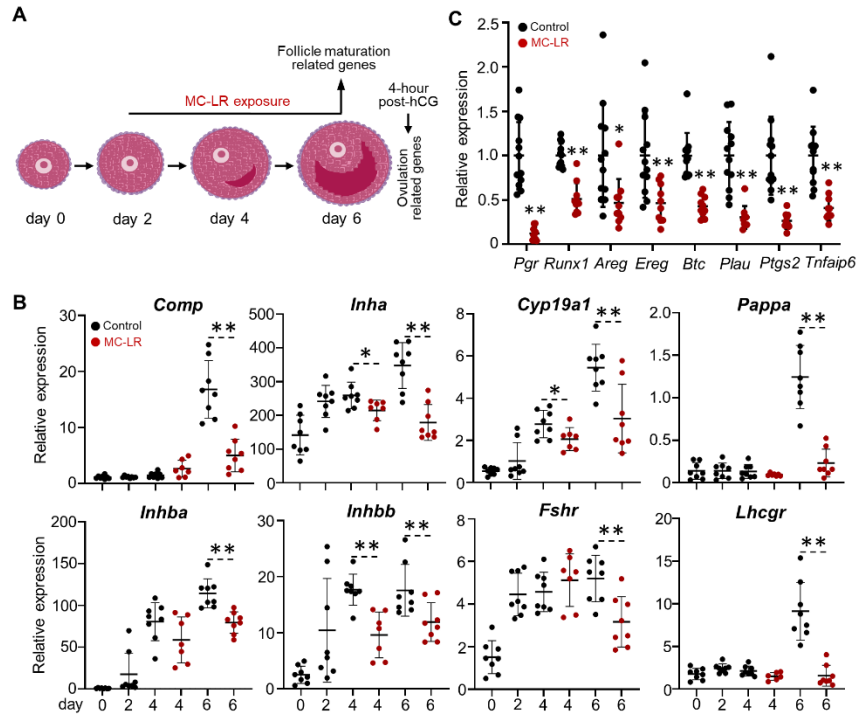


**Figure 3.6** MC-LR treatment affects the follicle maturation and ovulation during eIVFG. (A) A schematic of experimental design for examining the effect of MC-LR on follicle maturation and ovulation during eIVFG. (B) mRNA expression levels of follicle maturation-related genes in control and MC-LR treatment follicles on days 0, 2, 4, and 6.  $n = 7-8$  follicles in each group. (C) mRNA expression levels of follicle ovulation-related genes in control and MC-LR treatment follicles at 4 hours during in vitro ovulation.  $n = 10-12$  follicles in each group. Error bar: standard deviation; \* $p < 0.05$  and \*\* $p < 0.01$ .

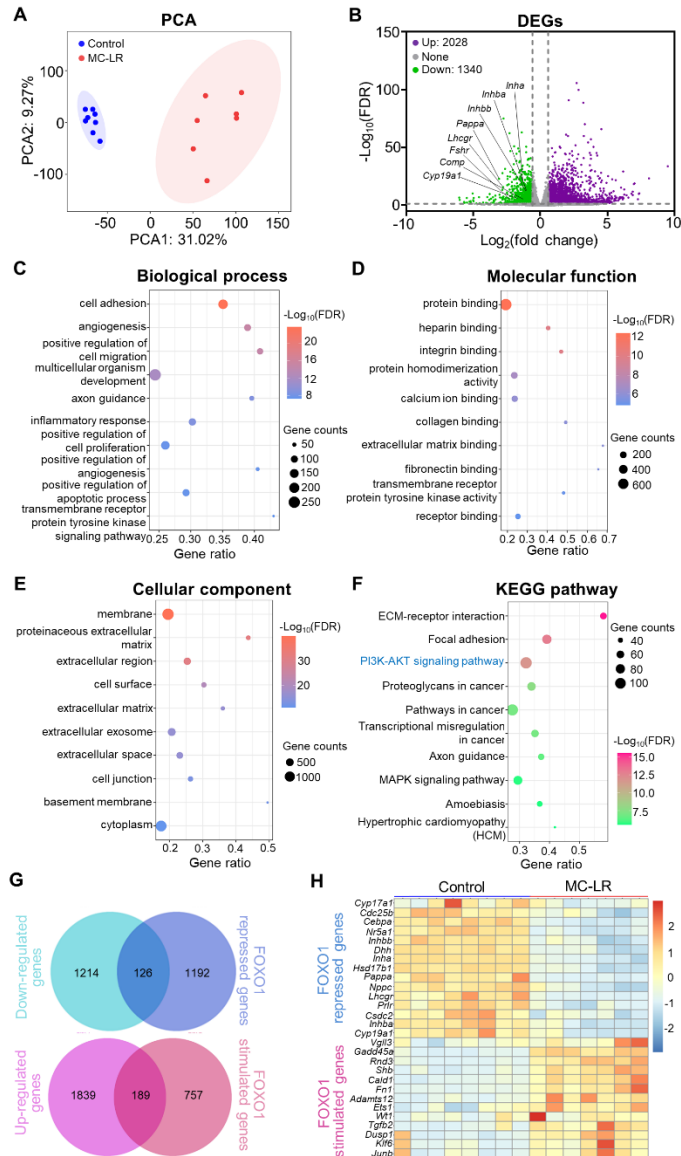


**Figure 3.7** Single-follicle RNA-sequencing identifies that PI3K/AKT/FOXO1 signaling pathway is involved in the MC-LR-disrupted follicle maturation. (A) Principal component analysis (PCA) of the first two principal components between control and MC-LR-treated follicles on day 6 during eIVFG. All follicles were located within the 95% confidence interval, represented by the blue (control) and red (MC-LR) ellipses.  $n=7-8$  follicles in each group. (B) Volcano plot of differentially expressed genes (DEGs,  $FDR < 0.05$ , absolute fold change  $>1.5$  in MC-LR-treated follicles compared to control follicles). Purple: up-regulated genes; gray: non-significantly altered genes; green: down-regulated genes. (C-E) Gene Ontology (GO) analyses of DEGs, including top 10 biological process enrichment results (C), top 10 molecular function enrichment results (D), and top 10 cellular component enrichment results (E). (F) The top 10 KEGG pathway enrichment results of DEGs. KEGG: Kyoto Encyclopedia of Genes and Genomes. (G) Venn diagram showing the number of overlapping genes between MC-LR-induced down-regulated genes and FOXO1-repressed genes (top panel) and the number of overlapping genes between MC-LR-induced up-regulated genes and FOXO1-stimulated genes (bottom panel). (H) Heatmap for representative overlapping genes between MC-LR-induced DEGs and FOXO1-regulated genes.

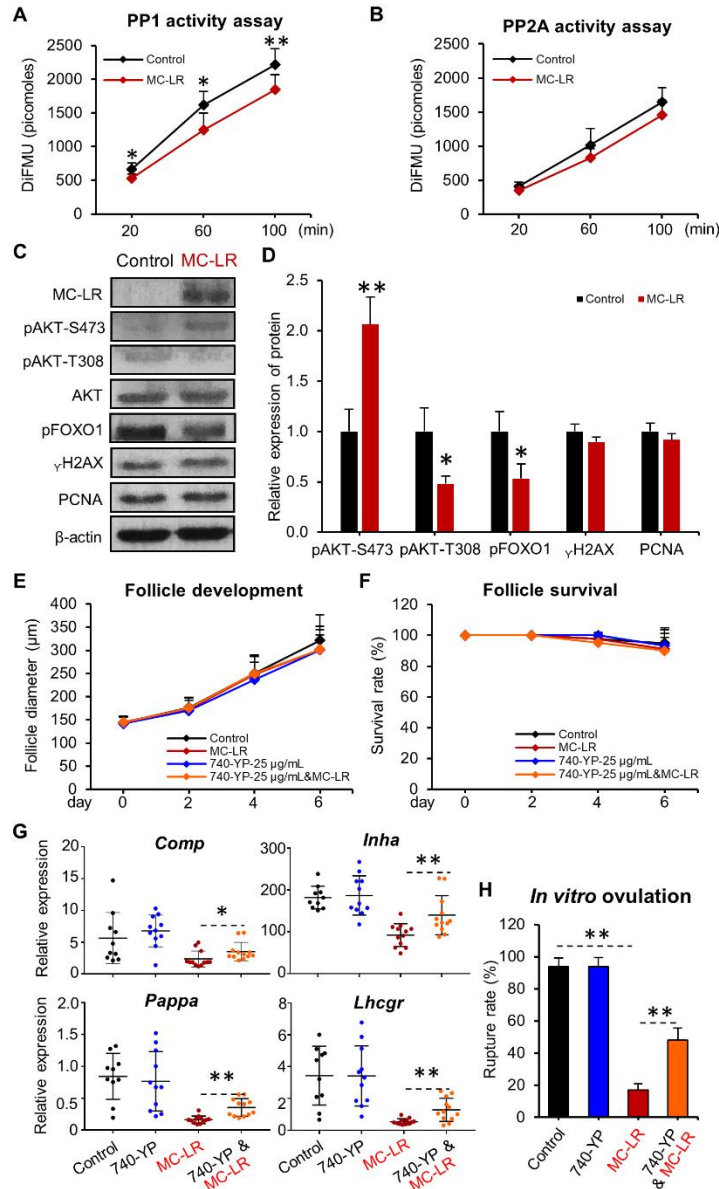


**Figure 3.8** MC-LR inhibits the PP1/PI3K/AKT/FOXO1 signaling pathway. (A and B) A time course of PP1 (A) and PP2A (B) activity assay for MC-LR-treated or untreated follicles. Three independent experiments were performed. (C) Western blotting analysis of MC-LR, YH2AX, PCNA, and PI3K/AKT pathway-related proteins in the follicles treated with or without MC-LR. Three independent experiments were performed. (D) Quantification of the expression of detected proteins. (E) Follicle diameters and (F) follicle survival rates of follicles treated with or without 10 μM MC-LR in the presence or absence of 25 μg/mL 740-YP from day 0 to 6 during eIVFG. n = 12-15 follicles in each experimental group and replicate and 3 replicates were included. (G) mRNA expression levels of follicle maturation-related genes in control, MC-LR treatment, 740-YP treatment, and MC-LR and 740-YP co-treatment follicles on day 6. n = 10-12 follicles in each group. (H) Percentage of ruptured follicles exposed to different treatment with MC-LR and 740-YP during eIVFG. n = 10-12 follicles in each experimental group and replicate and 3 replicates were included. Error bar: standard deviation; \*p<0.05 and \*\*p<0.01.

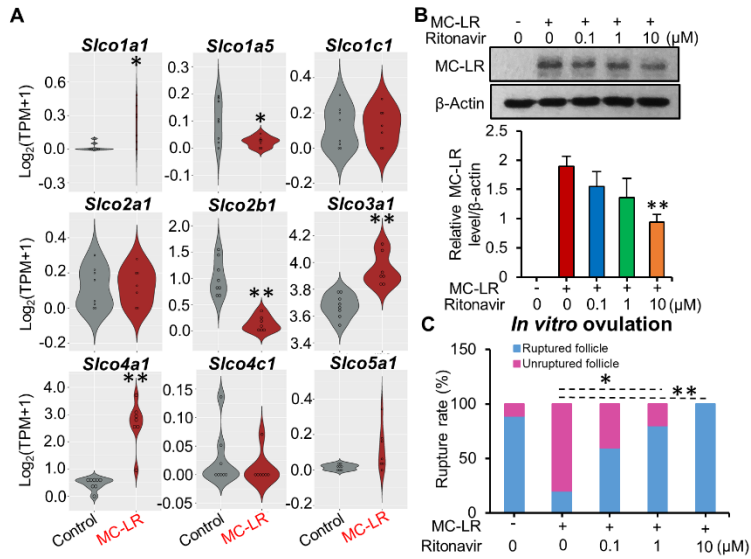


**Figure 3.9** OATP inhibitor Ritonavir blocks the accumulation of MC-LR in follicles and rescues the MC-LR-disrupted follicle ovulation. (A) mRNA expression levels of OATP encoding genes in control and MC-LR treatment follicles.  $n = 7-8$  follicles in each experimental group. (B) Follicle diameters (top panel) and follicle survival rates (bottom panel) of follicles treated with or without 10  $\mu\text{M}$  MC-LR in the presence of different concentrations of Ritonavir from day 0 to 6 during eIVFG.  $n = 10$  follicles in each experimental group. (C) Accumulation of MC-LR examined by western blotting in follicles treated with or without MC-LR in the presence of different concentrations of Ritonavir. The histograms indicated the relative accumulation levels of MC-LR comparing to  $\beta$ -actin. Error bar: standard deviation; \*\* $p < 0.01$ . Three replicates were performed. (D) Percentage of ruptured follicles exposed to different treatment with MC-LR and Ritonavir during eIVFG.  $n = 9-10$  follicles in each experimental group. \* $p < 0.05$  and \*\* $p < 0.01$ .

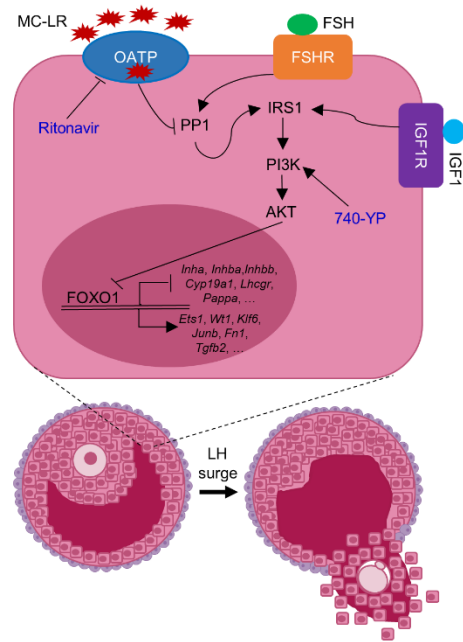


**Figure 3.10** A proposed model for MC-LR-affected follicle maturation and ovulation.

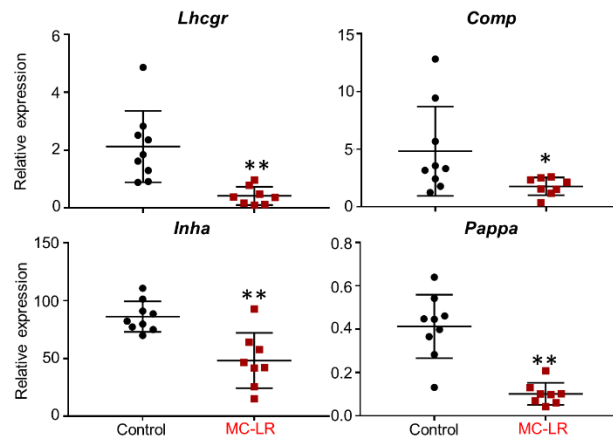


**Figure 3.11** mRNA expression levels of follicle maturation-related genes in the granulosa cells of control and MC-LR treatment follicles on day 6 of eIVFG. n = 8-9 follicles in each group. Error bar: standard deviation; \*p< 0.05 and \*\*p<0.01.

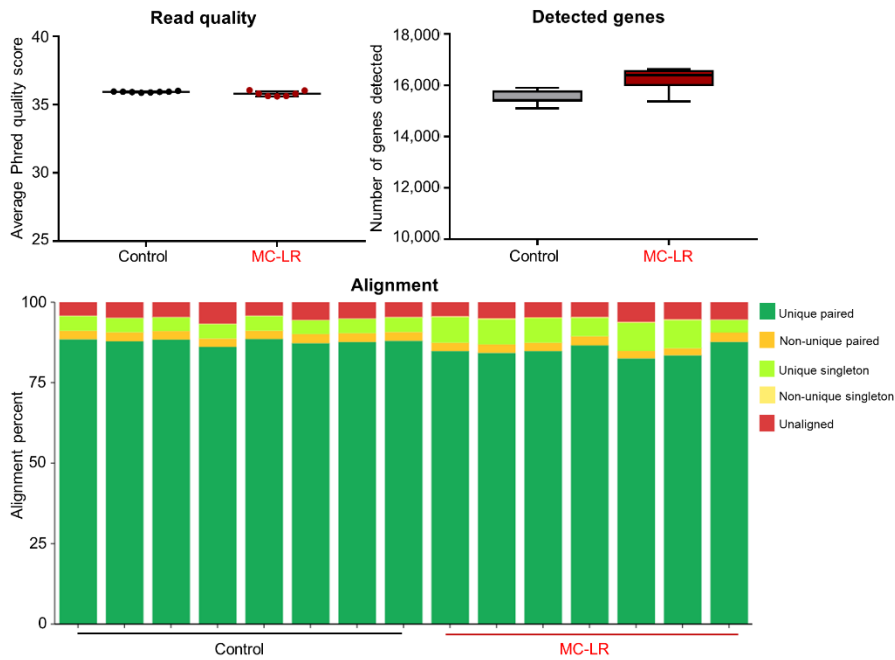


**Figure 3.12** Quality control analysis of single-follicle RNA sequencing for the control and MC-LR treatment follicles.

CHAPTER 4

A CLOSED VITRIFICATION SYSTEM ENABLES A MURINE  
OVARIAN FOLLICLE BANK FOR HIGH-THROUGHPUT  
OVOTOXICITY SCREENING, WHICH DISCOVERS THE ENDOCRINE  
DISRUPTING EFFECT OF MICROCYSTINS

---

Yingzheng Wang, Jingshan Xu, Jessica E. Stanley, Murong Xu, Bryan W. Brooks, Geoffrey I. Scott, Saurabh Chatterjee, Qiang Zhang, Mary B. Zelinski, Shuo Xiao. A closed vitrification system enables a murine ovarian follicle bank for high-throughput ovotoxicity screening, which identifies endocrine disrupting activity of microcystins. *Reprod Toxicol.* 2022 Vol. 93 Pages 118-130.

Reprinted here with the permission of the publisher.

## Abstract

Increasing evidence reveals that a broad spectrum of environmental chemicals and pharmaceutical compounds cause female ovarian toxicity (ovotoxicity). The current gold standard of ovotoxicity testing largely relies on whole laboratory animals, but *in vivo* models are time consuming, costly, and present animal welfare concerns. We previously demonstrated that the 3D encapsulated *in vitro* follicle growth (eIVFG) is a robust *in vitro* model for ovotoxicity testing. However, the follicle preparation process is complex and highly dependent on technical skills. Here, we aimed to use vitrification methods to cryopreserve murine immature follicles for a high-content eIVFG, chemical exposure, and ovotoxicity screening. Results indicated that a closed vitrification system combined with optimized vitrification protocols preserved mouse follicle viability and functionality and vitrified follicles exhibited comparable follicle and oocyte reproductive outcomes to freshly harvested follicles during eIVFG, including follicle survival and development, ovarian steroidogenesis, and oocyte maturation and ovulation. Moreover, vitrified follicles consistently responded to ovotoxic chemical, doxorubicin (DOX). We further used vitrified follicles to test the response of microcystins (MCs), an emerging category of environmental contaminants produced by cyanobacteria associated with harmful algal blooms (HABs), and found that different congeners of MCs exhibited differential ovotoxicities. In summary, our study demonstrates that vitrification enables a long-term-storage and ready-to-use ovarian follicle bank for high-throughput ovotoxicity screening, which identifies endocrine disrupting effects of MCs.

**Keywords:** Vitrification, *in vitro* follicle growth, high-throughput, ovotoxicity, microcystin

#### 4.1 INTRODUCTION

The ovary is the primary female reproductive organ and consists of various developmental stages of follicles as the basic functional unit. Each follicle contains a central germ cell oocyte and the surrounding somatic cells, and functions to secrete steroid and peptide hormones and to mature oocytes for ovulation and fertilization. It is believed that the ovarian follicle pool is established prior to birth and is non-renewable [245]. Thus, chemicals or other factors that compromise the quality and quantity of follicles will result in ovarian toxicity (ovotoxicity) [246]. For instance, increasing evidence reveals that a broad spectrum of both environmental contaminants (e.g., endocrine disrupting chemicals, EDCs) and pharmaceutical compounds (e.g., chemotherapeutics) cause ovotoxicity and increase women's risks of premature ovarian failure (POF), hormonal imbalance, and infertility [31-33].

Thus far, the gold standard for testing the ovotoxicity of chemicals largely relies on the use of whole laboratory animals. However, *in vivo* models are time consuming, costly, and harmful to animals. Additionally, the specific reproductive endpoints in the ovary such as follicle development, oocyte maturation, and ovulation are difficult to monitor in real time without dissecting animals. Furthermore, over 84,000 chemicals are registered and used daily in consumer products, and about 2,000 new chemicals are being introduced each year, making the safety evaluation of all chemicals using whole animals not feasible [41]. These facts indicate that there is an urgent and unmet need to develop an efficient and reliable *in vitro* ovotoxicity screening platform.

In our previous studies, we have used the alginate hydrogel encapsulation method to grow both mouse and human immature follicles *in vitro*, termed encapsulated *in vitro* follicle growth (eIVFG) [34, 35, 247]. The eIVFG maintains the 3D architecture of follicles and support follicle development for maturation, ovarian steroidogenesis, and ovulation, as well as the acquisition of both oocyte meiotic and developmental competence. We further demonstrated that eIVFG is a robust *in vitro* model to screen for the ovotoxicity of xenobiotic exposures [37, 38]. However, the follicle preparation procedure for eIVFG is a complex process and requires multiple rounds of follicle isolation and culture. Furthermore, the ovotoxicity screening costs several weeks or months to complete the chemical exposure and ovotoxicity assessment with multiple concentrations, times, and replicates. These shortfalls make the eIVFG not optimal for a high-throughput ovotoxicity screening, particularly when a rapid screening is desired in the face of unpredictable and emerging environmental threats such as the Deepwater Horizon oil spill in Gulf of Mexico.

Cryopreservation is a process by which cells, tissues, and organs are stored at deep cryogenic temperatures (e.g., -196 °C) for years, including slow freezing and vitrification. Compared to slow freezing, vitrification, a process that allows biological samples to be transformed into a glass-like state at ultra-rapid cooling rate without both extra- and intra-cellular ice formation, is simple, cost-effective, and requires less procedural time. Previous studies have used vitrification method to cryopreserve preantral follicles from various species as an additional option of female fertility preservation [42-48]. However, the recovered follicles have not been performed a systemic evaluation of folliculogenesis and oogenesis or the follicle and/or oocyte quality are compromised. Additionally, it is also

largely unknown whether these vitrified follicles will consistently respond to ovotoxic chemicals compared to freshly harvested follicles.

In the present study, we used a closed vitrification system combined with optimized vitrification protocols to cryopreserve individual murine preantral follicles and demonstrated that vitrification preserved follicle viability and functionality, and vitrified follicles exhibited comparable follicle/oocyte reproductive outcomes to freshly harvested follicles. Moreover, we used doxorubicin (DOX), a commonly used chemotherapeutic chemical that has ovotoxicity [37, 49-51], as the positive control to compare the response of vitrified and fresh follicles during eIVFG. Further, we used vitrified follicles and eIVFG to screen for the ovotoxicity of microcystins (MCs), an emerging category of environmental contaminants associated with harmful algal blooms (HABs) which can present transformational threats to the environment and public health [178]. Our results demonstrate that vitrification enables a long-term-storage and ready-to-use ovarian follicle bank for high-throughput ovotoxicity screening; different MC congeners have differential ovotoxic effects on ovarian follicles, and MC-LF may exhibit endocrine disrupting effects on the ovary.

## 4.2 MATERIALS AND METHODS

### **Animals and follicle isolation**

Animals were treated according to the NIH Guideline for the Care and Use of Laboratory Animals and the approved Institutional Animal Care and Use Committee (IACUC) protocol at the University of South Carolina (UofSC). The CD-1 mouse breeding colony (Charles River Laboratory, Wilmington, MA) was housed in a temperature- and light-controlled animal facility (22°C ± 1°C; 12 h light:12 h dark) with 40-60% humidity

and provided with food and water ad libitum. Pregnant females were checked daily to record the accurate date of birth of pups. Ovaries were removed from 15- or 16-day-old female mice and multilayered secondary follicles were mechanically isolated using insulin syringe needles. Morphologically normal follicles with three to five layers of granulosa cells, intact basement membrane and theca cell layers, and 130-160  $\mu\text{m}$  in diameters were distributed into different experimental groups.

### **Vitrification protocol development, follicle vitrification and warming**

To develop a vitrification protocol that can efficiently and effectively cryopreserve individual follicles, we performed a systemic review of previous studies that vitrified both ovarian tissues or individual follicles of multiple species (Supplemental Table 4.1). It was found that various types of cryo-devices, compositions of CPAs, equilibration time, cooling and warming procedure, and animal species have been used and inconsistent follicle and oocyte reproductive outcomes were observed, indicating that there is no standardized follicle vitrification protocol thus far. For the cryo-device and cooling and warming procedures, here, we elected to use a closed vitrification system with cooling in liquid nitrogen (LN<sub>2</sub>) vapor and a two-phase warming procedure, because Ting *et al.* used this method to cryopreserve macaque ovarian cortex tissues and demonstrated that the ovarian tissues after vitrification and warming maintained follicle integrity and the isolated macaque secondary follicles were able to survive and grow to antral stage using eIVFG [248-250].

To establish an effective murine follicle vitrification protocol, two recipes of vitrification solutions were tested because both of them have shown promising results on cryopreserving ovarian tissues [248-252]. The first vitrification solution used ethylene

glycol (EG) and glycerol (G) as CPAs and synthetic polymers of PXZ (polyvinylpyrrolidone (PVP) K-12; Acros Organics, New Jersey, polyvinylalcohol and polyvinylacetate (PVA); Supercool X-1000TM, and polyglycerol; Supercool Z-1000TM, PXZ; 21st Century Medicine, Fontana, CA) to further inhibit ice nucleation and formation, which was referred to EG+PXZ below. The second vitrification solution used EG, dimethyl sulfoxide (DMSO; Sigma-Aldrich, St. Louis, MO), and sucrose as CPAs, which was referred to EDS below. The EDS vitrification solution has been used to vitrify mouse ovarian tissues and obtained live pups after ovarian tissue transplant, and this recipe has also been clinically applied for cryopreserving ovarian tissues from cancer patients [252, 253]. The detailed recipes of EG+PXZ and EDS vitrification solutions are shown in Table 4.1.

Since the volume of individual follicles are significantly smaller than ovarian cortex tissues, we first performed a preliminary experiment by testing different equilibration times in both vitrification solutions, which allowed us to gain complete follicle vitrification as well as to minimize CPA-induced cytotoxicity. The follicle vitrification procedure and equilibration time are shown in Fig. 4.1. Specifically, for the EG+PXZ vitrification protocol, freshly harvested follicles were sequentially equilibrated in four vitrification solutions containing increasing concentrations of CPAs for 1, 1, and 1 minutes (min) and 10 seconds (sec), respectively (Fig. 4.1). For the EDS vitrification protocol, follicles were sequentially equilibrated in three vitrification solutions containing increasing concentrations of CPAs for 1 min, 3 min, and 10 sec, respectively (Fig. 4.1). Following equilibration, 10-15 follicles were loaded into each 0.25 cc straw (Agtech Inc., Manhattan, KS) containing 100  $\mu$ L of the final vitrification solution and then heat sealed of both ends

and cooled in LN2 vapor for 2 min. Finally, the straws with vitrified follicles were immediately plunged into LN2 for long-term storage.

For both EG+PXZ and EDS vitrification protocols, follicles were warmed using a two-phase warming procedure because it has been demonstrated that this method can effectively avoid devitrification or re-crystallization, a major lethal mechanism to vitrified cells during warming, and can preserve ovarian cell viability and functionality [248]. Briefly, straws containing vitrified follicles were removed from LN2, exposed to room temperature air at 25°C for 5 sec, and then immediately plunged into a 42°C water bath with gentle shaking for 5 sec. Follicles were released by cutting both straw ends and serially incubated in 5 warming solutions with decreasing concentrations of sucrose for 1, 2, 3, 3, and 5 min, respectively (Fig. 4.1). The detailed recipes of warming solutions are shown in Table 4.1. Warmed follicles were transferred and placed in dissection media containing L-15 media with 1% FBS for alginate encapsulation and eIVFG.

### **Follicle encapsulation and eIVFG**

Both freshly harvested follicles and follicles after vitrification and warming were encapsulated for eIVFG as we previously described [34, 35, 247]. Briefly, follicles were individually encapsulated in 0.5% alginate hydrogel (Sigma-Aldrich). Alginate beads were placed into maintenance media containing minimum essential medium ( $\alpha$ MEM Glutamax; Gibco, Grand Island, NY) with 1% FBS for 30 min at 37°C in 5% CO<sub>2</sub> incubator. Then, encapsulated follicles were placed individually in 96-well plate, with each well containing 100  $\mu$ l growth media (50%  $\alpha$ MEM Glutamax and 50% F-12 Glutamax supplemented with 3 mg/mL bovine serum albumin (BSA; Fisher Scientific, Denver, CO), 10 mIU/mL recombinant follicle-stimulating hormone (rFSH; from A.F. Parlow, National Hormone

and Peptide Program, National Institute of Diabetes and Digestive and Kidney Diseases, Bethesda, MD), 1 mg/mL bovine fetuin (Sigma-Aldrich), 5 µg/mL insulin, 5 µg/mL transferrin, and 5 ng/mL selenium (ITS; Sigma-Aldrich). Follicles were cultured at 37°C in 5% CO<sub>2</sub> for 8 days and half of the culture media (50 µl) was exchanged every other day. Follicles were imaged at each media change for survival and diameter assessments using an Olympus inverted microscope with 10x objective (Olympus Optical Co Ltd, Tokyo, Japan). Follicles were considered dead if they had unhealthy appearing oocytes and/or granulosa cells, or if the integrity of the oocyte and somatic cell interface was visibly compromised. The follicle diameter was calculated by averaging 2 perpendicular measurements from one side to another side of basement membrane per follicle using ImageJ software (National Institutes of Health, Bethesda, MD).

### ***In vitro* maturation**

On day 8 of eIVFG, follicles grown to antral stage were removed from alginate beads and treated with  $\alpha$ MEM-based maturation media containing 10% FBS, 1.5 IU/mL human chorionic gonadotropin (hCG), and 10 ng/mL epidermal growth factor (EGF; BD Biosciences, Franklin Lakes, NJ) for 14-16 h at 37°C in 5% CO<sub>2</sub> to trigger *in vitro* ovulation and oocyte maturation. Then, follicles were incubated in L-15 media supplemented with 0.3% hyaluronidase (Sigma-Aldrich) for 3 min at 37 °C and the oocytes were denuded from surrounding cumulus cells by gentle aspiration. The oocytes were considered as metaphase II (MII) oocytes if a polar body was present in the perivitelline space and the MII oocyte percentage was calculated.

### **Oocyte diameter and polar body size measurement**

After *in vitro* maturation, about 30 MII oocytes in each group was randomly selected to detect the oocyte diameter as we previously described [51]. Briefly, the oocyte diameter was obtained from two perpendicular measurements, including the zona pellucida. The first measurement detected the widest diameter of oocyte and the second measurement originated at a right angle from the midpoint of the first measurement. Next, the final oocyte diameter was calculated by averaging these two diameters. Twenty-four to 32 MII oocytes were randomly selected to quantify the first polar body size for the fresh and vitrification groups. The polar body area was measured using ImageJ software (National Institutes of Health, Bethesda, MD) to indicate the polar body size.

### **Oocyte spindle and chromosome structure analysis**

Oocytes retrieved after *in vitro* maturation were fixed in 4% paraformaldehyde (PFA; Sigma-Aldrich) for 30 min and incubated with 0.5% Triton X-100 (Sigma-Aldrich) for 20 min at RT. After incubation in the blocking solution containing 1 x PBS with 0.3% BSA and 0.01% Tween-20 for 1 h, oocytes were incubated with anti- $\alpha$ -tubulin antibody (1:100, Cell Signaling Technology, Danvers, MA) in blocking solution overnight, and the blocking solution without antibody was used as negative control. Oocytes were washed 3 times with blocking solution and mounted using Vectashield containing DAPI (Vector Laboratories, Burlingame, CA). Finally, oocytes were examined using a laser scanning confocal microscope (Carl Zeiss LSM 700, Oberkochen, Germany). Oocytes with barrel-shaped bipolar spindles and well-organized microtubule fibers, along with tightly aligned chromosomes on the metaphase plate was indicated as normal. All other configurations were considered as abnormal.

### **Hormone assay**

The concentration of 17 $\beta$ -estradiol (E2) in the follicle culture media was measured using an ELISA kit (Calbiotech, Spring Valley, CA) according to manufacturer's instructions. Briefly, the anti-estradiol capture antibodies pre-coated wells were incubated with E2 standards, conditioned culture media, and Estradiol Biotin Reagent for 45 min. Next, the Estradiol Enzyme Reagent was added and incubated for another 45 min. After washing the wells with washing buffer three times, the solution of TMB reagent was added and incubated at room temperature for 20 min, resulting in the development of blue color. Last, the reaction was stopped by the addition of Stop Solution and the absorbance was measured using a BioTek Synergy HT microplate reader (BioTek Instruments, Inc., Winooski, VT) at 450 nm within 15 min.

### **Quantitative RT-PCR**

Both freshly harvested and vitrified follicles were collected on day 8 of eIVFG for examining the expression of genes involved in ovarian steroidogenesis and oocyte-specific genes by quantitative reverse transcription PCR (qRT-PCR). Total RNA was extracted using TRIzol (Invitrogen, Carlsbad, CA) according to manufacturer's instructions with 20-30 follicles in each group. Total RNA was then reverse transcribed into cDNA using Superscript III reverse transcriptase with random hexamer primers (Invitrogen, Carlsbad, CA) and stored at -80°C. qPCR was performed in 384-well plate using Power SYBR Green PCR Master Mix (Applied Biosystems, Foster City, CA) on Bio-Rad CFX384 real time system (Bio-Rad, Hercules, CA). qPCR thermocycle was programmed for 10 min at 95 °C, followed by 40 cycles of 15 s at 95 °C and 40 s at 60 °C, and finally a melting stage to determine the specificity of primers. The mRNA expression levels of each genes were

normalized by the expression of glyceraldehyde-3-phosphate dehydrogenase (*Gapdh*). The primer sequences were: *Gapdh* forward: CATCACTGCCACCCAGAAGACTG, *Gapdh* reversed: ATGCCAGTGAGCTTCCCGTTCAG; *Gdf9* forward: GATGGGACTGACAGGTCTGG, *Gdf9* reversed: CAGCGGTCCTGTACCTG; *Bmp15* forward: AAGGGAGAACCGCACGATTG, *Bmp15* reversed: TGCTTGGTCCGGCATTTAGG; *Zp1* forward: TACAAAGGCTGCCACGTTCTA, *Zp1* reversed: TTGGGACAGATCAGTGTGACA; *Zp2* forward: AAGCCTTCCTCAGTCCGAGAA, *Zp2* reversed: CCAGAGCATAAGTGCAGTTCA; *Zp3* forward: ATGGCGTCAAGCTATTTCCCTC, *Zp3* reversed: CGTGCCAAAAGGTCTCTACT; *Star* forward: TTGGGCATACTCAACAACCA, *Star* reversed: CCTTGACATTTGGGTTCCAC, *Cyp11a1* forward: TCAAAGCCAGCATCAAGGAGA, *Cyp11a1* reversed: TGGCAAAGCTAGCCACCTGTA; *Hsd3b1* forward: AGTGATGGAAAAAGGGCAGGT, *Hsd3b1* reversed: GCAAGTTTGTGAGTGGGTTAG; *Cyp17a1* forward: AGTCAAAGACACCTAATGCCAAG, *Cyp17a1* reversed: ACGTCTGGGGAGAAACGGT; *Hsd17b1* forward: ACTGTGCCAGCAAGTTTGCG, *Hsd17b1* reversed: AAGCGGTTCGTGGAGAAGTAG; *Cyp19a1* forward: CATGGTCCCGGAAACTGTGA, *Cyp19a1* reversed: GTAGTAGTTGCAGGCACTTC.

### **Histology and TUNEL assay**

Follicles were fixed in 4% PFA for 2 h at RT and processed for paraffin embedding and serial sectioning at 5 µm. Follicle sections were stained with hematoxylin and eosin (H&E, ThermoFisher Scientific, Waltham, MA) for histological evaluation between

freshly harvested follicles and vitrified-warmed follicles. After DOX exposure, follicle apoptosis was determined using Terminal Deoxynucleotidyl Transferase (TdT) – mediated dUTP Nick-End Labeling (TUNEL) assay using the DeadEnd™ Fluorometric TUNEL System (G3250, Promega, Madison, MI) following manufacturer's instructions.

### **DOX and MCs exposure**

Isolated multilayered secondary follicles were vitrified using EDS based vitrification protocol and were stored in LN2 tank. Upon chemical exposure and eIVFG, follicles were warmed as described in Fig. 4.1. To investigate whether vitrified follicles consistently respond to ovotoxic chemicals compared to freshly harvested follicle, both freshly harvested and vitrified follicles were treated with DOX (Sigma-Aldrich) at 100 nM, a clinically relevant but ovotoxic concentration as we previously demonstrated [37]. Follicles were collected at 6 h and 12 h post treatment and fixed in 4% PFA for paraffin processing.

For the ovotoxicity screening of MCs, vitrified follicles were warmed and exposed to four most common types of MCs, including MC-LA (Cayman Chemicals, Ann Arbor, MI), MC-LF (Enzo Life Sciences, Farmingdale, NY), MC-LR (Cayman Chemicals), and MC-LY (Enzo Life Sciences). Previous studies reported that the serum concentration of MC-LR, the most potent congener of MCs, was at 0.05-1.8 nM in fishermen in Lake Chaohu, China, and 7.6-31.4 nM in patients treated with contaminated dialysate fluids in Caruaru, Brazil [77, 78]. Unfortunately, the effects of MC-LR on female reproductive health, particularly on the ovary, have been scarcely investigated [189]. Thus, we decided to include a broad range of exposure concentrations to gain the first insight into the response of ovarian follicles to MC-LR, including a human relevant exposure

concentration at 0.1  $\mu\text{M}$  and two higher concentrations at 1 and 10  $\mu\text{M}$  during the entire period of eIVFG. Because the *in vivo* exposure data for the other types of MCs are very limited but have been reported to be at the similar order of magnitude to MC-LR [254, 255], we chose the same exposure concentration range from 0 to 10  $\mu\text{M}$  for the MC-LA, MC-LF, and MC-LY. The reproductive endpoints of follicle survival and development, E2 secretion, *in vitro* ovulation, and oocyte meiosis were evaluated as described above.

### **Statistical Analyses**

One-way ANOVA followed by a Tukey's multiple comparisons test was performed to analyze the follicle growth, survival, oocyte and polar body size, and E2 concentration in comparing the freshly isolated follicles and vitrified follicles and in different MC congeners-treated groups at a single time point. Kruskal-Wallis with a Dunn's multiple comparisons test was performed to analyze the steroidogenesis related genes and oocyte-specific genes expression, MII oocyte percentage, and percentage of MII oocytes with normal spindle and chromosome structure.  $P < 0.05$  was considered statistically significant.

## **4.3 RESULTS**

### **Vitrified follicles displayed normal follicle morphology after warming**

The morphology of vitrified follicles was first examined to determine the impact of vitrification on overall follicle and oocyte health. The morphologically normal follicles were defined by the complete granulosa cell and theca cell layers, intact basement membrane, and round shape of central germ cell oocytes. After warming,  $69 \pm 10\%$  and  $97 \pm 3\%$  of vitrified follicles showed normal morphological appearance using EG+PXZ and EDS vitrification solutions, respectively (Fig. 4.2A and 4.2B). For vitrified follicles with abnormal morphology,  $> 90\%$  of them showed distorted oocytes but with normal somatic

cell layers (Fig. 4.2A). Consistently, the morphologically normal vitrified follicles also had normal histological appearance of the somatic cells, oocytes, and entire follicle architecture compared to freshly harvested follicles (Fig. 4.2C).

### **Vitrified follicles had comparable survival rate and development pattern to freshly harvested follicles during eIVFG**

We next included vitrified follicles with normal morphology after warming for eIVFG and compared their follicle and oocyte reproductive outcomes with freshly harvested follicles. The results of eIVFG indicated that the alginate hydrogel encapsulation maintained the 3D architecture of both freshly harvested and vitrified follicles, and supported follicle growth and development from multilayered secondary stage on day 0 to antral stage on day 8 (Fig. 4.3A). For freshly harvested follicles, the follicle diameter increased from  $144 \pm 12 \mu\text{m}$  on day 0 to  $349 \pm 46 \mu\text{m}$  on day 8 (Fig. 4.3B) and the follicle survival rate was  $91 \pm 7\%$  on day 8 (Fig. 4.3C). For vitrified follicles using EG+PXZ and EDS vitrification solutions, the follicle terminal diameters on day 8 were  $339 \pm 34 \mu\text{m}$  and  $324 \pm 27 \mu\text{m}$  and the survival rates were  $90 \pm 8\%$  and  $93 \pm 6\%$ , respectively, which were comparable to freshly harvested follicles (Fig. 4.3B and 4.3C). These results indicate that vitrification preserves follicle viability and vitrified follicles have normal survival rate and developmental pattern during eIVFG.

### **Vitrified follicles exhibited comparable ovarian steroidogenesis to freshly harvested follicles during eIVFG**

To evaluate the ovarian steroidogenesis of vitrified follicles during eIVFG, the expression of steroidogenesis-related genes and hormonal secretion of E2 were examined. Compared to freshly harvested follicles on day 8, qRT-PCR results showed that vitrified

follicles using both EG+PXZ and EDS vitrification protocols had comparable mRNA expression levels of genes that are critical for ovarian steroidogenesis, including *Star*, *Cyp11a1*, *Hsd3b1*, *Cyp17a1*, *Hsd17b1*, and *Cyp19a1* (Fig. 4.4A and 4.4C). At hormonal secretion level, there was no significant difference for the E2 concentrations in follicle culture media on day 8 of eIVFG between freshly harvested follicles and vitrified follicles using both vitrification solutions (Fig. 4.4B). These results suggest that vitrified follicles have normal ovarian steroidogenesis during eIVFG.

#### **Vitrified follicles exhibited normal *in vitro* ovulation and oocyte meiotic maturation**

On day 8 of eIVFG, grown antral follicles were treated with hCG to trigger *in vitro* ovulation and oocyte meiotic division. The ovulated MII oocytes from vitrified follicles had normal appearance (Fig. 4.5A, bright field) and the MII oocyte percentages of vitrified follicles using EG+PXZ and EDS vitrification solutions were  $61 \pm 21\%$  and  $69 \pm 3\%$ , respectively, which were comparable to the MII oocyte percentage of freshly harvested follicles at  $66 \pm 1\%$  (Fig. 4.5B). Moreover, there was no significant difference for the size of both entire MII oocytes and extruded first polar bodies among different groups (Fig. 4.5C and 4.5D).

Because we and others have previously demonstrated that the oocyte polar body extrusion is not a sufficient indicator for oocyte quality, and that a functional spindle is also essential for proper chromosome segregation and producing a haploid gamete [34, 37, 247, 256], we therefore further examined oocyte spindle morphology and chromosome alignment by immunofluorescent staining of oocyte  $\alpha$ -tubulin and chromosomes. Results indicated that  $89 \pm 5\%$  of MII oocytes from freshly harvested follicles had barrel-shaped bipolar spindles and tightly aligned chromosomes on the metaphase plate (Fig. 4.5A and

4.5E), suggesting normal oocyte meiotic division upon in vitro maturation. The MII oocytes from vitrified follicles using EG+PXZ and EDS vitrification solutions had the percentages of normal spindle morphology and chromosome alignment at  $82 \pm 6\%$  and  $82 \pm 4\%$ , respectively, which were slightly decreased compared to freshly harvested follicles but with the difference not statistically significant (Fig. 4.5A and 4.5E). Taken together, these results indicate that vitrified follicles maintain normal functions of in vitro ovulation and oocyte meiotic division.

### **Vitrified follicles had comparable expression of oocyte-specific genes to freshly harvested follicles**

At mRNA level, we further performed qRT-PCR to investigate the expression of 5 oocyte-specific genes, including *Gdf9* and *Bmp15*, two oocyte-derived growth factors in transforming growth factor- $\beta$  (TGF- $\beta$ ) superfamily that are essential for folliculogenesis and oogenesis [257, 258], and *Zp1*, *Zp2*, and *Zp3*, three oocyte zona pellucida-specific genes that are critical for oogenesis, fertilization, and preimplantation embryo development [259, 260]. Results showed that the mRNA expression of all examined oocyte-specific genes were comparable between freshly harvested follicles and vitrified follicles (Fig. 4.5F). These results demonstrate that vitrification preserve normal transcription of oocyte specific genes that are essential for folliculogenesis and oogenesis.

### **DOX exhibited consistent ovotoxicities in vitrified and freshly isolated follicles**

Using both eIVFG and *in vivo* animal models, we have recently demonstrated that the clinically relevant exposure of DOX has a dose-dependent ovotoxicity [37, 38]. At the cellular level, DOX primarily induces DNA damage and apoptosis of granulosa cells and then results in entire follicle apoptosis. Here, we used DOX as a positive control to

determine whether vitrified follicles consistently respond to ovotoxic chemicals [37]. TUNEL staining results showed that DOX at 100 nM primarily induced theca cell apoptosis at 6 h post-DOX treatment and more positive signals were found in both granulosa cell and theca cell layers at 12 h in both vitrified and freshly harvested follicles (Fig. 4.6). These results reveal that DOX consistently induces follicular cell DNA damage and apoptosis in vitrified follicles, providing an efficient and reliable model for eIVFG and *in vitro* ovotoxicity screening.

### **eIVFG using vitrified follicles discovered differential ovotoxicities of different MC congeners**

We next warmed vitrified follicles for eIVFG and screened for the potential ovotoxicity of MCs, including MC-LA, LF, LR, and LY, by investigating the follicle survival and development, E2 secretion, *in vitro* ovulation, and oocyte meiotic maturation. Ovotoxicity screening results indicated that MC-LR was the least ovotoxic MC with comparable follicle survival rates at all exposure concentrations but significantly decreased follicle terminal diameter at 10  $\mu$ M on day 8 of eIVFG (Fig. 4.7A and Supplemental Fig. 4.2). MC-LA, LF, and LY significantly decreased follicle survival rates and inhibited follicle growth at 10  $\mu$ M, however, there was no significant difference when the exposure levels of MC-LA and -LY were at 0.1 and 1  $\mu$ M (Fig. 4.7A and Supplemental Fig. 4.1 and 4.3). MC-LF was found to be the most ovotoxic MC congener and exhibited dose-dependent ovotoxicity (Fig. 4.7). Specifically, MC-LF at 0.1  $\mu$ M did not significantly impact follicle survival and development during eIVFG. However,  $69 \pm 28\%$  of follicles were dead on day 8 when the exposure level was at 1  $\mu$ M, and the average follicle diameter was significantly decreased to  $219 \pm 77 \mu$ m compared to the average follicle diameter at

319 ± 79 μm in the control group (Fig. 4.7). At 10 μM, MC-LF resulted in 100% follicle death on day 2, which were characterized by the dark granulosa cell layers and compromised follicle integrity (Fig. 4.7). We next treated all survived follicles with hCG to trigger *in vitro* ovulation and found that all tested MC congeners did not significantly affect follicle ovulation and oocyte meiotic division if treated follicles could survive and develop to antral stage on day 8 (Fig. 4.7A).

Estradiol is primarily produced in growing follicles and is essential for follicle development and oocyte maturation as well as for the functions of downstream reproductive tract organs such as the uterus and systemic health. Therefore, we next measured the E2 secretion in the conditioned follicle culture media on day 8. ELISA results showed that there was no significant difference for the E2 secretion between control group and follicles treated with MC-LA, LR, and LY at 0.1 and 1 μM (Fig. 4.8). The extremely low concentrations of E2 from follicles treated with MC-LA and LY at 10 μM and MC-LF at 1 and 10 μM (Fig. 4.8) reflected the fact that most of follicles were dead on day 8 (Fig. 4.7). Surprisingly, follicles treated with MC-LF at 0.1 μM did not affect follicle survival and development (Fig. 4.7). However, the E2 secretion was significantly decreased compared to control group (Fig. 4.8). In summary, these results demonstrate that different congeners of MCs exhibit differential ovotoxicities, and MC-LF has dose-dependent toxicities on follicle survival, follicle development, and hormone secretion.

#### 4.4 DISCUSSION

In the present study, we aimed to cryopreserve mouse preantral follicles through vitrification to establish a long-term-storage and ready-to-use ovarian follicle bank, which can be used for a high-throughput *in vitro* ovotoxicity screening. We tested two commonly

used vitrification protocols for cryopreserving ovarian tissues or individual follicles with minor modifications. For the EG+PXZ vitrification protocol, Ting *et al.* used this method to cryopreserve macaque ovarian cortex tissues and demonstrated that the isolated secondary follicles were able to grow to antral stage [248]. Compared to individual cells, larger volume of tissues/organs usually requires longer exposure time and higher concentrations of CPAs to facilitate CPA penetration and avoid intra- and extra-cellular ice formation [261, 262]. However, CPAs are also cytotoxic [263]. Since individual follicles are much smaller than ovarian cortical pieces, we decreased the equilibration time in vitrification solutions to minimize CPA-induced cytotoxicity. For the EDS-based vitrification solution, it has been widely used to cryopreserve ovarian tissues or follicles (Supplemental Table 4.1). Lee *et al.* compared four different compositions of CPAs and found that the EDS-based vitrification solution produced the best follicle survival rates after warming (96%) as well as after an 8-day 2D *in vitro* follicle culture (88%). However, they also discovered that the follicle growth and oocyte maturation outcomes were significantly compromised [264]. Similarly, another three studies also reported that the EDS vitrification protocol was able to result in > 85% follicle survival rate after warming and > 70% survival rate after 2D *in vitro* follicle culture, however, the follicle growth or MII oocyte percentage after *in vitro* maturation was decreased [45, 265, 266]. Compared to their vitrification solution recipes, we increased the final concentration of EG and DMSO from 30% to 40%. As we did in the EG+PXZ vitrification protocol, we also used a closed vitrification system with cooling in LN2 vapor and a two-phase warming procedure, and further included one more step of equilibration in HM without CPA to decrease the potential osmotic shock induced by high concentration of FBS in the following vitrification

solutions [267]. After integrating the optimized cryo-device, vitrification solutions, and cooling and warming procedures, our results demonstrate that both EG+PXZ and EDS protocols can successfully vitrify mouse preantral follicles and the follicle survival rate and developmental pattern during eIVFG are comparable to freshly harvested follicles.

Ovarian steroidogenesis requires bi-communications between theca cells and granulosa cells and multiple steps of enzymatic conversion to produce the final sex steroid hormone, E2 (Fig. 4A) [268]. Most of previously published results showed that vitrified follicles from multiple species had significantly decreased secretion of E2 during *in vitro* follicle/tissue culture, suggesting that the ovarian steroidogenesis pathway was interfered by vitrification (Supplemental Table 4.1). Our study revealed that vitrified follicles using both modified EG+PXZ and EDS vitrification protocols had comparable E2 secretion and mRNA expression of all examined steroidogenesis related genes on day 8 of eIVFG compared to freshly harvested follicles. Therefore, our optimized vitrification protocols maintain hormone synthesis and secretion of follicular somatic cells and the vitrified follicles are good models to study the effect of xenobiotic exposure on ovarian steroidogenesis.

The normal spindle assembly and chromosome alignment during oocyte meiotic division are essential for the formation of a haploid gamete to ensure the success of subsequent fertilization, embryo development, and full-term pregnancy [269]. A majority of previous studies did not examine the spindle and chromosome organization after *in vitro* oocyte maturation (Table 4.2). For the three studies which did, no defect was found [45, 47, 264]. Consistently, our results also showed that vitrified follicles using both EG+PXZ and EDS vitrification protocols produced MII oocytes with normal MII percentage, oocyte

and polar body size, and normal spindle and chromosome organization compared to freshly harvested follicles, suggesting a good in vitro model to study the impact of environmental factors on oocyte meiotic maturation.

Although vitrified preantral mouse follicles can produce live birth following in vitro follicle growth, oocyte maturation, IVF, and embryo transfer, oocytes derived from vitrified follicles had lower developmental competence compared to oocytes grown in vivo [46]. Moreover, vitrification has been found to induce oocyte zona pellucida hardening which might be caused by the presence of calcium in vitrification solution [270, 271]. Our results revealed that vitrification maintain normal expression of two key oocyte-derived growth factors, *Gdf-9* and *Bmp-15*, as well as three zona pellucida related genes, *Zp1*, *Zp2*, and *Zp3*, indicating that the optimized vitrification protocols and eIVFG might be able to maintain oocyte developmental competence. However, future studies such as IVF and in vitro embryo development are necessary to obtain more promising evidence before we use vitrified follicles to study the effect of environmental exposures on oocyte developmental competence during folliculogenesis and oogenesis.

Thus far, there has been no study investigating whether the vitrified-warmed follicles consistently respond to ovotoxic chemicals. We previously demonstrated that DOX induced DNA damage in follicles in a time and cell type dependent manner using cultured freshly isolated follicles [37]. Compared to freshly isolated follicles, our results showed that vitrified follicles had consistent toxic responses after DOX treatment, which enables us to use vitrified follicles for a high-content eIVFG, chemical exposure, and ovotoxicity screening.

HABs have increased significantly and globally in magnitude, frequency, and duration over the past few decades [179, 180]. People can be exposed to HAB toxins through seafood, drinking water, swimming, and contaminated medical solutions [186]. HAB toxins have been demonstrated to exhibit neurotoxicity, hepatotoxicity, and dermal toxicity, etc [89, 188, 189]. However, their impacts on female reproductive health and fertility have not been well studied. MCs are a family of cyclic heptapeptides produced from cyanobacteria (also termed blue-green algae) and are the most common and hazardous type of HAB toxins. The general chemical structure of MCs is cyclo-(D-Ala<sub>1</sub>-X<sub>2</sub>-D-MeAsp<sub>3</sub>-Z<sub>4</sub>-Adda<sub>5</sub>-D-Glu<sub>6</sub>-Mdha<sub>7</sub>), with two variable L-amino acids at the positions two (X) and four (Z) [183]. MCs has been well-characterized as a selective inhibitor of protein serine/threonine phosphatases 2A (PP2A) [272, 273], which results in hyperphosphorylation of proteins, leading to cytoskeleton disruption, oxidative stress, mitochondria dysfunction, endoplasmic reticulum (ER) stress, and DNA damage [94, 274].

Among different MC congeners, MC-LR has been reported to be the most potent PP2A inhibitor [275, 276]. Therefore, most of previous studies only used MC-LR for toxicity testing. However, it is poorly understood whether the other types of MC congeners exhibit similar toxicity or they can disrupt cellular functions through other mechanisms. Our dose-response ovotoxicity screening results revealed that MC-LF, but not the more commonly studied MC-LR, was the most ovotoxic MC congener. More surprisingly, compared to MC-LA, LF, and LY, MC-LR even showed the least adverse impact on follicle survival and development. Similar to our results, MC-LF has been shown to have a more pronounced cytotoxic effects on Caco-2 cells and neuronal cells than MC-LR [188, 277]. These results suggest that, at these higher and pharmacological concentrations, MC-

LA, LF, and LY may cause follicle death through other molecular mechanisms besides the inhibition of PP2A. However, the underlying mechanism of MCs-induced differential ovotoxicities is still unknown and further studies are required. For example, the organic acid transporter polypeptides (OATPs) are the primary transporters to facilitate the uptake and export of MCs in multiple tissues [210]. Therefore, it is worth investigating the expression profile and function of OATPs in the ovary and whether OATPs exert different transporting activities to different MC congeners, which have been poorly studied so far.

Although we found toxic effects of MCs on follicle survival and development when the exposure concentrations were at 1-10  $\mu\text{M}$ , the reported highest human serum level of MCs was at 31.4 nM in patients treated with contaminated dialysate fluids [78], which are 30- to 300-fold lower compared to the ovotoxic concentrations we discovered here. These results suggest that the human relevant exposure level of MCs may not severely affect ovarian follicle survival and development. However, our ovotoxicity screening results also discovered that MC-LF at 0.1  $\mu\text{M}$ , which is only about 3-fold higher than the peak MC serum concentration in humans, significantly inhibit E2 secretion during eIVFG, indicating that the human relevant exposure of MC-LF may interfere with ovarian steroidogenesis and exert an endocrine disrupting effect on the ovary. However, these *in vitro* ovotoxicity screening results will need to be validated using *in vivo* animal models and even human epidemiological studies and the underlying molecular mechanism are necessary to be defined in our future studies.

In summary, our optimized vitrification protocols can be used to establish a long-term-storage and ready-to-use follicle bank, enabling for a high-throughput *in vitro* follicle culture, chemical exposure, and ovotoxicity screening. This platform is not meant to

replace *in vivo* animal models, but it can efficiently and significantly help prioritize chemicals with high ovotoxicity concern for more targeted and mechanistic *in vitro* and *in vivo* toxicity assessments. Additionally, our ovotoxicity screening results show that MCs exhibit endocrine disrupting effect on the ovary. Furthermore, our optimized follicle vitrification protocol provides an additional fertility preservation option, particularly for prepubertal cancer patients who have no mature gametes or embryos available and are also concerned for the risk of metastasis after ovarian tissue transplantation [278].

**Table 4.1** Recipes of vitrification and warming solutions.

<b>Vitrification solutions (EG+PXZ)</b>					
	Solution 1	Solution 2	Solution 3	Solution 4	
Total CPA concentration	5%	15%	30%	50%	
CPA composition	5% G	7.5% G + 7.5% EG	15% G + 15% EG	25% G + 25% EG	
PXZ polymers	NA	NA	NA	3%	
Base medium	L-15 supplemented with 15% FBS and 1 $\mu$ M L-Ascorbic acid 2-phosphate sesquimagnesium salt hydrate (AA2P)				
<b>Vitrification solutions (EDS)</b>					
	Solution 1	Solution 2	Solution 3		
Total CPA concentration	0%	15%	40%		
CPA composition	NA	7.5% EG + 7.5% DMSO	20% EG + 20% DMSO + 0.5 M sucrose		
Base medium	L-15 supplemented with 20% FBS				
<b>Warming solutions (EG+PXZ and EDS)</b>					
	Solution 1	Solution 2	Solution 3	Solution 4	Solution 5
Sucrose concentration	1 M	0.75 M	0.5 M	0.25 M	0 M
Base medium	L-15 supplemented 15% FBS and 1 $\mu$ M AA2P				

\*Notes: G: glycerol; EG: ethylene glycol; P: polyvinylpyrrolidone (PVP); X: Supercool X-1000TM; Z: Supercool Z-1000TM; DMSO: dimethyl sulfoxide; M: mol/L; NA: not applicable.

**Table 4.2:** A summary of previous studies that vitrified ovarian tissues or individual follicles

Ovarian tissue or follicle	Cryo-device	<i>In vitro</i> culture method	Culture period	Vitrification solution recipe	Examined ovarian tissue, follicle, or oocyte reproductive outcomes	Ref
<b>Human</b>						
Preantral follicles	stainless steel mesh	3D	7-d	Vit-1: 10% EG Vit-2: 25% EG Vit-3: 40% EG + 0.6 M sucrose Base media: DPBS with 10% or 20% HSA	81.2% of survival rate immediately after warming; No significant difference in follicle growth; A relatively higher trend of ultrastructure alterations	[42]
Ovarian tissue	Cryovial	3D	8-d	Vit-1: 7.5% EG + 7.5% DMSO Vit-2: 15% EG + 15% DMSO + 0.5 M sucrose Base media: DPBS with 20% HSA	Higher percentage of damaged oocytes and granulosa cells; Delayed follicle growth; Down-regulation of mRNA levels of Zp3, Cyp11a, and Amh	[279]
<b>Macaque</b>						
Ovarian tissue	Aluminum foil and cryovial	3D	10-w	Vit-1: 10% glycerol Vit-2: 10% glycerol + 20% EG Vit-3: 25% glycerol + 25% EG	Vitrification maintained morphology of stoma and secondary follicles; Diminished BrdU uptake; Decreased <i>in vitro</i> follicle survival and growth; Delayed steroid production	[249]

Ovarian tissue	Aluminum foil and cryotube	3D	5-w	Vit-1: 10% glycerol Vit-2: 10% glycerol + 20% EG Vit-3: 25% glycerol + 25% EG + PXZ polymers	Reduced proportion of normal oocytes in secondary follicles; Reduced five-week follicle survival rate and growth; Similar E2 production using polymers	[250]
Ovarian tissue	2 ml high-security tissue straw	3D	6-w	Vit-1: 5% glycerol Vit-2: 25% Vit-4 Vit-3: 50% Vit-4 Vit-4: 27% EG + 27% glycerol Base media: HM supplemented with PXZ, 15% SPS, and 19 µg/ml ascorbic acid phosphate	Reduced E2 production of cultured tissue; Similar six-week follicle survival rate; Smaller follicle diameter at week 6; Similar E2 and P4 production of follicles	[248]
<b>Mouse</b> Preantral follicles	Sterile plastic straw (Cryo-Top method)	2D	12-d	Vit-1: 7.5% EG + 7.5% DMSO Vit-2: 15% EG + 15% DMSO + 0.5 M sucrose Base media: HAMS F-10 with 15% FCS	Partial or total loss of oocyte-granulosa cell apposition and TZPs; Delayed follicle growth; Similar oocyte growth pattern and spindle and chromosomal constitution; Comparable DNA methylation pattern in oocytes	[45]
Preantral follicles	Cryolock	2D	12- d	Vit-1: 7.5% EG + 7.5% DMSO Vit-2: 15% EG + 15% DMSO + 0.5 M sucrose Base media: αMEM with 20%	77.3-84.6% of follicle survival rate at the end of culture; 39.5-66.7% of MII oocyte rate	[265]
Preantral follicles	Cryotop	2D	14-d	Vit-1: 7.5% EG + 7.5% DMSO Vit-2: 15% EG + 15% DMSO + 0.5 M sucrose Base media: αMEM with 20% FBS	97.56% of survival rate after warming; 83.52% of survival rate at the end of culture; Decreased MII oocyte rate; Expression level of Bcl-2, survivin, Bax, Fas, P53 was similar	[280]

Preantral follicles	0.25 ml French straw	Membrane inserts (OGCs culture)	10-d	Vit-1: 2 M EG Vit-2: 6 M EG + 0.3 M raffinose Base media: L-15 with 10% FCS	Lower Viability of OGCs; Proportions of MII oocytes and blastocytes were similar, but lower than the follicles grown <i>in vivo</i>	[46]
Preantral follicles	Nylon mesh, electron microscopy grid, micro-capillary tips	Transwell inserts	10-d	Vit-1: 2 M EG Vit-2: 6 M EG + 0.3 M raffinose Base media: L-15 with 20% SSS	55-62% of follicle survival at the end of IVC; 51-60% of MII oocyte rate; Normal Meiotic spindle assembly	[47]
Secondary follicles	Cryotop	2D	10-d	Vit-1: 7.5% EG + 7.5% DMSO Vit-2: 15% EG + 15% DMSO + 0.5 M sucrose Base media: L-15 with 20% FBS	95.7% of follicle viability after warming; Follicle survival and growth was compromised; 32.7% of MII oocyte rate; Normal Meiotic spindle formation	[264]
Preantral follicles	Cryoloop	2D	10-d	Vit-1: 7.5% EG + 7.5% DMSO Vit-2: 15% EG + 15% DMSO + 0.696 M sucrose + 10 mg/ml Ficoll 70 Base media: MEM with 0.5% BSA	94.0% of follicle recovery rate after warming; 82.3% of survival rate after two days' culture; 70.7% of follicle survival rate at the end of culture; 70.2% of MII oocyte rate	[281]
Ovary	Acupuncture needle	3D	12-d	Vit-1: 7.5% EG + 7.5% DMSO Vit-2: 15% EG + 15% DMSO + 0.5 M sucrose Base media: $\alpha$ MEM with 20% FBS	Decreased follicle survival rate; Similar oocyte maturation rate; Comparable expression levels of Gdf9, Bmp15, Fgf8, KitL, Kit, and Amh	[282]

Ovary	Acupuncture needle	3D	12-d	Vit-1: 1.35 M EG + 1.05 M DMSO Vit-2: 2.70 M EG + 2.10 M DMSO + 0.5 M sucrose Base media: $\alpha$ -MEM supplemented with 20% FBS	Oocyte shrinkage was observed; Number of isolated healthy follicles was decreased; Viability of follicles was significantly decreased; MII oocyte rate was similar; Oocyte maturation genes and oocyte specific genes expressions were similar	[44]
Ovary	Acupuncture needle	2D and 3D	12-d	Vit-1: 7.5% EG + 7.5% DMSO Vit-2: 15% EG + 15% DMSO + 0.5 sucrose Base media: MEM with 20% FBS	77.54% and 65% of survival rates at the end of culture for 2D and 3D culture; 3D culture did not affect the follicle growth; Expression of Gdf9, Bmp15, and Bmp6 was similar	[283]
Ovarian tissue	0.5 ml plastic straw	2D	10-d	40% EG + 30% Ficoll 70 + 1 M sucrose	80% of follicle survival rate after warming; 66.9% of follicle survival rate at the end of culture; Increased expression level of Fas; Lower percentage of intact cells	[285]
Ovary	Transmission electron microscope copper grid	2D	4-h	Vit-1: 7.5% EG + 7.5% DMSO Vit-2: 20% EG + 20% DMSO + 0.5 M sucrose Base media: DPBS with 20% FBS	Decreased number of morphologically intact follicles; Increased apoptotic follicles after culture; EDS showed the best results in ovary vitrification	[286]

**Rat**

Preantral follicles	Open-pulled straw (OPS) and solid-surface (SSV)	3D	3-d	Vit-1: 4% EG Vit-2: 40% EG + 0.5 M sucrose Base media: DPBS with 10% FBS	Decreased viable follicles percentage; Ultrastructural alteration; Decreased follicle growth; Inhibited E2 secretion	[287]
<b>Bovine</b> Secondary follicles	Cryotop	3D	4-w	Vit-1: 7.5% EG + 7.5% DMSO Vit-2: 15% EG + 15% DMSO + 0.5 M sucrose Base media: TCM199 with 20% FCS	50% of follicles were degenerated after 1 week; Similar follicle growth	[288]
Preantral follicles	Metal mesh High Security Vitrification straws	2D and 3D	4-d	Vit-1: 7.5% EG + 7.5% DMSO Vit-2: 15% EG + 15% DMSO + 0.5 M sucrose Base media: M199 with 10 mg/ml BSA	2D culture was more effective in vitrifying follicles; Embedding in alginate allowed to handle follicles more efficiency	[289]
Ovarian tissue	Aluminum foil	3D	20-d	Vit-1: 10% glycerol Vit-2: 10% glycerol + 20% EG Vit-3: 25% glycerol + 25% EG	20% of follicle survival rate at the end of culture; Similar Follicle diameter; Lower antrum formation rate	[290]
<b>Ovine</b>						
Secondary follicles	Metal cube	2D	6-d	Vit-1: 12.5% Vit-4 Vit-2: 25% Vit-4 Vit-3: 50% Vit-4 Vit-4: 2.60 M acetamide + 2.62 M DMSO + 1.31 M PrOH + 0.0075 M PEG Base media: MEM with 10% FBS	Decreased follicle viability; Decreased daily follicular growth rate	[292]
Secondary follicles	Metal cube	2D	18-d	Vit-1: 12.5% Vit-4 Vit-2: 25% Vit-4 Vit-3: 50% Vit-4	Compromised follicle growth; Decreased expression of Cx37 and 43; Decreased oocyte maturation rate	[293]

				Vit-4: 2.60 M acetamide + 2.62 M DMSO + 1.31 M 1,2-propanediol + 0.0075 M polyethylene glycol Base media: MEM with 10% FBS		
Secondary follicles and ovarian tissue	Metal cube	2D	18-d	Vit-1: 12.5% Vit-4 Vit-2: 25% Vit-4 Vit-3: 50% Vit-4 Vit-4: 2.60 M acetamide + 2.62 M DMSO + 1.31 M 1,2- propanediol + 0.0075 M polyethylene glycol Base media: MEM with 10% FBS	97.5% of morphologically normal follicles; Similar follicle growth; Decreased E2 production; Increased progesterone secretion; No MII oocyte	[48]
Preantral follicles	Stainless mess	3D	10-d	Vit-1: 7.5% EG + 7.5% DMSO Vit-2: 20% EG + 20% DMSO + 0.5 M sucrose Base media: TCM-199 with 20% SSS	Decreased E2 and progesterone production	[251]

---

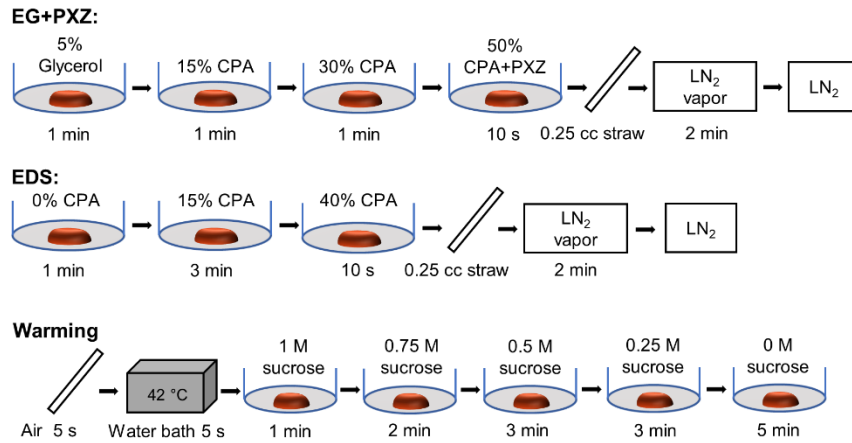


**Figure. 4.1** Procedures of ovarian follicle vitrification and warming. Freshly harvested follicles were sequentially equilibrated in EG+PXZ and EDS vitrification solutions containing increasing concentrations of CPAs. Follicles were next loaded into 0.25 cc straw, cooled in LN<sub>2</sub> vapor, and plunged into LN<sub>2</sub> for long-term storage. The follicle retrieval was performed using a two-phase warming procedure followed by five sequential incubations in warming solutions with decreasing concentrations of sucrose. CPA, cryoprotective agents; PXZ, polyvinylpyrrolidone (PVP) K-12, Supercool X-1000TM, and Supercool Z-1000TM; LN<sub>2</sub>, liquid nitrogen.

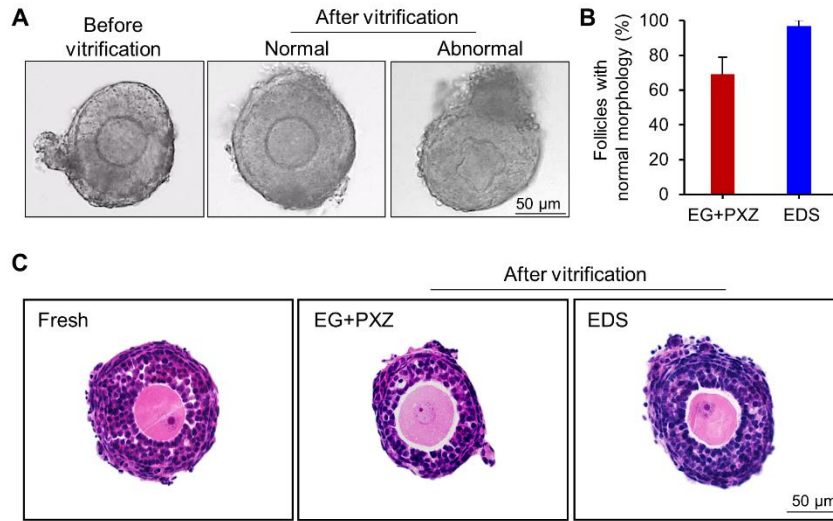


**Figure 4.2** Follicle morphology after vitrification and warming. (A) Representative images of freshly harvested follicles and vitrified follicles immediately after warming. (B) Percentage of vitrified follicles with normal morphology using EG+PXZ and EDS vitrification solutions. Error bar: standard deviation. (C) Representative histological images of freshly harvested and vitrified follicles with normal morphology. N=20-40 follicles in each experimental group and 5 replicates were performed.

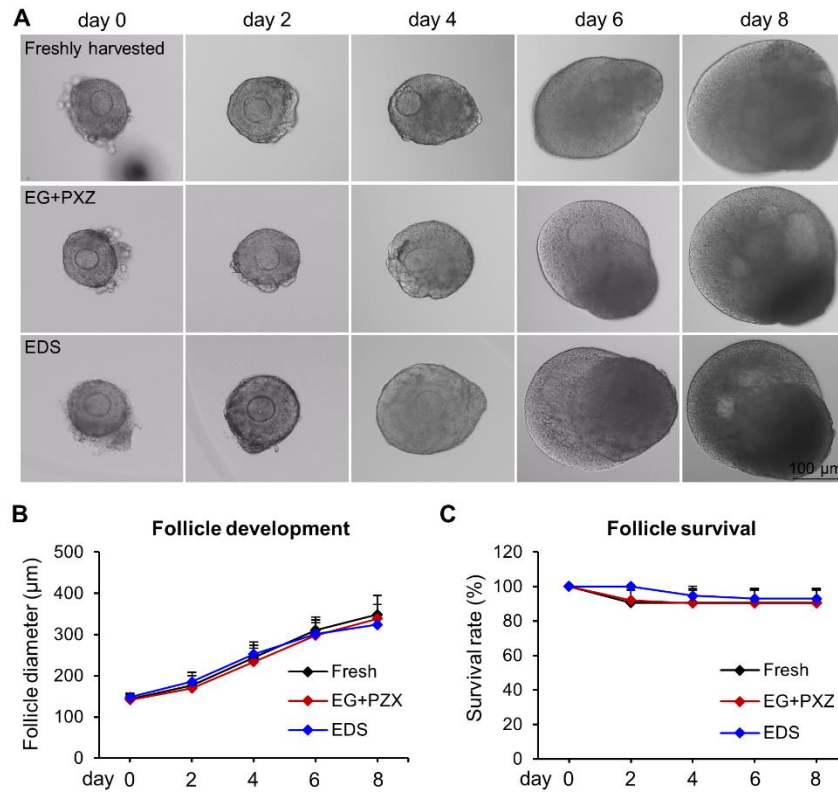


**Figure 4.3** Effect of vitrification on follicle growth and survival during encapsulated *in vitro* follicle growth (eIVFG). (A) Representative images of freshly harvested and vitrified follicles on days 0, 2, 4, 6, and 8 of eIVFG. (B) Follicle diameters and (C) follicle survival rates from day 0 to 8 during eIVFG. Error bar: standard deviation. N=15-20 follicles for each experimental group and 3 replicates of eIVFG were performed.

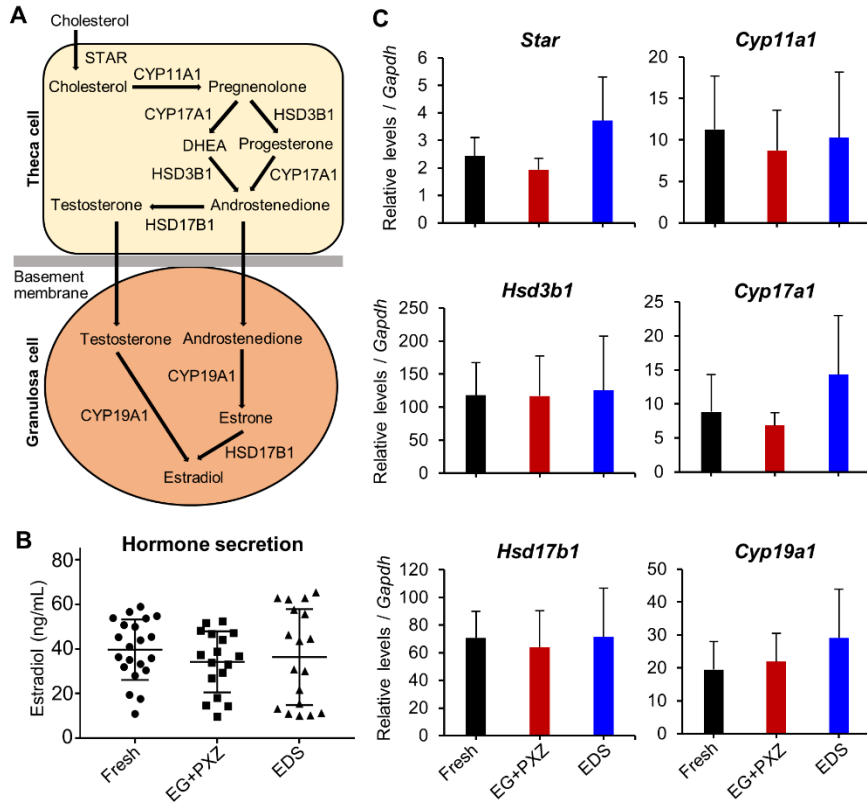


**Figure 4.4** Effect of vitrification on the mRNA expression of ovarian steroidogenesis related genes and 17 $\beta$ -estradiol (E2) secretion. (A) Classic ovarian steroidogenesis pathway in follicular cells. (B) Concentration of E2 in follicle culture media on day 8 of eIVFG measured by ELISA. (C) mRNA expression levels of steroidogenesis related genes in freshly harvested and vitrified follicles on day 8 of eIVFG. Error bar: standard deviation. For E2 concentration analysis, N=6-7 follicles in each group for each replicate and three replicates was performed. For mRNA expression analysis, N=20-30 follicles in each group for each replicate and three replicates were included.

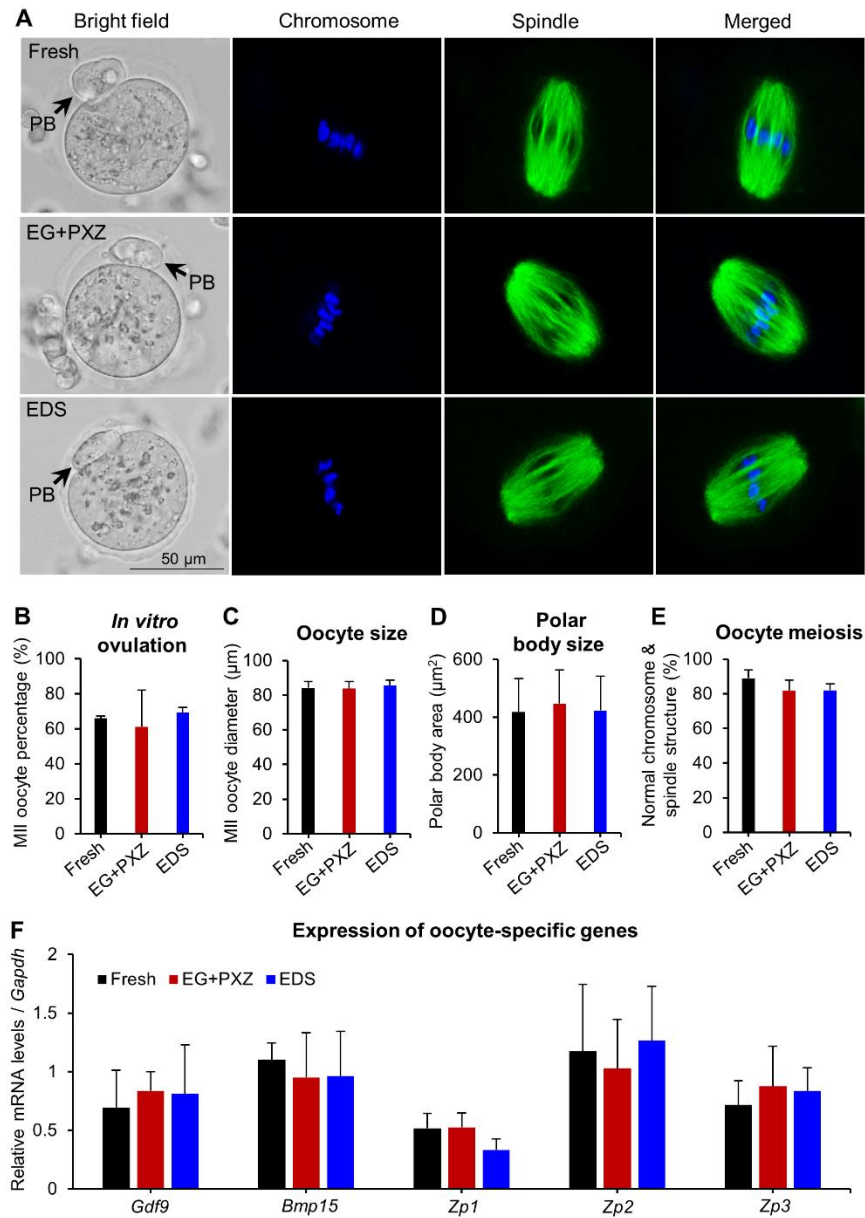


**Figure 4.5** Effect of vitrification on oocyte meiotic maturation after *in vitro* maturation. (A) Representative images of metaphase II (MII) oocyte morphology, chromosome distribution (blue) and spindle morphology (green) from freshly harvested and vitrified follicles. PB: polar body. Blue: DAPI; green:  $\alpha$ -tubulin. (B) MII oocyte percentage after *in vitro* oocyte maturation. (C) MII oocyte diameter after *in vitro* oocyte maturation. (D) The size of first polar body after *in vitro* oocyte maturation. (E) Percentage of oocytes with normal spindle morphology and chromosome alignment. (F) mRNA expression of oocyte specific genes in freshly harvested and vitrified follicles on day 8 of eIVFG. For all examined parameters in A-E, there were N=7-20 follicles in each experimental group and replicate and 3 replicates were included. For mRNA expression analysis, N=20-30 follicles in each group for each replicate and three replicates were included.

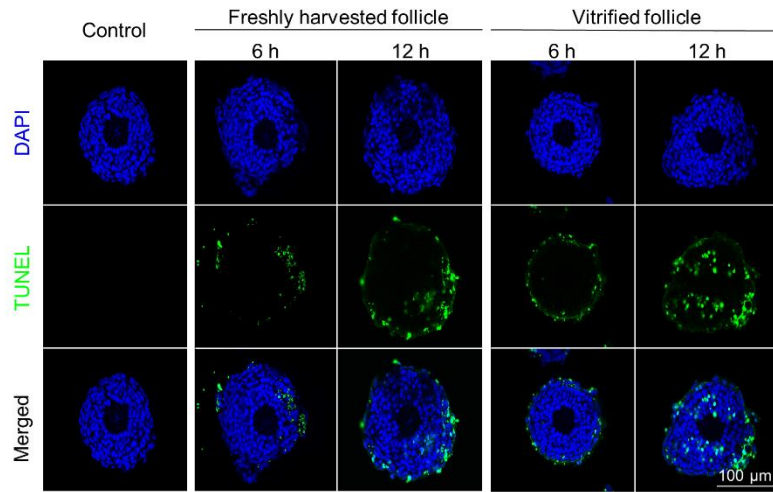


**Figure 4.6** Ovotoxicity testing of doxorubicin (DOX) using vitrified and warmed follicles, with representative TUNEL images of follicles treated with DOX at 100 nM for 0, 6, and 12 hours. Blue: DAPI; green: DNA fragmentation revealed by TUNEL staining. N=5-6 follicles in each experimental group for each time point and replicate and three replicates were performed.

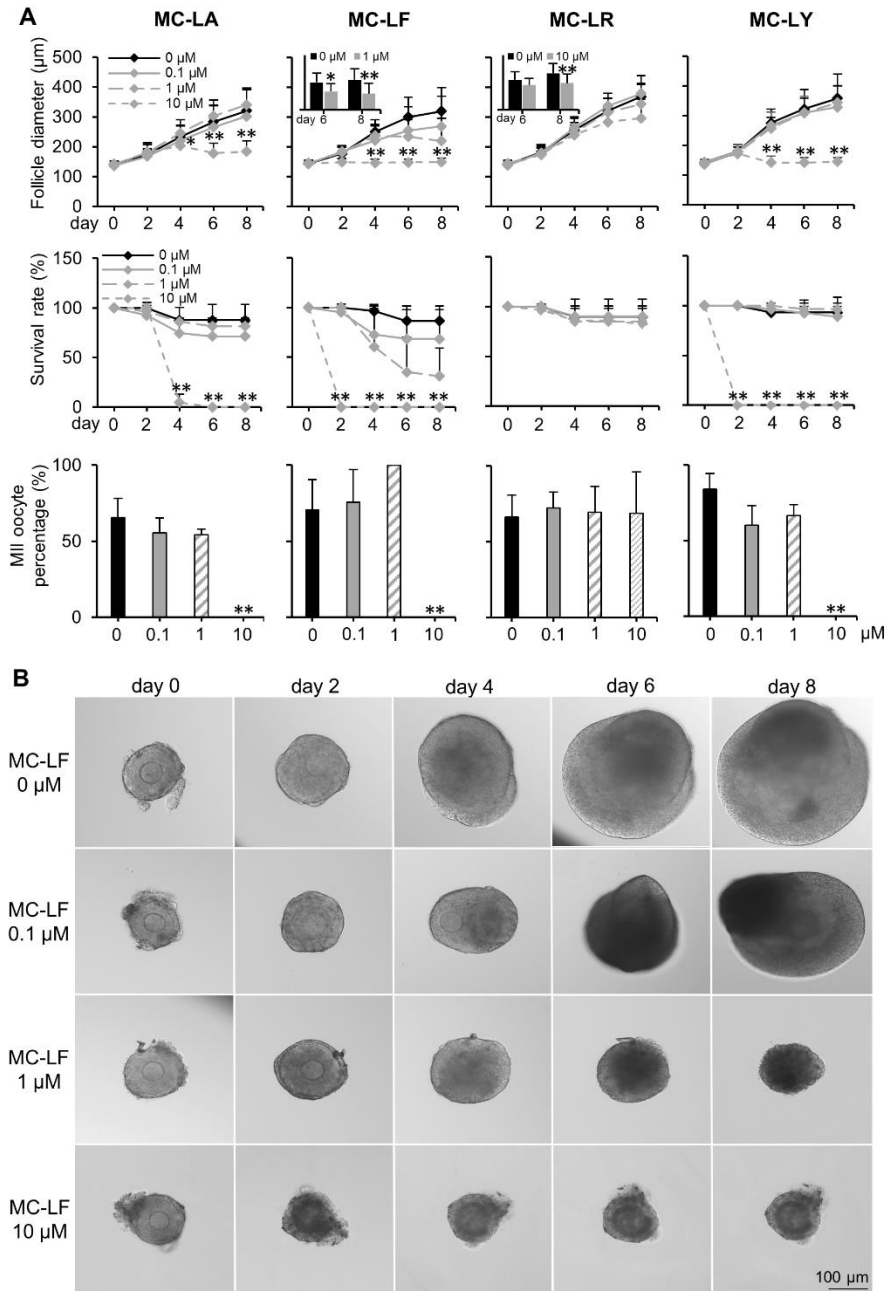


**Figure 4.7** Effect of different congeners of microcystins (MCs) on follicle growth, survival, and oocyte maturation during encapsulated in vitro follicle growth (eIVFG) using vitrified and warmed follicles. (A) Follicle diameter, survival rate, and MII oocyte percentage after in vitro oocyte maturation upon different congeners and concentrations of MCs exposure. (B) Representative images of follicles treated with different concentrations of MC-LF on days 0, 2, 4, 6, and 8 during eIVFG. Error bar: standard deviation; \* $p < 0.05$  and \*\* $p < 0.01$ .  $N = 8-10$  follicles in each group for each replicate and 3 replicates were performed.

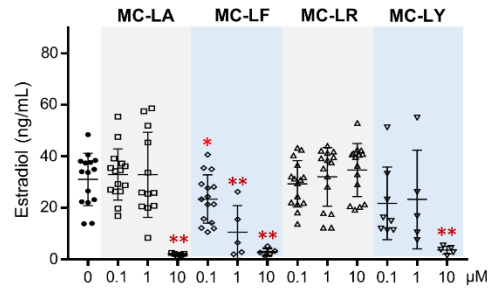


**Figure 4.8** Effect of different congeners and concentrations of microcystins (MCs) on 17 $\beta$ -estradiol (E2) secretion of *in vitro* cultured vitrified and warmed follicles on day 8 of eIVFG. Error bar: standard deviation; \* $p < 0.05$  and \*\* $p < 0.01$ . N=5-15 follicles in each group and 3 replicates were performed.

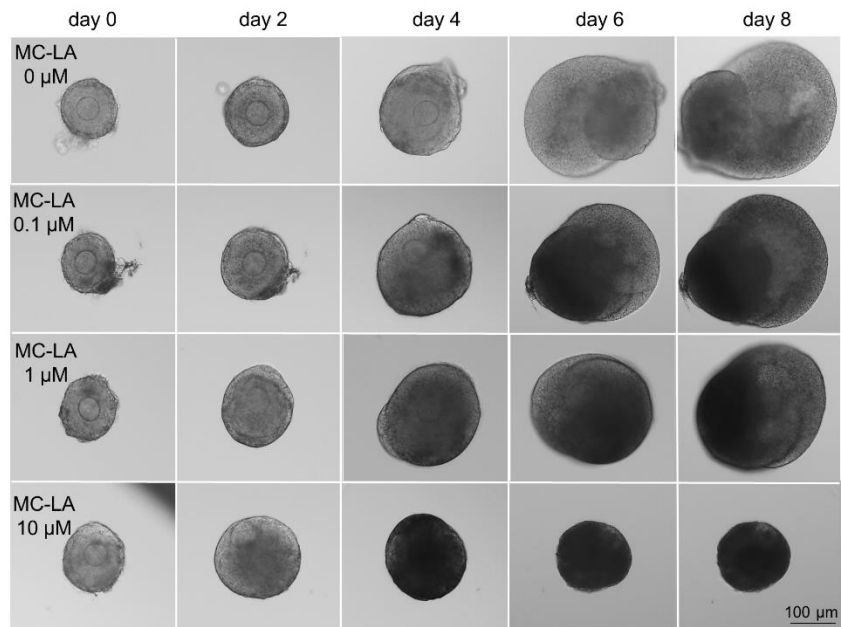


**Figure 4.9** Representative images of follicles treated with different concentrations of microcystin-LA (MC-LA) on days 0, 2, 4, 6, and 8 during eIVFG. N=7-10 follicles in each group for each replicate and 3 replicates were performed.

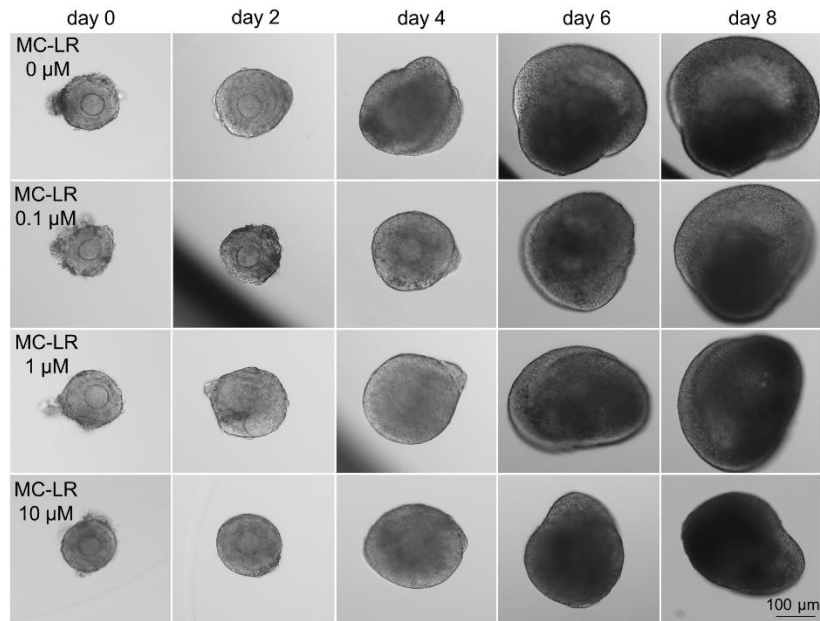


**Figure 4.10** Representative images of follicles treated with different concentrations of microcystin-LR (MC-LR) on days 0, 2, 4, 6, and 8 during eIVFG. N=8-10 follicles in each group for each replicate and 3 replicates were performed.

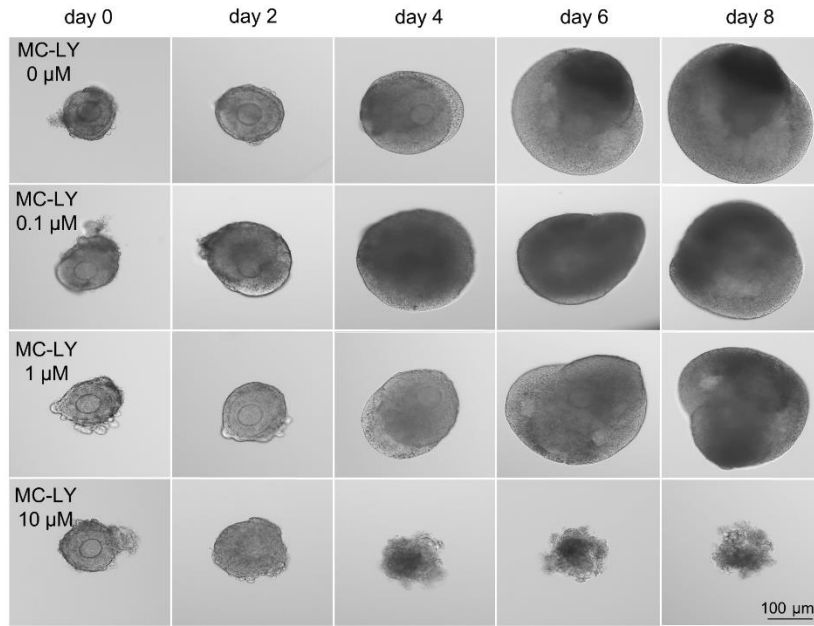


**Figure 4.11** Representative images of follicles treated with different concentrations of microcystin-LY (MC-LY) on days 0, 2, 4, 6, and 8 during eIVFG. N=8-10 follicles in each group for each replicate and 3 replicates were performed.

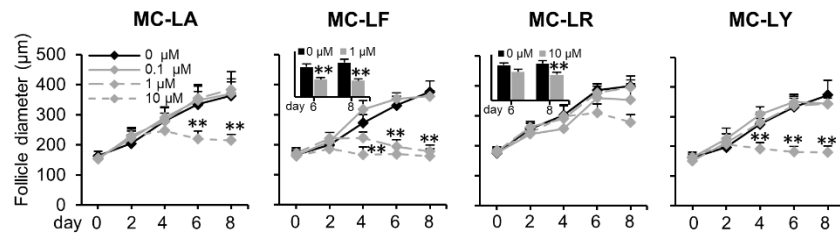


**Figure 4.12** Effect of different congeners of microcystins (MCs) on follicle growth during encapsulated *in vitro* follicle growth (eIVFG) using freshly harvested follicles. Error bar: standard deviation; \*\* $p < 0.01$ . N=8-12 follicles in each group.

## CHAPTER 5

### CONCLUSION

Due to the climate change-associated temperature rise and anthropogenic eutrophication, harmful algal blooms have become a global emerging environmental concern in water bodies. Increasing evidence demonstrates that HAB-produced toxin MCs pose a threat to the health of humans and animals. Here, I focused on investigating the toxic effects and mechanisms of HAB toxin MC-LR on the female reproduction. I found that MC-LR could accumulate in the ovarian cells, including ovarian stroma cells, theca cells, and granulosa cells of antral follicles. Using both *in vivo* mouse exposure model and *in vitro* 3D follicle culture model, results revealed that MC-LR did not affect follicle growth, but disrupted FSH-dependent follicle maturation. Furthermore, in-depth mechanistic studies suggested that MC-LR disrupted PP1-mediated activation of PI3K/AKT/FOXO1 signaling in follicular granulosa cells to compromise the FSH-dependent follicle maturation which further damaged the following ovulation.

To develop an efficient and reliable *in vitro* ovotoxicity screening platform, I used a closed vitrification system combined with optimized vitrification protocols to cryopreserve murine immature follicles for a high-content eIVFG and ovotoxicity screening. Results indicated that the newly developed vitrification protocol preserved mouse follicle viability and functionality and vitrified follicles exhibited comparable follicle and oocyte reproductive outcomes to freshly harvested follicles during eIVFG, including follicle survival and development, ovarian steroidogenesis, and oocyte

maturation and ovulation. I further used vitrified follicles to test four MC congeners, including MC-LA, LF, LR, and LY, and found that different congeners of MCs exhibited differential ovotoxicities. These results demonstrate that vitrification enables a long-term-storage and ready-to-use ovarian follicle bank for high-throughput ovotoxicity screening.

Overall, my research has shown that HAB toxin MC-LR can adversely affect the female reproduction by compromising follicle maturation and ovulation. Moreover, I developed an efficient and reliable *in vitro* ovotoxicity screening platform using vitrified follicles which enables a high-throughput screening the ovotoxicity of MC congeners and other environmental contaminants.

## REFERENCES

1. Sandifer, P.A., et al., *Chapter 12 - Oceans and Human Health and the New Blue Economy*, in *Preparing a Workforce for the New Blue Economy*, L. Hotaling and R.W. Spinrad, Editors. 2021, Elsevier. p. 213-236.
2. Sellner, K.G., G.J. Doucette, and G.J. Kirkpatrick, *Harmful algal blooms: causes, impacts and detection*. J Ind Microbiol Biotechnol, 2003. **30**(7): p. 383-406.
3. Pham, T.L. and M. Utsumi, *An overview of the accumulation of microcystins in aquatic ecosystems*. J Environ Manage, 2018. **213**: p. 520-529.
4. Breda-Alves, F., V.D. Fernandes, and M.A. Chia, *Understanding the environmental roles of herbicides on cyanobacteria, cyanotoxins, and cyanoHABs*. Aquatic Ecology, 2021. **55**(2): p. 347-361.
5. Du, X., et al., *The Diversity of Cyanobacterial Toxins on Structural Characterization, Distribution and Identification: A Systematic Review*. Toxins (Basel), 2019. **11**(9).
6. Buratti, F.M., et al., *Cyanotoxins: producing organisms, occurrence, toxicity, mechanism of action and human health toxicological risk evaluation*. Arch Toxicol, 2017. **91**(3): p. 1049-1130.
7. Christiansen, G., et al., *Microcystin biosynthesis in planktothrix: genes, evolution, and manipulation*. J Bacteriol, 2003. **185**(2): p. 564-72.
8. Xie, L., et al., *The impact of environmental parameters on microcystin production in dialysis bag experiments*. Sci Rep, 2016. **6**: p. 38722.
9. Bouaicha, N., et al., *Structural Diversity, Characterization and Toxicology of Microcystins*. Toxins (Basel), 2019. **11**(12).
10. Ferrao-Filho Ada, S. and B. Kozlowsky-Suzuki, *Cyanotoxins: bioaccumulation and effects on aquatic animals*. Mar Drugs, 2011. **9**(12): p. 2729-72.
11. Wijewickrama, M.M. and P.M. Manage, *Accumulation of Microcystin-LR in Grains of Two Rice Varieties (Oryza sativa L.) and a Leafy Vegetable, Ipomoea aquatica*. Toxins (Basel), 2019. **11**(8).
12. Vidal, F., et al., *Recreational Exposure during Algal Bloom in Carrasco Beach, Uruguay: A Liver Failure Case Report*. Toxins (Basel), 2017. **9**(9).
13. Pouria, S., et al., *Fatal microcystin intoxication in haemodialysis unit in Caruaru, Brazil*. Lancet, 1998. **352**(9121): p. 21-6.
14. *Cyanobacterial toxins: microcystins. Background document for development of WHO Guidelines for drinking-water quality and Guidelines for safe recreational water environments*.  
  
*Geneva: World Health Organization; 2020 (WHO/HEP/ECH/WSH/2020.6). Licence: CC BY-NC-SA 3.0 IGO.*
15. USEPA, *Recommendations for Cyanobacteria and Cyanotoxin Monitoring in Recreational Waters*. 2019.
16. Graham, J.L., et al., *Cyanotoxin mixtures and taste-and-odor compounds in cyanobacterial blooms from the Midwestern United States*. Environ Sci Technol, 2010. **44**(19): p. 7361-8.

17. Lu, H., et al., *Characterization of organic anion transporting polypeptide 1b2-null mice: essential role in hepatic uptake/toxicity of phalloidin and microcystin-LR*. *Toxicol Sci*, 2008. **103**(1): p. 35-45.
18. Komatsu, M., et al., *Involvement of mitogen-activated protein kinase signaling pathways in microcystin-LR-induced apoptosis after its selective uptake mediated by OATP1B1 and OATP1B3*. *Toxicol Sci*, 2007. **97**(2): p. 407-16.
19. Kaur, G., et al., *Human MRP2 exports MC-LR but not the glutathione conjugate*. *Chemico-Biological Interactions*, 2019. **311**.
20. Roth, M., A. Obaidat, and B. Hagenbuch, *OATPs, OATs and OCTs: the organic anion and cation transporters of the SLCO and SLC22A gene superfamilies*. *Br J Pharmacol*, 2012. **165**(5): p. 1260-87.
21. Schulte, R.R. and R.H. Ho, *Organic Anion Transporting Polypeptides: Emerging Roles in Cancer Pharmacology*. *Mol Pharmacol*, 2019. **95**(5): p. 490-506.
22. Lone, Y., M. Bhide, and R.K. Koiri, *Microcystin-LR Induced Immunotoxicity in Mammals*. *J Toxicol*, 2016. **2016**: p. 8048125.
23. Arman, T. and J.D. Clarke, *Microcystin Toxicokinetics, Molecular Toxicology, and Pathophysiology in Preclinical Rodent Models and Humans*. *Toxins (Basel)*, 2021. **13**(8).
24. McLellan, N.L. and R.A. Manderville, *Toxic mechanisms of microcystins in mammals*. *Toxicol Res (Camb)*, 2017. **6**(4): p. 391-405.
25. Zhang, S., et al., *The latest advances in the reproductive toxicity of microcystin-LR*. *Environ Res*, 2021. **192**: p. 110254.
26. Yuan, L., et al., *Epigenetic modification of H3K4 and oxidative stress are involved in MC-LR-induced apoptosis in testicular cells of SD rats*. *Environ Toxicol*, 2020. **35**(2): p. 277-291.
27. Wang, X., et al., *Microcystin-LR causes sexual hormone disturbance in male rat by targeting gonadotropin-releasing hormone neurons*. *Toxicol*, 2016. **123**: p. 45-55.
28. Zhou, Y., et al., *The toxic effects of microcystin-LR on rat spermatogonia in vitro*. *Toxicol Lett*, 2012. **212**(1): p. 48-56.
29. Huang, H., et al., *Microcystin-LR Induced Apoptosis in Rat Sertoli Cells via the Mitochondrial Caspase-Dependent Pathway: Role of Reactive Oxygen Species*. *Front Physiol*, 2016. **7**: p. 397.
30. Hainaut, M. and H.J. Clarke, *Germ cells of the mammalian female: A limited or renewable resource? dagger*. *Biol Reprod*, 2021. **105**(4): p. 774-788.
31. Bhattacharya, P. and A.F. Keating, *Impact of environmental exposures on ovarian function and role of xenobiotic metabolism during ovotoxicity*. *Toxicol Appl Pharmacol*, 2012. **261**(3): p. 227-35.
32. Spears, N., et al., *Ovarian damage from chemotherapy and current approaches to its protection*. *Hum Reprod Update*, 2019. **25**(6): p. 673-693.
33. Vabre, P., et al., *Environmental pollutants, a possible etiology for premature ovarian insufficiency: a narrative review of animal and human data*. *Environ Health*, 2017. **16**(1): p. 37.
34. Xiao, S., et al., *In vitro follicle growth supports human oocyte meiotic maturation*. *Sci Rep*, 2015. **5**: p. 17323.
35. Xiao, S., et al., *A microfluidic culture model of the human reproductive tract and 28-day menstrual cycle*. *Nat Commun*, 2017. **8**: p. 14584.
36. Wang, Y., et al., *A closed vitrification system enables a murine ovarian follicle bank for high-throughput ovotoxicity screening, which identifies endocrine disrupting activity of microcystins*. *Reprod Toxicol*, 2020. **93**: p. 118-130.
37. Xiao, S., et al., *Doxorubicin Has Dose-Dependent Toxicity on Mouse Ovarian Follicle Development, Hormone Secretion, and Oocyte Maturation*. *Toxicol Sci*, 2017. **157**(2): p. 320-329.

38. Wang, Y., et al., *Multidrug Resistance Protein 1 Deficiency Promotes Doxorubicin-Induced Ovarian Toxicity in Female Mice*. *Toxicol Sci*, 2018. **163**(1): p. 279-292.
39. Xu, J., et al., *A Tiered Female Ovarian Toxicity Screening Identifies Toxic Effects of Checkpoint Kinase 1 Inhibitors on Murine Growing Follicles*. *Toxicol Sci*, 2020. **177**(2): p. 405-419.
40. Jiang, K., et al., *A platform utilizing Drosophila ovulation for nonhormonal contraceptive screening*. *Proc Natl Acad Sci U S A*, 2021. **118**(28).
41. Roundtable on Environmental Health Sciences, R., and Medicine; Board on Population Health and Public Health Practice; Institute of Medicine., *Identifying and reducing environmental health risks of chemicals in our society: Workshop summary- the challenge: Chemicals in today's society.*, in *Identifying and Reducing Environmental Health Risks of Chemicals in Our Society: Workshop Summary*. 2014: Washington (DC).
42. Bian, J., et al., *Vitreous cryopreservation of human preantral follicles encapsulated in alginate beads with mini mesh cups*. *J Reprod Dev*, 2013. **59**(3): p. 288-95.
43. Camboni, A., et al., *Alginate beads as a tool to handle, cryopreserve and culture isolated human primordial/primary follicles*. *Cryobiology*, 2013. **67**(1): p. 64-9.
44. Asgari, F., et al., *Three dimensional in vitro culture of preantral follicles following slow-freezing and vitrification of mouse ovarian tissue*. *Cryobiology*, 2015. **71**(3): p. 529-36.
45. Trapphoff, T., et al., *DNA integrity, growth pattern, spindle formation, chromosomal constitution and imprinting patterns of mouse oocytes from vitrified pre-antral follicles*. *Hum Reprod*, 2010. **25**(12): p. 3025-42.
46. dela Pena, E.C., et al., *Birth of pups after transfer of mouse embryos derived from vitrified preantral follicles*. *Reproduction*, 2002. **123**(4): p. 593-600.
47. Desai, N., et al., *Mouse ovarian follicle cryopreservation using vitrification or slow programmed cooling: assessment of in vitro development, maturation, ultra-structure and meiotic spindle organization*. *J Obstet Gynaecol Res*, 2011. **37**(1): p. 1-12.
48. Lunardi, F.O., et al., *Ovine secondary follicles vitrified out the ovarian tissue grow and develop in vitro better than those vitrified into the ovarian fragments*. *Theriogenology*, 2016. **85**(7): p. 1203-10.
49. Ben-Aharon, I., et al., *Doxorubicin-induced ovarian toxicity*. *Reprod Biol Endocrinol*, 2010. **8**: p. 20.
50. Roti Roti, E.C., et al., *Acute doxorubicin insult in the mouse ovary is cell- and follicle-type dependent*. *PLoS One*, 2012. **7**(8): p. e42293.
51. Wang, Y., et al., *Doxorubicin obliterates mouse ovarian reserve through both primordial follicle atresia and overactivation*. *Toxicol Appl Pharmacol*, 2019. **381**: p. 114714.
52. Kimambo, O.N., J.R. Gumbo, and H. Chikoore, *The occurrence of cyanobacteria blooms in freshwater ecosystems and their link with hydro-meteorological and environmental variations in Tanzania*. *Heliyon*, 2019. **5**(3): p. e01312.
53. Kaebernick, M. and B.A. Neilan, *Ecological and molecular investigations of cyanotoxin production*. *Fems Microbiology Ecology*, 2001. **35**(1): p. 1-9.
54. Du, X.D., et al., *The Diversity of Cyanobacterial Toxins on Structural Characterization, Distribution and Identification: A Systematic Review*. *Toxins*, 2019. **11**(9).
55. Tillett, D., et al., *Structural organization of microcystin biosynthesis in Microcystis aeruginosa PCC7806: an integrated peptide-polyketide synthetase system*. *Chem Biol*, 2000. **7**(10): p. 753-64.
56. Bouaicha, N., et al., *Structural Diversity, Characterization and Toxicology of Microcystins*. *Toxins*, 2019. **11**(12).
57. Rapala, J., et al., *Variation of microcystins, cyanobacterial hepatotoxins, in Anabaena spp. as a function of growth stimuli*. *Applied and Environmental Microbiology*, 1997. **63**(6): p. 2206-2212.

58. Hesse, K. and J.-G. Kohl, *Effects of light and nutrient supply on growth and microcystin content of different strains of Microcystis*. Cyanotoxins: occurrence, causes, consequences, 2012.
59. Martins, J.C. and V.M. Vasconcelos, *Microcystin dynamics in aquatic organisms*. J Toxicol Environ Health B Crit Rev, 2009. **12**(1): p. 65-82.
60. Xiang, L., et al., *Bioaccumulation and Phytotoxicity and Human Health Risk from Microcystin-LR under Various Treatments: A Pot Study*. Toxins (Basel), 2020. **12**(8).
61. Tencalla, F. and D. Dietrich, *Biochemical characterization of microcystin toxicity in rainbow trout (*Oncorhynchus mykiss*)*. Toxicon, 1997. **35**(4): p. 583-95.
62. Ito, E., F. Kondo, and K. Harada, *First report on the distribution of orally administered microcystin-LR in mouse tissue using an immunostaining method*. Toxicon, 2000. **38**(1): p. 37-48.
63. Benson, J.M., et al., *The toxicity of microcystin LR in mice following 7 days of inhalation exposure*. Toxicon, 2005. **45**(6): p. 691-8.
64. Nishiwaki, R., et al., *Two significant aspects of microcystin-LR: specific binding and liver specificity*. Cancer Lett, 1994. **83**(1-2): p. 283-9.
65. Wang, Q., et al., *Distribution of microcystins in various organs (heart, liver, intestine, gonad, brain, kidney and lung) of Wistar rat via intravenous injection*. Toxicon, 2008. **52**(6): p. 721-7.
66. Greer, B., J.P. Meneely, and C.T. Elliott, *Uptake and accumulation of Microcystin-LR based on exposure through drinking water: An animal model assessing the human health risk*. Sci Rep, 2018. **8**(1): p. 4913.
67. Xie, L.Q., et al., *Organ distribution and bioaccumulation of microcystins in freshwater fish at different trophic levels from the eutrophic Lake Chaohu, China*. Environmental Toxicology, 2005. **20**(3): p. 293-300.
68. Zhang, W., et al., *Why mammals more susceptible to the hepatotoxic microcystins than fish: evidences from plasma and albumin protein binding through equilibrium dialysis*. Ecotoxicology, 2013. **22**(6): p. 1012-9.
69. Setlikova, I. and C. Wiegand, *Hepatic and branchial glutathione S-transferases of two fish species: substrate specificity and biotransformation of microcystin-LR*. Comp Biochem Physiol C Toxicol Pharmacol, 2009. **149**(4): p. 515-23.
70. Robinson, N.A., et al., *Tissue distribution, excretion and hepatic biotransformation of microcystin-LR in mice*. J Pharmacol Exp Ther, 1991. **256**(1): p. 176-82.
71. Kondo, F., et al., *Detection and identification of metabolites of microcystins formed in vivo in mouse and rat livers*. Chem Res Toxicol, 1996. **9**(8): p. 1355-9.
72. Buratti, F.M., et al., *Human glutathione transferases catalyzing the conjugation of the hepatotoxin microcystin-LR*. Chem Res Toxicol, 2011. **24**(6): p. 926-33.
73. Schmidt, J.R., S.W. Wilhelm, and G.L. Boyer, *The fate of microcystins in the environment and challenges for monitoring*. Toxins (Basel), 2014. **6**(12): p. 3354-87.
74. Kondo, F., et al., *Formation, characterization, and toxicity of the glutathione and cysteine conjugates of toxic heptapeptide microcystins*. Chem Res Toxicol, 1992. **5**(5): p. 591-6.
75. Miles, C.O., et al., *Conjugation of Microcystins with Thiols Is Reversible: Base-Catalyzed Deconjugation for Chemical Analysis*. Chem Res Toxicol, 2016. **29**(5): p. 860-70.
76. Li, W., et al., *Rapid conversion and reversible conjugation of glutathione detoxification of microcystins in bighead carp (*Aristichthys nobilis*)*. Aquat Toxicol, 2014. **147**: p. 18-25.
77. Chen, J., et al., *First identification of the hepatotoxic microcystins in the serum of a chronically exposed human population together with indication of hepatocellular damage*. Toxicol Sci, 2009. **108**(1): p. 81-9.

78. Hilborn, E.D., et al., *A simple colorimetric method to detect biological evidence of human exposure to microcystins*. *Toxicol*, 2005. **46**(2): p. 218-21.
79. Hagenbuch, B. and B. Stieger, *The SLCO (former SLC21) superfamily of transporters*. *Mol Aspects Med*, 2013. **34**(2-3): p. 396-412.
80. Steckelbroeck, S., et al., *Steroid sulfatase (STS) expression in the human temporal lobe: enzyme activity, mRNA expression and immunohistochemistry study*. *J Neurochem*, 2004. **89**(2): p. 403-17.
81. Obaidat, A., M. Roth, and B. Hagenbuch, *The expression and function of organic anion transporting polypeptides in normal tissues and in cancer*. *Annu Rev Pharmacol Toxicol*, 2012. **52**: p. 135-51.
82. Badee, J., et al., *Meta-analysis of expression of hepatic organic anion-transporting polypeptide (OATP) transporters in cellular systems relative to human liver tissue*. *Drug Metab Dispos*, 2015. **43**(4): p. 424-32.
83. Yu, J., et al., *Intestinal Drug Interactions Mediated by OATPs: A Systematic Review of Preclinical and Clinical Findings*. *J Pharm Sci*, 2017. **106**(9): p. 2312-2325.
84. Li, Y., et al., *A cross-sectional investigation of chronic exposure to microcystin in relationship to childhood liver damage in the Three Gorges Reservoir Region, China*. *Environ Health Perspect*, 2011. **119**(10): p. 1483-8.
85. Fawell, J.K., et al., *The toxicity of cyanobacterial toxins in the mouse: I microcystin-LR*. *Hum Exp Toxicol*, 1999. **18**(3): p. 162-7.
86. Lad, A., et al., *Chronic Low Dose Oral Exposure to Microcystin-LR Exacerbates Hepatic Injury in a Murine Model of Non-Alcoholic Fatty Liver Disease*. *Toxins (Basel)*, 2019. **11**(9).
87. Chen, L. and P. Xie, *Mechanisms of Microcystin-induced Cytotoxicity and Apoptosis*. *Mini Rev Med Chem*, 2016. **16**(13): p. 1018-31.
88. Campos, A. and V. Vasconcelos, *Molecular mechanisms of microcystin toxicity in animal cells*. *Int J Mol Sci*, 2010. **11**(1): p. 268-87.
89. Zhou, M., W.W. Tu, and J. Xu, *Mechanisms of microcystin-LR-induced cytoskeletal disruption in animal cells*. *Toxicol*, 2015. **101**: p. 92-100.
90. Nasa, I. and A.N. Kettenbach, *Coordination of Protein Kinase and Phosphoprotein Phosphatase Activities in Mitosis*. *Front Cell Dev Biol*, 2018. **6**: p. 30.
91. Toivola, D.M., J.E. Eriksson, and D.L. Brautigan, *Identification of protein phosphatase 2A as the primary target for microcystin-LR in rat liver homogenates*. *FEBS Lett*, 1994. **344**(2-3): p. 175-80.
92. Goldberg, J., et al., *Three-dimensional structure of the catalytic subunit of protein serine/threonine phosphatase-1*. *Nature*, 1995. **376**(6543): p. 745-53.
93. Xing, Y., et al., *Structure of protein phosphatase 2A core enzyme bound to tumor-inducing toxins*. *Cell*, 2006. **127**(2): p. 341-53.
94. Meng, G., et al., *Microcystin-LR induces cytoskeleton system reorganization through hyperphosphorylation of tau and HSP27 via PP2A inhibition and subsequent activation of the p38 MAPK signaling pathway in neuroendocrine (PC12) cells*. *Toxicology*, 2011. **290**(2-3): p. 218-29.
95. Yang, F., et al., *Involvement of MAPK/ERK1/2 pathway in microcystin-induced microfilament reorganization in HL7702 hepatocytes*. *J Toxicol Environ Health A*, 2018. **81**(21): p. 1135-1141.
96. Christen, V., N. Meili, and K. Fent, *Microcystin-LR induces endoplasmic reticulum stress and leads to induction of NFkappaB, interferon-alpha, and tumor necrosis factor-alpha*. *Environ Sci Technol*, 2013. **47**(7): p. 3378-85.
97. Kwon, Y.G., et al., *Cell cycle-dependent phosphorylation of mammalian protein phosphatase 1 by cdc2 kinase*. *Proc Natl Acad Sci U S A*, 1997. **94**(6): p. 2168-73.

98. Vagnarelli, P., et al., *Repo-Man coordinates chromosomal reorganization with nuclear envelope reassembly during mitotic exit*. Dev Cell, 2011. **21**(2): p. 328-42.
99. Mochida, S., *Regulation of alpha-endosulfine, an inhibitor of protein phosphatase 2A, by multisite phosphorylation*. FEBS J, 2014. **281**(4): p. 1159-69.
100. Lorca, T. and A. Castro, *The Greatwall kinase: a new pathway in the control of the cell cycle*. Oncogene, 2013. **32**(5): p. 537-43.
101. Ramos, F., et al., *Role of protein phosphatases PPI, PP2A, PP4 and Cdc14 in the DNA damage response*. Cell Stress, 2019. **3**(3): p. 70-85.
102. Li, D.W., et al., *Protein serine/threonine phosphatase-1 dephosphorylates p53 at Ser-15 and Ser-37 to modulate its transcriptional and apoptotic activities*. Oncogene, 2006. **25**(21): p. 3006-22.
103. Chen, B.Y., et al., *The K898E germline variant in the PPI-binding motif of BRCA1 causes defects in DNA Repair*. Sci Rep, 2014. **4**: p. 5812.
104. Goodarzi, A.A., et al., *Autophosphorylation of ataxia-telangiectasia mutated is regulated by protein phosphatase 2A*. Embo Journal, 2004. **23**(22): p. 4451-4461.
105. Harman, L.S., et al., *One- and two-electron oxidation of reduced glutathione by peroxidases*. J Biol Chem, 1986. **261**(4): p. 1642-8.
106. Pflugmacher, S., et al., *Identification of an enzymatically formed glutathione conjugate of the cyanobacterial hepatotoxin microcystin-LR: the first step of detoxication*. Biochim Biophys Acta, 1998. **1425**(3): p. 527-33.
107. Guo, X., et al., *Quantitatively evaluating detoxification of the hepatotoxic microcystin-LR through the glutathione (GSH) pathway in SD rats*. Environ Sci Pollut Res Int, 2015. **22**(23): p. 19273-84.
108. Chen, L., et al., *The role of GSH in microcystin-induced apoptosis in rat liver: Involvement of oxidative stress and NF-kappaB*. Environ Toxicol, 2016. **31**(5): p. 552-60.
109. Venditti, P., L. Di Stefano, and S. Di Meo, *Mitochondrial metabolism of reactive oxygen species*. Mitochondrion, 2013. **13**(2): p. 71-82.
110. Murphy, M.P., *How mitochondria produce reactive oxygen species*. Biochemical Journal, 2009. **417**: p. 1-13.
111. Guo, C., et al., *Oxidative stress, mitochondrial damage and neurodegenerative diseases*. Neural Regen Res, 2013. **8**(21): p. 2003-14.
112. Ding, W.X., H.M. Shen, and C.N. Ong, *Critical role of reactive oxygen species and mitochondrial permeability transition in microcystin-induced rapid apoptosis in rat hepatocytes*. Hepatology, 2000. **32**(3): p. 547-555.
113. Weng, D., et al., *The role of ROS in microcystin-LR-induced hepatocyte apoptosis and liver injury in mice*. Toxicology, 2007. **232**(1-2): p. 15-23.
114. Shi, Y., et al., *Oxidative stress and histopathological alterations in liver of Cyprinus carpio L. induced by intraperitoneal injection of microcystin-LR*. Ecotoxicology, 2015. **24**(3): p. 511-9.
115. Wickstrom, M.L., et al., *Alterations in microtubules, intermediate filaments, and microfilaments induced by microcystin-LR in cultured cells*. Toxicol Pathol, 1995. **23**(3): p. 326-37.
116. Chen, D.N., et al., *Hyperphosphorylation of intermediate filament proteins is involved in microcystin-LR-induced toxicity in HL7702 cells*. Toxicol Lett, 2012. **214**(2): p. 192-9.
117. Huang, X., et al., *Involvement of oxidative stress and cytoskeletal disruption in microcystin-induced apoptosis in CIK cells*. Aquat Toxicol, 2015. **165**: p. 41-50.
118. Wang, Q., et al., *Microcystin-leucine arginine blocks vasculogenesis and angiogenesis through impairing cytoskeleton and impeding endothelial cell migration by downregulating integrin-mediated Rho/ROCK signaling pathway*. Environ Sci Pollut Res Int, 2021.

119. Chen, L., et al., *The interactive effects of cytoskeleton disruption and mitochondria dysfunction lead to reproductive toxicity induced by microcystin-LR*. PLoS One, 2013. **8**(1): p. e53949.
120. Zhang, X., et al., *Vitamin C Protects Porcine Oocytes From Microcystin-LR Toxicity During Maturation*. Front Cell Dev Biol, 2020. **8**: p. 582715.
121. Jiang, J., et al., *Microcystin-LR induced reactive oxygen species mediate cytoskeletal disruption and apoptosis of hepatocytes in Cyprinus carpio L*. PLoS One, 2013. **8**(12): p. e84768.
122. Galluzzi, L., et al., *Molecular mechanisms of cell death: recommendations of the Nomenclature Committee on Cell Death 2018*. Cell Death Differ, 2018. **25**(3): p. 486-541.
123. Zegura, B., et al., *Different sensitivities of human colon adenocarcinoma (CaCo-2), astrocytoma (IPDDC-A2) and lymphoblastoid (NCNC) cell lines to microcystin-LR induced reactive oxygen species and DNA damage*. Toxicol, 2008. **52**(3): p. 518-25.
124. Dias, E., et al., *Microcystin-LR activates the ERK1/2 kinases and stimulates the proliferation of the monkey kidney-derived cell line Vero-E6*. Toxicol In Vitro, 2010. **24**(6): p. 1689-95.
125. Dias, E., et al., *Comparative study of the cytotoxic effect of microcystin-LR and purified extracts from Microcystis aeruginosa on a kidney cell line*. Toxicol, 2009. **53**(5): p. 487-95.
126. Alverca, E., et al., *Morphological and ultrastructural effects of microcystin-LR from Microcystis aeruginosa extract on a kidney cell line*. Toxicol, 2009. **54**(3): p. 283-94.
127. Li, Y., et al., *Microcystin-LR induces mitochondria-mediated apoptosis in human bronchial epithelial cells*. Exp Ther Med, 2016. **12**(2): p. 633-640.
128. Ji, Y., et al., *Microcystin-LR Induces Apoptosis via NF-kappa B/iNOS Pathway in INS-1 Cells*. International Journal of Molecular Sciences, 2011. **12**(7): p. 4722-4734.
129. Piyathilaka, M.A., et al., *Microcystin-LR-induced cytotoxicity and apoptosis in human embryonic kidney and human kidney adenocarcinoma cell lines*. Microbiology (Reading), 2015. **161**(Pt 4): p. 819-28.
130. Chen, T., et al., *Induction of apoptosis in mouse liver by microcystin-LR: a combined transcriptomic, proteomic, and simulation strategy*. Mol Cell Proteomics, 2005. **4**(7): p. 958-74.
131. Ji, Y., et al., *Microcystin-LR induces apoptosis via NF-kappaB/iNOS pathway in INS-1 cells*. Int J Mol Sci, 2011. **12**(7): p. 4722-34.
132. Denton, D. and S. Kumar, *Autophagy-dependent cell death*. Cell Death Differ, 2019. **26**(4): p. 605-616.
133. Yang, Y., et al., *Influence of microcystins-LR (MC-LR) on autophagy in human neuroblastoma SK-N-SH cells*. J Toxicol Environ Health A, 2019. **82**(21): p. 1129-1136.
134. Liu, H., et al., *Oxidative Stress Mediates Microcystin-LR-Induced Endoplasmic Reticulum Stress and Autophagy in KK-1 Cells and C57BL/6 Mice Ovaries*. Front Physiol, 2018. **9**: p. 1058.
135. Chen, Y., et al., *Microcystin-LR induces autophagy and apoptosis in rat Sertoli cells in vitro*. Toxicol, 2013. **76**: p. 84-93.
136. Zhang, S., et al., *Novel Role of ER Stress and Autophagy in Microcystin-LR Induced Apoptosis in Chinese Hamster Ovary Cells*. Front Physiol, 2016. **7**: p. 527.
137. Woolbright, B.L., et al., *Microcystin-LR induced liver injury in mice and in primary human hepatocytes is caused by oncotic necrosis*. Toxicol, 2017. **125**: p. 99-109.
138. Du, X., et al., *Microcystin-LR induces ovarian injury and apoptosis in mice via activating apoptosis signal-regulating kinase 1-mediated P38/JNK pathway*. Ecotoxicol Environ Saf, 2021. **213**: p. 112066.

139. Wu, J., et al., *MC-LR Exposure Leads to Subfertility of Female Mice and Induces Oxidative Stress in Granulosa Cells*. *Toxins (Basel)*, 2015. **7**(12): p. 5212-23.
140. Wu, J., et al., *Reproductive toxicity on female mice induced by microcystin-LR*. *Environ Toxicol Pharmacol*, 2014. **37**(1): p. 1-6.
141. Selman, K., et al., *Stages of oocyte development in the zebrafish, Brachydanio rerio*. *J Morphol*, 1993. **218**(2): p. 203-224.
142. Liu, W., et al., *Sex-dependent effects of microcystin-LR on hypothalamic-pituitary-gonad axis and gametogenesis of adult zebrafish*. *Sci Rep*, 2016. **6**: p. 22819.
143. Zhan, C., et al., *Microcystin-LR promotes zebrafish (Danio rerio) oocyte (in vivo) maturation by activating ERK1/2-MPF signaling pathways, and cAMP is involved in this process*. *Environ Pollut*, 2020. **259**: p. 113843.
144. Trinchet, I., et al., *Pathological modifications following sub-chronic exposure of medaka fish (Oryzias latipes) to microcystin-LR*. *Reprod Toxicol*, 2011. **32**(3): p. 329-40.
145. Liu, W., et al., *Microcystin-LR influences the in vitro oocyte maturation of zebrafish by activating the MAPK pathway*. *Aquat Toxicol*, 2019. **215**: p. 105261.
146. Hou, J., et al., *Damage and recovery of the ovary in female zebrafish i.p.-injected with MC-LR*. *Aquat Toxicol*, 2014. **155**: p. 110-8.
147. Shi, F., et al., *Microcystin-LR exposure results in aberrant spindles and induces apoptosis in porcine oocytes*. *Theriogenology*, 2020. **158**: p. 358-367.
148. Liu, H., et al., *Microcystin-leucine arginine exposure contributes to apoptosis and follicular atresia in mice ovaries by endoplasmic reticulum stress-upregulated Ddit3*. *Sci Total Environ*, 2021. **756**: p. 144070.
149. Ma, Y., et al., *IRE1 and CaMKKbeta pathways to reveal the mechanism involved in microcystin-LR-induced autophagy in mouse ovarian cells*. *Food Chem Toxicol*, 2021. **147**: p. 111911.
150. Gacsi, M., et al., *Comparative study of cyanotoxins affecting cytoskeletal and chromatin structures in CHO-K1 cells*. *Toxicol In Vitro*, 2009. **23**(4): p. 710-8.
151. Kawan, A., et al., *Recovery of reproductive function of female zebrafish from the toxic effects of microcystin-LR exposure*. *Aquatic Toxicology*, 2019. **214**.
152. Deng, D.F., et al., *Toxic threshold of dietary microcystin (-LR) for quart medaka*. *Toxicon*, 2010. **55**(4): p. 787-94.
153. Jacquet, C., et al., *Effects of microcystin-LR on development of medaka fish embryos (Oryzias latipes)*. *Toxicon*, 2004. **43**(2): p. 141-147.
154. Oberemm, A., J. Fastner, and C.E.W. Steinberg, *Effects of microcystin-LR and cyanobacterial crude extracts on embryo-larval development of zebrafish (Danio rerio)*. *Water Research*, 1997. **31**(11): p. 2918-2921.
155. Zhao, S., et al., *Microcystin-LR exposure decreased the fetal weight of mice by disturbance of placental development and ROS-mediated endoplasmic reticulum stress in the placenta*. *Environ Pollut*, 2020. **256**: p. 113362.
156. Gao, L., et al., *Paternal exposure to microcystin-LR induces fetal growth restriction partially through inhibiting cell proliferation and vascular development in placental labyrinth*. *Environ Sci Pollut Res Int*, 2021. **28**(42): p. 60032-60040.
157. Bagur, A.C. and C.A. Mautalen, *Risk for developing osteoporosis in untreated premature menopause*. *Calcif Tissue Int*, 1992. **51**(1): p. 4-7.
158. Hu, F.B., et al., *Age at natural menopause and risk of cardiovascular disease*. *Archives of Internal Medicine*, 1999. **159**(10): p. 1061-1066.
159. Bush, T.L., et al., *Cardiovascular Mortality and Noncontraceptive Use of Estrogen in Women - Results from the Lipid Research Clinics Program Follow-up-Study*. *Circulation*, 1987. **75**(6): p. 1102-1109.

160. Qiao, Q., et al., *Female zebrafish (Danio rerio) are more vulnerable than males to microcystin-LR exposure, without exhibiting estrogenic effects*. *Aquatic Toxicology*, 2013. **142**: p. 272-282.
161. Zhao, Y., L. Xie, and Y. Yan, *Microcystin-LR impairs zebrafish reproduction by affecting oogenesis and endocrine system*. *Chemosphere*, 2015. **120**: p. 115-22.
162. Hou, J., et al., *Reproduction impairment and endocrine disruption in female zebrafish after long-term exposure to MC-LR: A life cycle assessment*. *Environ Pollut*, 2016. **208**(Pt B): p. 477-85.
163. Li, X., et al., *MC-LR induced overproduction of progesterone via inhibiting miR-3473g: in vitro and in vivo evidence*. *Reproduction*, 2020. **159**(1): p. 81-89.
164. Chen, L., et al., *Effects of acute exposure to microcystins on hypothalamic-pituitary-adrenal (HPA), -gonad (HPG) and -thyroid (HPT) axes of female rats*. *Sci Total Environ*, 2021. **778**: p. 145196.
165. Oziol, L. and N. Bouaicha, *First evidence of estrogenic potential of the cyanobacterial heptotoxins the nodularin-R and the microcystin-LR in cultured mammalian cells*. *J Hazard Mater*, 2010. **174**(1-3): p. 610-5.
166. Chan, K.A., M.W. Tsoulis, and D.M. Sloboda, *Early-life nutritional effects on the female reproductive system*. *J Endocrinol*, 2015. **224**(2): p. R45-62.
167. Lin, W., et al., *Parental Transfer of Microcystin-LR-Induced Innate Immune Dysfunction of Zebrafish: A Cross-Generational Study*. *Environ Sci Technol*, 2020. **54**(2): p. 1014-1023.
168. Zhan, C., et al., *Microcystin-LR triggers different endoplasmic reticulum stress pathways in the liver, ovary, and offspring of zebrafish (Danio rerio)*. *J Hazard Mater*, 2020. **386**: p. 121939.
169. Zhao, S., G. Li, and J. Chen, *A proteomic analysis of prenatal transfer of microcystin-LR induced neurotoxicity in rat offspring*. *J Proteomics*, 2015. **114**: p. 197-213.
170. Martin, R.M., M.S. Bereman, and K.C. Marsden, *Exposure to a mixture of BMAA and MCLR synergistically modulates behavior in larval zebrafish while exacerbating molecular changes related to neurodegeneration*. *bioRxiv*, 2020: p. 2020.07.15.205617.
171. Freitas, M., et al., *Effects of microcystin-LR, cylindrospermopsin and a microcystin-LR/cylindrospermopsin mixture on growth, oxidative stress and mineral content in lettuce plants (Lactuca sativa L.)*. *Ecotoxicol Environ Saf*, 2015. **116**: p. 59-67.
172. Pinheiro, C., et al., *The interactive effects of microcystin-LR and cylindrospermopsin on the growth rate of the freshwater algae Chlorella vulgaris*. *Ecotoxicology*, 2016. **25**(4): p. 745-58.
173. Myhre, O., et al., *Repeated five-day administration of L-BMAA, microcystin-LR, or as mixture, in adult C57BL/6 mice - lack of adverse cognitive effects*. *Scientific Reports*, 2018. **8**(1): p. 2308.
174. Roy, A., et al., *Nanomaterials for Remediation of Environmental Pollutants*. *Bioinorg Chem Appl*, 2021. **2021**: p. 1764647.
175. Cheng, H., et al., *Adverse reproductive performance in zebrafish with increased bioconcentration of microcystin-LR in the presence of titanium dioxide nanoparticles*. *Environmental science. Nano*, 2018. **5**: p. 1208-1217.
176. Wang, S., et al., *Combined exposure to 3-chloro-4-dichloromethyl-5-hydroxy-2(5H)-furanone and microcystin-LR increases genotoxicity in Chinese hamster ovary cells through oxidative stress*. *Environ Sci Technol*, 2013. **47**(3): p. 1678-87.
177. Lin, Y., et al., *Single and combined exposure of microcystin-LR and nitrite results in reproductive endocrine disruption via hypothalamic-pituitary-gonadal-liver axis*. *Chemosphere*, 2018. **211**: p. 1137-1146.

178. Brooks, B.W., et al., *Are harmful algal blooms becoming the greatest inland water quality threat to public health and aquatic ecosystems?* Environ Toxicol Chem, 2016. **35**(1): p. 6-13.
179. EPA. *Climate Change and Harmful Algal Blooms*. 2011; Available from: <https://www.epa.gov/nutrientpollution/climate-change-and-harmful-algal-blooms>.
180. CDC. *Harmful algal blooms (HABs)-Associated Illness*. 2018; Available from: <https://www.cdc.gov/habs/index.html>.
181. Landrigan, P.J., J.J. Stegeman, and L.E. Fleming, *Human Health and Ocean Pollution*. Ann Glob Health, 2020. **86**(1): p. 151.
182. Preece, E.P., et al., *A review of microcystin detections in Estuarine and Marine waters: Environmental implications and human health risk*. Harmful Algae, 2017. **61**: p. 31-45.
183. Rastogi, R.P., R.P. Sinha, and A. Incharoensakdi, *The cyanotoxin-microcystins: current overview*. Reviews in Environmental Science and Bio-Technology, 2014. **13**(2): p. 215-249.
184. Tsuji, K., et al., *Stability of microcystins from cyanobacteria--II. Effect of UV light on decomposition and isomerization*. Toxicon, 1995. **33**(12): p. 1619-31.
185. Tsuji, K., et al., *Stability of microcystins from cyanobacteria: effect of light on decomposition and isomerization*. Environ Sci Technol, 1994. **28**(1): p. 173-7.
186. Drobac, D., et al., *Human exposure to cyanotoxins and their effects on health*. Arh Hig Rada Toksikol, 2013. **64**(2): p. 119-30.
187. Jochimsen, E.M., et al., *Liver failure and death after exposure to microcystins at a hemodialysis center in Brazil*. N Engl J Med, 1998. **338**(13): p. 873-8.
188. Hinojosa, M.G., et al., *Neurotoxicity induced by microcystins and cylindrospermopsin: A review*. Sci Total Environ, 2019. **668**: p. 547-565.
189. Chen, L., et al., *A review of reproductive toxicity of microcystins*. J Hazard Mater, 2016. **301**: p. 381-99.
190. Mackintosh, C., et al., *Cyanobacterial Microcystin-Lr Is a Potent and Specific Inhibitor of Protein Phosphatase-1 and Phosphatase-2a from Both Mammals and Higher-Plants*. Febs Letters, 1990. **264**(2): p. 187-192.
191. Wlodarchak, N. and Y.N. Xing, *PP2A as a master regulator of the cell cycle*. Critical Reviews in Biochemistry and Molecular Biology, 2016. **51**(3): p. 162-184.
192. Shi, Y., B. Reddy, and J.L. Manley, *PPI/PP2A phosphatases are required for the second step of Pre-mRNA splicing and target specific snRNP proteins*. Mol Cell, 2006. **23**(6): p. 819-29.
193. Zegura, B., A. Straser, and M. Filipic, *Genotoxicity and potential carcinogenicity of cyanobacterial toxins - a review*. Mutat Res, 2011. **727**(1-2): p. 16-41.
194. Rogers, E.D., et al., *Global gene expression profiling in larval zebrafish exposed to microcystin-LR and microcystis reveals endocrine disrupting effects of Cyanobacteria*. Environ Sci Technol, 2011. **45**(5): p. 1962-9.
195. Liu, W.J., et al., *Sex-dependent effects of microcystin-LR on hypothalamic-pituitary-gonad axis and gametogenesis of adult zebrafish*. Scientific Reports, 2016. **6**.
196. Cheng, H., et al., *Parental exposure to microcystin-LR induced thyroid endocrine disruption in zebrafish offspring, a transgenerational toxicity*. Environ Pollut, 2017. **230**: p. 981-988.
197. Jia, Y.L., et al., *Cyanobacterial blooms act as sink and source of endocrine disruptors in the third largest freshwater lake in China*. Environmental Pollution, 2019. **245**: p. 408-418.
198. Mallia, V., et al., *Investigation of In Vitro Endocrine Activities of Microcystis and Planktothrix Cyanobacterial Strains*. Toxins (Basel), 2020. **12**(4).
199. Kumar, T.R., et al., *Follicle stimulating hormone is required for ovarian follicle maturation but not male fertility*. Nat Genet, 1997. **15**(2): p. 201-4.

200. Dierich, A., et al., *Impairing follicle-stimulating hormone (FSH) signaling in vivo: targeted disruption of the FSH receptor leads to aberrant gametogenesis and hormonal imbalance*. Proc Natl Acad Sci U S A, 1998. **95**(23): p. 13612-7.
201. Zhang, F.P., et al., *Normal prenatal but arrested postnatal sexual development of luteinizing hormone receptor knockout (LuRKO) mice*. Mol Endocrinol, 2001. **15**(1): p. 172-83.
202. Pakarainen, T., et al., *Knockout of luteinizing hormone receptor abolishes the effects of follicle-stimulating hormone on preovulatory maturation and ovulation of mouse graafian follicles*. Mol Endocrinol, 2005. **19**(10): p. 2591-602.
203. Zeleznik, A.J., *The physiology of follicle selection*. Reprod Biol Endocrinol, 2004. **2**: p. 31.
204. Mukherjee, A., O.K. Park-Sarge, and K.E. Mayo, *Gonadotropins induce rapid phosphorylation of the 3',5'-cyclic adenosine monophosphate response element binding protein in ovarian granulosa cells*. Endocrinology, 1996. **137**(8): p. 3234-45.
205. Carlone, D.L. and J.S. Richards, *Evidence that functional interactions of CREB and SF-1 mediate hormone regulated expression of the aromatase gene in granulosa cells and constitutive expression in R2C cells*. Journal of Steroid Biochemistry and Molecular Biology, 1997. **61**(3-6): p. 223-231.
206. Law, N.C. and M.E. Hunzicker-Dunn, *Insulin Receptor Substrate 1, the Hub Linking Follicle-stimulating Hormone to Phosphatidylinositol 3-Kinase Activation*. J Biol Chem, 2016. **291**(9): p. 4547-60.
207. Law, N.C., M.F. White, and M.E. Hunzicker-Dunn, *G protein-coupled receptors (GPCRs) That Signal via Protein Kinase A (PKA) Cross-talk at Insulin Receptor Substrate 1 (IRS1) to Activate the phosphatidylinositol 3-kinase (PI3K)/AKT Pathway*. J Biol Chem, 2016. **291**(53): p. 27160-27169.
208. Nair, A.B. and S. Jacob, *A simple practice guide for dose conversion between animals and human*. J Basic Clin Pharm, 2016. **7**(2): p. 27-31.
209. Lin, H., et al., *Determination of Environmental Exposure to Microcystin and Aflatoxin as a Risk for Renal Function Based on 5493 Rural People in Southwest China*. Environ Sci Technol, 2016. **50**(10): p. 5346-56.
210. EPA, *Drinking Water Health Advisories for the Cyanobacterial Microcystin Toxins*, O.o. Water, Editor. 2015: Washington, DC.
211. EPA. *Guideline and Recommendations*. 2018 [cited 2018 June 11]; Available from: <https://www.epa.gov/nutrient-policy-data/guidelines-and-recommendations>.
212. Byers, S.L., et al., *Mouse estrous cycle identification tool and images*. PLoS One, 2012. **7**(4): p. e35538.
213. Pedersen, T. and H. Peters, *Proposal for a classification of oocytes and follicles in the mouse ovary*. J Reprod Fertil, 1968. **17**(3): p. 555-7.
214. Luo, C., et al., *Superovulation Strategies for 6 Commonly Used Mouse Strains*. Journal of the American Association for Laboratory Animal Science, 2011. **50**(4): p. 471-478.
215. Michalak, A.M., et al., *Record-setting algal bloom in Lake Erie caused by agricultural and meteorological trends consistent with expected future conditions*. Proc Natl Acad Sci U S A, 2013. **110**(16): p. 6448-52.
216. Wang, Y., et al., *Vitrification preserves murine ovarian follicular cell transcriptome in a 3D encapsulated in vitro follicle growth system*. Biol Reprod, 2021. **105**(6): p. 1378-1380.
217. Fan, H.Y., et al., *MAPK3/1 (ERK1/2) in ovarian granulosa cells are essential for female fertility*. Science, 2009. **324**(5929): p. 938-41.
218. Herndon, M.K., et al., *Forkhead box O member FOXO1 regulates the majority of follicle-stimulating hormone responsive genes in ovarian granulosa cells*. Mol Cell Endocrinol, 2016. **434**: p. 116-26.

219. Vanhaesebroeck, B. and D.R. Alessi, *The PI3K-PDK1 connection: more than just a road to PKB*. *Biochemical Journal*, 2000. **346**: p. 561-576.
220. Shitara, Y., K. Takeuchi, and T. Horie, *Long-lasting inhibitory effects of saquinavir and ritonavir on OATP1B1-mediated uptake*. *J Pharm Sci*, 2013. **102**(9): p. 3427-35.
221. Karlgren, M., et al., *Classification of inhibitors of hepatic organic anion transporting polypeptides (OATPs): influence of protein expression on drug-drug interactions*. *J Med Chem*, 2012. **55**(10): p. 4740-63.
222. Ho, J.C., A.M. Michalak, and N. Pahlevan, *Widespread global increase in intense lake phytoplankton blooms since the 1980s*. *Nature*, 2019. **574**(7780): p. 667-+.
223. Zhao, Y., et al., *Long-term environmental exposure to microcystins increases the risk of nonalcoholic fatty liver disease in humans: A combined fisher-based investigation and murine model study*. *Environ Int*, 2020. **138**: p. 105648.
224. Kishi, H., et al., *Expression of the gonadotropin receptors during follicular development*. *Reprod Med Biol*, 2018. **17**(1): p. 11-19.
225. Law, N.C., et al., *Lhcgr expression in granulosa cells: roles for PKA-phosphorylated beta-catenin, TCF3, and FOXO1*. *Mol Endocrinol*, 2013. **27**(8): p. 1295-310.
226. Nyegaard, M., et al., *Lack of functional pregnancy-associated plasma protein-A (PAPPA) compromises mouse ovarian steroidogenesis and female fertility*. *Biol Reprod*, 2010. **82**(6): p. 1129-38.
227. Norris, R.P., et al., *Cyclic GMP from the surrounding somatic cells regulates cyclic AMP and meiosis in the mouse oocyte*. *Development*, 2009. **136**(11): p. 1869-78.
228. Zhang, M., et al., *Granulosa cell ligand NPPC and its receptor NPR2 maintain meiotic arrest in mouse oocytes*. *Science*, 2010. **330**(6002): p. 366-9.
229. Egbert, J.R., et al., *Dephosphorylation and inactivation of NPR2 guanylyl cyclase in granulosa cells contributes to the LH-induced decrease in cGMP that causes resumption of meiosis in rat oocytes*. *Development*, 2014. **141**(18): p. 3594-604.
230. Gao, L.L., et al., *SET/PP2A system regulates androgen production in ovarian follicles in vitro*. *Mol Cell Endocrinol*, 2013. **374**(1-2): p. 108-16.
231. Hu, M.W., et al., *Scaffold Subunit Aalpha of PP2A Is Essential for Female Meiosis and Fertility in Mice*. *Biology of Reproduction*, 2014. **91**(1).
232. Bollen, M., et al., *The extended PP1 toolkit: designed to create specificity*. *Trends Biochem Sci*, 2010. **35**(8): p. 450-8.
233. Thayyullathil, F., et al., *Protein Phosphatase 1-Dependent Dephosphorylation of Akt Is the Prime Signaling Event in Sphingosine-Induced Apoptosis in Jurkat Cells*. *Journal of Cellular Biochemistry*, 2011. **112**(4): p. 1138-1153.
234. Makanji, Y., et al., *Inhibin at 90: From Discovery to Clinical Application, a Historical Review*. *Endocrine Reviews*, 2014. **35**(5): p. 747-794.
235. Skory, R.M., et al., *Microarray analysis identifies COMP as the most differentially regulated transcript throughout in vitro follicle growth*. *Molecular Reproduction and Development*, 2013. **80**(2): p. 132-144.
236. Ghosh, D., et al., *Structural basis for androgen specificity and oestrogen synthesis in human aromatase*. *Nature*, 2009. **457**(7226): p. 219-23.
237. Simoni, M., J. Gromoll, and E. Nieschlag, *The follicle-stimulating hormone receptor: biochemistry, molecular biology, physiology, and pathophysiology*. *Endocr Rev*, 1997. **18**(6): p. 739-73.
238. Robker, R.L., L.K. Akison, and D.L. Russell, *Control of oocyte release by progesterone receptor-regulated gene expression*. *Nucl Recept Signal*, 2009. **7**: p. e012.
239. Jo, M. and T.E. Curry, Jr., *Luteinizing hormone-induced RUNX1 regulates the expression of genes in granulosa cells of rat periovulatory follicles*. *Mol Endocrinol*, 2006. **20**(9): p. 2156-72.

240. Richards, J.S. and S.A. Pangas, *The ovary: basic biology and clinical implications*. J Clin Invest, 2010. **120**(4): p. 963-72.
241. Duffy, D.M., et al., *Ovulation: Parallels With Inflammatory Processes*. Endocr Rev, 2019. **40**(2): p. 369-416.
242. Takahashi, T., et al., *Cyclooxygenase-2-derived prostaglandin E(2) directs oocyte maturation by differentially influencing multiple signaling pathways*. J Biol Chem, 2006. **281**(48): p. 37117-29.
243. Lim, H., et al., *Multiple female reproductive failures in cyclooxygenase 2-deficient mice*. Cell, 1997. **91**(2): p. 197-208.
244. Mukhopadhyay, D., et al., *Two distinct populations of tumor necrosis factor-stimulated gene-6 protein in the extracellular matrix of expanded mouse cumulus cell-oocyte complexes*. Arch Biochem Biophys, 2001. **394**(2): p. 173-81.
245. Grive, K.J. and R.N. Freiman, *The developmental origins of the mammalian ovarian reserve*. Development, 2015. **142**(15): p. 2554-63.
246. Goswami, D. and G.S. Conway, *Premature ovarian failure*. Hum Reprod Update, 2005. **11**(4): p. 391-410.
247. Xiao, S., et al., *Size-specific follicle selection improves mouse oocyte reproductive outcomes*. Reproduction, 2015. **150**(3): p. 183-92.
248. Ting, A.Y., et al., *Morphological and functional preservation of pre-antral follicles after vitrification of macaque ovarian tissue in a closed system*. Hum Reprod, 2013. **28**(5): p. 1267-79.
249. Ting, A.Y., et al., *In vitro development of secondary follicles from cryopreserved rhesus macaque ovarian tissue after slow-rate freeze or vitrification*. Hum Reprod, 2011. **26**(9): p. 2461-72.
250. Ting, A.Y., et al., *Synthetic polymers improve vitrification outcomes of macaque ovarian tissue as assessed by histological integrity and the in vitro development of secondary follicles*. Cryobiology, 2012. **65**(1): p. 1-11.
251. Nikiforov, D., et al., *Innovative multi-protectoral approach increases survival rate after vitrification of ovarian tissue and isolated follicles with improved results in comparison with conventional method*. J Ovarian Res, 2018. **11**(1): p. 65.
252. Kagawa, N., S. Silber, and M. Kuwayama, *Successful vitrification of bovine and human ovarian tissue*. Reprod Biomed Online, 2009. **18**(4): p. 568-77.
253. Kagawa, N., et al., *Production of the first offspring from oocytes derived from fresh and cryopreserved pre-antral follicles of adult mice*. Reprod Biomed Online, 2007. **14**(6): p. 693-9.
254. Meneely, J.P. and C.T. Elliott, *Microcystins: measuring human exposure and the impact on human health*. Biomarkers, 2013. **18**(8): p. 639-49.
255. Haddad, S.P., et al., *Determination of microcystins, nodularin, anatoxin-a, cylindrospermopsin, and saxitoxin in water and fish tissue using isotope dilution liquid chromatography tandem mass spectrometry*. J Chromatogr A, 2019. **1599**: p. 66-74.
256. Li, Y., et al., *Confocal microscopic analysis of the spindle and chromosome configurations of human oocytes matured in vitro*. Fertil Steril, 2006. **85**(4): p. 827-32.
257. Su, Y.Q., et al., *Synergistic roles of BMP15 and GDF9 in the development and function of the oocyte-cumulus cell complex in mice: genetic evidence for an oocyte-granulosa cell regulatory loop*. Dev Biol, 2004. **276**(1): p. 64-73.
258. de Castro, F.C., M.H. Cruz, and C.L. Leal, *Role of Growth Differentiation Factor 9 and Bone Morphogenetic Protein 15 in Ovarian Function and Their Importance in Mammalian Female Fertility - A Review*. Asian-Australas J Anim Sci, 2016. **29**(8): p. 1065-74.
259. Wassarman, P.M., L. Jovine, and E.S. Litscher, *Mouse zona pellucida genes and glycoproteins*. Cytogenet Genome Res, 2004. **105**(2-4): p. 228-34.

260. Epifano, O., et al., *Coordinate expression of the three zona pellucida genes during mouse oogenesis*. *Development*, 1995. **121**(7): p. 1947-56.
261. Gao, D. and J.K. Critser, *Mechanisms of cryoinjury in living cells*. *ILAR J*, 2000. **41**(4): p. 187-96.
262. Bakhach, J., *The cryopreservation of composite tissues: Principles and recent advancement on cryopreservation of different type of tissues*. *Organogenesis*, 2009. **5**(3): p. 119-26.
263. Elliott, G.D., S. Wang, and B.J. Fuller, *Cryoprotectants: A review of the actions and applications of cryoprotective solutes that modulate cell recovery from ultra-low temperatures*. *Cryobiology*, 2017. **76**: p. 74-91.
264. Lee, J., et al., *Establishment of an improved vitrification protocol by combinations of vitrification medium for isolated mouse ovarian follicles*. *Theriogenology*, 2018. **121**: p. 97-103.
265. Oryan Abkenar, Z., et al., *Vitrification and subsequent in vitro maturation of mouse preantral follicles in presence of growth factors*. *Cell J*, 2014. **16**(3): p. 271-8.
266. Taghavi, S.A., et al., *Vitrification of mouse preantral follicles versus slow freezing: Morphological and apoptosis evaluation*. *Anim Sci J*, 2015. **86**(1): p. 37-44.
267. Gstraunthaler, G., *Alternatives to the use of fetal bovine serum: Serum-free cell culture*. *Altex-Alternativen Zu Tierexperimenten*, 2003. **20**(4): p. 275-281.
268. Segawa, T., et al., *Changes in estrone and estradiol levels during follicle development: a retrospective large-scale study*. *Reprod Biol Endocrinol*, 2015. **13**: p. 54.
269. Bennabi, I., M.E. Terret, and M.H. Verlhac, *Meiotic spindle assembly and chromosome segregation in oocytes*. *J Cell Biol*, 2016. **215**(5): p. 611-619.
270. Wiesak, T., et al., *Effect of vitrification on the zona pellucida hardening and follistatin and cathepsin B genes expression and developmental competence of in vitro matured bovine oocytes*. *Cryobiology*, 2017. **76**: p. 18-23.
271. Larman, M.G., C.B. Sheehan, and D.K. Gardner, *Calcium-free vitrification reduces cryoprotectant-induced zona pellucida hardening and increases fertilization rates in mouse oocytes*. *Reproduction*, 2006. **131**(1): p. 53-61.
272. MacKintosh, C., et al., *Cyanobacterial microcystin-LR is a potent and specific inhibitor of protein phosphatases 1 and 2A from both mammals and higher plants*. *FEBS Lett*, 1990. **264**(2): p. 187-92.
273. Runnegar, M.T., S. Kong, and N. Berndt, *Protein phosphatase inhibition and in vivo hepatotoxicity of microcystins*. *Am J Physiol*, 1993. **265**(2 Pt 1): p. G224-30.
274. Wang, H., et al., *MCLR-induced PP2A inhibition and subsequent Rac1 inactivation and hyperphosphorylation of cytoskeleton-associated proteins are involved in cytoskeleton rearrangement in SMMC-7721 human liver cancer cell line*. *Chemosphere*, 2014. **112**: p. 141-53.
275. Ikehara, T., et al., *A protein phosphatase 2A (PP2A) inhibition assay using a recombinant enzyme for rapid detection of microcystins*. *Toxicon*, 2008. **51**(8): p. 1368-73.
276. Ikehara, T., et al., *The effect of structural variation in 21 microcystins on their inhibition of PP2A and the effect of replacing cys269 with glycine*. *Toxicon*, 2009. **54**(4): p. 539-44.
277. Vesterkvist, P.S., et al., *Comparative cellular toxicity of hydrophilic and hydrophobic microcystins on Caco-2 cells*. *Toxins (Basel)*, 2012. **4**(11): p. 1008-23.
278. Meirow, D., et al., *Searching for evidence of disease and malignant cell contamination in ovarian tissue stored from hematologic cancer patients*. *Hum Reprod*, 2008. **23**(5): p. 1007-13.
279. Wang, T.R., et al., *Human single follicle growth in vitro from cryopreserved ovarian tissue after slow freezing or vitrification*. *Hum Reprod*, 2016. **31**(4): p. 763-73.
280. Taghavi, S.A., et al., *Vitrification of mouse preantral follicles versus slow freezing: Morphological and apoptosis evaluation*. *Animal Science Journal*, 2015. **86**(1): p. 37-44.

281. Liu, L., et al., *Successful cryoloop vitrification and subsequent in vitro maturation of mouse preantral follicles*. Syst Biol Reprod Med, 2011. **57**(3): p. 149-53.
282. Sadr, S.Z., et al., *Utilizing Fibrin-Alginate and Matrigel-Alginate for Mouse Follicle Development in Three-Dimensional Culture Systems*. Biopreserv Biobank, 2018. **16**(2): p. 120-127.
283. Sadr, S.Z., et al., *Mouse preantral follicle development in two-dimensional and three-dimensional culture systems after ovarian tissue vitrification*. Eur J Obstet Gynecol Reprod Biol, 2015. **194**: p. 206-11.
284. Wang, X., et al., *Successful in vitro culture of pre-antral follicles derived from vitrified murine ovarian tissue: oocyte maturation, fertilization, and live births*. Reproduction, 2011. **141**(2): p. 183-91.
285. Mazoochi, T., et al., *Analysis of apoptosis and expression of genes related to apoptosis in cultures of follicles derived from vitrified and non-vitrified ovaries*. Mol Hum Reprod, 2009. **15**(3): p. 155-64.
286. Youm, H.W., et al., *Optimal vitrification protocol for mouse ovarian tissue cryopreservation: effect of cryoprotective agents and in vitro culture on vitrified-warmed ovarian tissue survival*. Hum Reprod, 2014. **29**(4): p. 720-30.
287. Xing, W., et al., *Solid-surface vitrification is an appropriate and convenient method for cryopreservation of isolated rat follicles*. Reprod Biol Endocrinol, 2010. **8**: p. 42.
288. Taketsuru, H., et al., *Bovine oocytes in secondary follicles grow in medium containing bovine plasma after vitrification*. J Reprod Dev, 2011. **57**(1): p. 99-106.
289. Bus, A., et al., *Effects of vitrification on the viability of alginate encapsulated isolated bovine pre-antral follicles*. J Assist Reprod Genet, 2018. **35**(7): p. 1187-1199.
290. Guedes, J.S., et al., *Follicle Viability after Vitrification of Bovine Ovarian Tissue*. Rev Bras Ginecol Obstet, 2017. **39**(11): p. 614-621.
291. Sadeghnia, S., et al., *Development of sheep primordial follicles encapsulated in alginate or in ovarian tissue in fresh and vitrified samples*. Cryobiology, 2016. **72**(2): p. 100-5.
292. Lunardi, F.O., et al., *Vitrified sheep isolated secondary follicles are able to grow and form antrum after a short period of in vitro culture*. Cell Tissue Res, 2015. **362**(1): p. 241-51.
293. Lunardi, F.O., et al., *Sheep Isolated Secondary Follicles Are Able to Produce Metaphase II Oocytes After Vitrification and Long-Term In Vitro Growth*. Biopreserv Biobank, 2017. **15**(4): p. 321-331.

# APPENDIX A

## COPYRIGHT PERMISSION FOR CHAPTER 4

**CCC RightsLink®** Home ? Help Email Support Sign In Create Account

 **A closed vitrification system enables a murine ovarian follicle bank for high-throughput ovotoxicity screening, which identifies endocrine disrupting activity of microcystins**  
Author: Yingzheng Wang, Jingshan Xu, Jessica E. Stanley, Murong Xu, Bryan W. Brooks, Geoffrey I. Scott, Saurabh Chatterjee, Qiang Zhang, Mary B. Zelinski, Shuo Xiao  
Publication: Reproductive Toxicology  
Publisher: Elsevier  
Date: April 2020  
© 2020 Elsevier Inc. All rights reserved.

**Journal Author Rights**  
Please note that, as the author of this Elsevier article, you retain the right to include it in a thesis or dissertation, provided it is not published commercially. Permission is not required, but please ensure that you reference the journal as the original source. For more information on this and on your other retained rights, please visit: <https://www.elsevier.com/about/our-business/policies/copyright#Author-rights>

[BACK](#) [CLOSE WINDOW](#)

© 2022 Copyright - All Rights Reserved | Copyright Clearance Center, Inc. | Privacy statement | Terms and Conditions  
Comments? We would like to hear from you. Email us at [customer-care@copyright.com](mailto:customer-care@copyright.com)